Nmr of phosphorus-containing solids

Philip John Wilkes

NMR OF PHOSPHORUS-CONTAINING SOLIDS

by

Philip John Wilkes

B. Sc., University of East Anglia (1984)

A thesis submitted for the degree of

Doctor of Philosophy

of the University of Durham

October 1987

MEMORANDUM

The research presented in this thesis has been carried out in the Department of Chemistry of the University of Durham between October 1984 and October 1987. It is the original work of the author unless stated otherwise. None of this work has been submitted for any other degree.

NMR of Phosphorus-Containing Solids

by

Philip John Wilkes

ABSTRACT

The purpose of this work has been the determination of structure in solids using the technique of solid-state nuclear magnetic resonance spectroscopy.

High-resolution ^{31}P NMR spectra have been obtained for a range of phosphate species. A number of techniques have been applied to these systems including cross-polarization, magic angle spinning, and high power proton decoupling. Characterisation using additional NMR techniques such as ^{1}H CRAMPS has been carried out wherever possible.

The results obtained yield molecular and crystallographic information consistent with data from X-ray diffraction when known. Shielding tensor components were determined from static and/or spinning spectra wherever possible. The phosphate species studied include a series of precipitated calcium phosphates. A particular model for the structure of amorphous calcium phosphate is favoured in the light of ^{31}P NMR measurements. One sample showed NMR evidence for changes in composition whilst in the solid state.

The origins of ^{31}P NMR linewidths in high-resolution solid-state spectra have been considered in some detail. Variation of ^{31}P NMR linewidth as function of spinning rate has been noted for a number phosphate compounds. Multiple pulse techniques have been applied on the phosphorus channel with pleasing improvements in spectral resolution.

Five solid binary phosphorus sulphides have also been studied using phosphorus MAS NMR, and the results compared to solution state data wherever possible. A number of anomalies between solution and solid-state data have been noted and discussed.

ACKNOWLEDGEMENTS

Firstly I would like to thank my advisors Professor Robin Harris and Dr. Peter Belton who have both offered me much advice, guidance and inspiration throughout the duration of this research. I would especially like to thank Robin for considerable support and encouragement whilst I was undergoing the ordeal of writing up and working at the same time.

Secondly I would like to express my thanks to Dr. Geoff Nesbitt who took on the unenviable task of training myself and others in the experimental aspects of solid-state NMR. The learning that ensued was made very much easier thanks to the company of Larry Merwin and Pete Jackson with whom I shared my three years at Durham. NMR just wouldn't have been the same without you guys!

Life outside of NMR has also been extremely enjoyable, my sanity has remained reasonably intact thanks to the friendship of Mike Parkinson, Hairy Dave, Ig, Ev, the Dude, Tex, Pete, Tony, the "boy wonder" and many others at the Graduate Society. Cheers to you all!

I am grateful to Drs D. W. L. Hukins and J. E. Harries (University of Manchester) and Dr. D Woollins and P Wood (Imperial College, London) for the preparation of the samples described in chapters five and seven respectively.

Thanks are also extended to the U. K. Science and Engineering Research Council and the AFRC Institute of Food

Research for providing my CASE studentship.

Last, but by no means least, none of this work would have been possible without considerable support, encouragement and understanding from Mum, Dad, Graham and Suzanne throughout my studies. Thanks for being there.

Table of Contents

To Mum and Dad

CHAPTER 1 - INTRODUCTION

In recent years many advances have been made in the area of solid-state nuclear magnetic resonance (NMR). The developments include improved understanding, new NMR methods and ever improving hardware. The combination of these factors has enabled the NMR spectroscopist to obtain new information previously inaccessible for solids. The application of "state of the art" methods enables the spectroscopist to move closer and closer towards liquid-like resolution for a wide range of solid materials. In some cases, studies of this type allow information concerning molecular and crystal structure to be determined.

The aim of the work presented in this thesis is to examine the solid-state structure of a range of phosphorus-containing solids. The main theme of the work is the characterisation of a range of phosphate species, especially calcium phosphates. Out of this work arose an additional question concerning the origin of ^{31}P NMR linewidths in the solid state. This prompted the development of additional line narrowing techniques for use in solid-state phosphorus NMR studies, and the study of the series of P_4S_n compounds.

The overall approach used in this work was firstly to demonstrate the suitability of solid-state NMR techniques by comparison with previously obtained structural data from, say X-ray crystallography, and secondly to then make conclusions solely from NMR data when no crystal data are available. A number of NMR methods have been applied to the systems of interest with varying degrees of success. The data obtained

should constitute a starting point for future studies of systems of the types considered here.

The next chapter will discuss the theory of NMR as it applies to the solid state. Nuclear spin interactions will be considered along with indirect spin-spin coupling. The three main averaging techniques used in this work will be examined. Brief mention will be given to the cross-polarization technique.

In Chapter Three, experimental considerations will be discussed. The various pulse sequences used in this work will be described. Some description of set-up techniques will be given, especially with regard to setting of the rotor angle.

Chapter Four considers a range of model phosphate compounds in the solid-state. A range of NMR techniques are applied making use of both ^{31}P and ^{1}H high-resolution techniques. ^{1}H wide-line spectra are also considered. Wherever possible the NMR spectra are explained in the light of crystal structure information. The compounds have been further characterised in terms of shielding tensor components. The data are compared with NMR data from other workers.

Chapter Five examines in some detail the structures of some precipitated calcium phosphates. The aim of this work was to identify and characterise as fully as possible a sample of amorphous calcium phosphate, and to monitor the way in which aging takes place whilst in solution. The selectivity of the cross-polarization sequence compared to the single pulse excitation method will be demonstrated. Other selective

NMR methods have also been applied. Changes in the composition of a multicomponent system is followed in the solid state using ^{31}P NMR.

The aim of Chapter Six is to examine the origin of ^{31}P NMR linewidths in the solid state. Evidence from spectra presented in Chapter Four suggested that magic angle spinning was not averaging effectively until very high spinning rates were used. Even using very high spinning rates, linewidths tended to be significantly broader than in the solution state. The chapter considers homogeneous and inhomogeneous broadening and determines the extent to which various mechanisms contribute to ^{31}P NMR linewidths. Multiple pulse sequences have been applied on the phosphorus channel with pleasing improvements in the spectral resolution obtained.

Finally, a series of binary phosphorus sulphides are studied in Chapter Seven. The spectra obtained are compared wherever possible with X-ray crystal data (if available). Solid-state NMR enables identification of the phase present and gives information regarding molecular structure and crystal packing.

CHAPTER 2 - SOLID-STATE NMR THEORY

2.1 INTRODUCTION

In the study of NMR, the interactions that govern the response of magnetic moments are anisotropic in nature. That is, the magnitude and direction of the effect experienced at the nucleus varies with the orientation of the environment with respect to the chosen frame of reference.

For the solution state, rapid molecular motion gives rise to averaging of the anisotropic interactions, resulting in high-resolution spectra being obtained. The response of a solution can be described in terms of scalar quantities rather than tensors. The molecular motion that takes place can result in complete removal of dipolar effects, for example. Other interactions, e.g. the chemical shift, take on their isotropic values. The extensive averaging that takes place in the solution state does, however, result in the loss of anisotropic information concerning the various interactions.

In the solid state the situation is effectively reversed. All motion is "frozen out". Most crystals are anisotropic and possess limited symmetry. Thus interactions which are anisotropic in nature dominate. Consequently isotropic information is obscured. For solids, NMR spectra consist of signals which may be up to tens of kHz wide. The aim of the solid-state techniques applied in the work

presented in this thesis is to selectively remove/suppress the dominating anisotropic interactions so that high-resolution fine structure can be once again achieved.

The line-narrowing techniques used for the work covered in this thesis were as follows;

(a) Magic Angle Spinning (MAS). This technique involves rapid macroscopic rotation of a powder sample about an axis inclined at an angle of 54.7° relative to the applied magnetic field. This method will in principle remove dipolar interactions and average the anisotropic chemical shielding to its isotropic value, provided the rotation rate is in excess of the magnitude of the interaction to be removed. If the rotation rate is lower than the magnitude of the interaction to be removed, spinning sideband patterns appear, with the centre-band taking the isotropic value. This effect can often be used to recover information regarding the shielding anisotropy by analysis of the sideband pattern obtained[1,2].

(b) High-power heteronuclear dipolar decoupling. The method is analogous to the decoupling technique used in solution-state studies although much higher power levels are required (typically kilowatts rather than ca. 20 watts). For the work in this thesis, dipolar $\{^{31}P\text{-}^{1}H\}$ interactions are removed using this technique

(c) Multiple-pulse sequences. For systems of abundant spins (e.g. ^{1}H or ^{19}F) homonuclear dipolar interactions can become too large to be removed by magic-angle spinning techniques. The magnitude of the interactions is in excess of currently attainable spinning rates. Thus an alternative line-narrowing method is required. Multiple-pulse sequences apply trains of carefully timed pulses with differing phases, such that the magnetisation behaves as if the dipolar coupling interaction is zero during certain observation windows.

Frequently a combination of the above techniques is used to simultaneously remove a number of interactions

2.2 NUCLEAR SPIN INTERACTIONS

The nuclear spin Hamiltonian that describes the response of magnetic moments can be written as the sum of the constituent Hamiltonians which contribute to the total interaction. The various interactions represent the coupling of nuclear spins to physical features of the system in which they reside. These physical features result from interactions which can be categorised as being either external or internal to the spin system itself. In the case considered here the external Hamiltonians are the Zeeman and

radio frequency terms, which are essentially under the control of the experimentalist. The internal Hamiltonians result the interactions from within the spin system itself.

The nuclear spin Hamiltonian can be tabulated as follows;

Table 1: The nuclear Spin Hamiltonian

$\hat{A}$ =	$\hat{A}_Z$	Zeeman	External
	$+\hat{A}_{RF}$	Radio Frequency	External
	$+\hat{A}_{CS}$	Shielding	Internal
	$+\hat{A}_{SR}$	Spin Rotation	Internal
	$+\hat{A}_Q$	Quadrupolar	Internal
	$+\hat{A}_D$	Dipolar Spin-Spin Coupling	Internal
	$+\hat{A}_J$	Indirect (Scalar) Spin-Spin Coupling	Internal

Several of the Hamiltonians in Table 1 are of little importance. The external terms simply allow the experiment to be performed and do not contain information of molecular importance. Of the internal terms, the quadrupolar contribution will not be considered since the work in this thesis involves no quadrupolar nuclei. The spin-rotation Hamiltonian will not be considered either, since it describes the interaction between nuclear spins and the angular momentum of a molecule. The effect is generally accepted to be small and can be ignored in solid state studies.

As was mentioned earlier in this chapter NMR interactions tend to be anisotropic in nature. Brief attention will now be given to the treatment of such anisotropic interactions using tensor notation. Representation of the various interactions in terms of tensors results in a common notation. The internal Hamiltonians describe the bilinear coupling of two vectors (spin i and spin j). Consequently, tensors can be used to relate the behaviour of the spins. In the case of the NMR interactions considered here, second-rank tensors are appropriate. Each of them can be expressed in terms of a 3x3 matrix. All the internal Hamiltonians may be expressed in the following general tensor notation (see for example, Harris [3] or Haeberlen [4]) :

$$\left(\frac{h}{2\pi}\right)^{-1} \hat{H}_\lambda = k_\lambda I . \underline{G}_\lambda . P_\lambda$$

where h is Planck's constant, $\hat{H}_\lambda$ is the Hamiltonian for the interaction of type λ, k_λ represents the constant associated with the tensor $\underline{G}_\lambda$, I represents the nuclear spin and P_λ represents the vector property to which the spin interaction is related. Tabulations of $\underline{G}_\lambda$, k_λ and P_λ may be found elsewhere[3,4]. Once the Hamiltonian is in tensor notation the axis system can be changed (if desired) to the principal axis system (PAS). In this chosen axis system the tensor is in a diagonal form, where the values of the components along the diagonal are known as the principal components. Having forced the tensor into this form, three additional properties may be defined, namely the trace, the anisotropy and the asymmetry. These properties are defined in chapter 3.

Each of the remaining internal spin Hamiltonians will now be considered in turn.

2.2.1 The Shielding Hamiltonian

The source of shielding of nuclear spins arises from the interaction of the magnetic field resulting from the orbital motion of surrounding electrons with the applied static

magnetic field. The magnitude and direction of the interaction will thus be dependent on orientation. Consequently the interaction is a tensor quantity.

The coupling of a spin I with the magnetic field B_0 can be described using the shielding tensor $\underline{\sigma}$ such that:

$$\left(\frac{h}{2\pi}\right)^{-1} \hat{H}_{CS} = \gamma I . \underline{\sigma} . B_0$$

where γ is the magnetogyric ratio. Clearly the equation applies for a single isolated spin. In a real system this is obviously not the case, and a summation over all spins is required;

$$\left(\frac{h}{2\pi}\right)^{-1} \hat{H}_{CS} = \sum_i \gamma_i . I_i . \underline{\sigma}_i . B_0$$

This form can readily be converted to the PAS so that isotropic shielding, shielding asymmetry and shielding anisotropy can be defined.

2.2.2 Dipolar Spin-Spin Coupling.

Between two nuclear magnets there is a direct through-space interaction referred to as dipolar spin-spin coupling. The interaction is analogous to the case of two macroscopic bar magnets. The energy of such a system involving two point magnetic dipoles μ_i and μ_j can be defined classically as follows;

$$U = \frac{\mu_o}{4\pi}\left\{\frac{(\underline{\mu}_i \cdot \underline{\mu}_j)}{r_{ij}^3} - \frac{3(\underline{\mu}_i \cdot \underline{r}_{ij})(\underline{\mu}_j \cdot \underline{r}_{ij})}{r_{ij}^5}\right\}$$

where μ_o is the permeability of free space, $\underline{r}_{ij}$ is the vector joining the two dipoles and r_{ij} is the distance separating them.

The equation can be obtained in quantum mechanical form by making the substitution;

$$\underline{\mu} = \gamma\left(\frac{h}{2\pi}\right)\hat{I}$$

which gives;

$$\hat{H}_D = \gamma_i\gamma_j\left(\frac{h}{2\pi}\right)^2 \cdot \frac{\mu_o}{4\pi}\left\{\frac{(\hat{I}_i \cdot \hat{I}_j)}{r_{ij}^3} - \frac{3(\hat{I}_i \cdot \underline{r}_{ij})(\hat{I}_j \cdot \underline{r}_{ij})}{r_{ij}^5}\right\}$$

where γ_i and γ_j are the magnetogyric ratios of spins i and j respectively. When expressed in terms of polar coordinates the dipolar Hamiltonian takes the form;

$$\hat{H}_D = \left(\frac{\gamma_i\gamma_j}{r^3}\right)\left(\frac{\mu_o}{4\pi}\right)\left(\frac{h}{2\pi}\right)^2 (A + B + C + D + E + F)$$

with;

$$A = -\hat{I}_{iz}\hat{I}_{jz}\left(3\cos^2\theta - 1\right)$$

$$B = \left(\frac{1}{4}\right)\left(\hat{I}_{i+}\hat{I}_{j-} + \hat{I}_{i-}\hat{I}_{j+}\right)\left(3\cos^2\theta - 1\right)$$

$$C = -\left(\frac{3}{2}\right)\left(\hat{I}_{iz}\hat{I}_{j+} + \hat{I}_{i+}\hat{I}_{jz}\right)\sin\theta\cos\theta\exp(-i\phi)$$

$$D = -\left(\frac{3}{2}\right)\left(\hat{I}_{iz}\hat{I}_{j-} + \hat{I}_{i-}\hat{I}_{jz}\right)\sin\theta\cos\theta\exp(-i\phi)$$

$$E = -\left(\frac{3}{4}\right)\hat{I}_{i+}\hat{I}_{j+}\sin^2\theta\exp(-2i\phi)$$

$$F = -\left(\frac{3}{4}\right)\hat{I}_{i-}\hat{I}_{j-}\sin^2\theta\exp(2i\phi)$$

where θ is the angle between the internuclear vector and the applied Zeeman field.

From the above expansion it is obvious that each of the terms (A - F) can be considered as the product of two terms; i.e. a spin part and a geometric part. The geometric terms will be considered later in this chapter when averaging techniques are discussed. Brief comment will now be given with regard to the spin terms.

The A term takes the form of a pair of interacting parallel dipoles and does not result in any spin transitions. The energy of this interaction is a small perturbation of the Zeeman energy levels.

The B term describes energy conserving transitions, and

is often referred to as the "flip-flop" term. This type of transition will only be readily allowed for like spins. In the rigid heteronuclear case the transitions would be forbidden since they are not energy conserving as a consequence of the $\alpha\beta$ and $\beta\alpha$ states having different Zeeman energies.

The remaining terms C, D, E, and F make negligible contributions to first order spectra and thus will not be considered in any detail. The C and D terms alter the state of one spin only. The E and F terms describe double quantum transitions, where both spins flip up or both spins flip down simultaneously.

As a consequence of the foregoing arguments the dipolar Hamiltonian for first-order spectra can be expressed in truncated form:

(i) Heteronuclear case;

$$\hat{H}_D = -\left(\frac{h}{2\pi}\right)^2\left(\frac{\mu_o}{4\pi}\right)\gamma_i\gamma_j r^{-3}\left(3\cos^2\theta - 1\right)\left(\hat{I}_{iz}\hat{I}_{jz}\right)$$

(ii) Homonuclear case;

$$\hat{H}_D = -\left(\frac{h}{2\pi}\right)^2\left(\frac{\mu_o}{4\pi}\right)\gamma^2 r^{-3}\left(3\cos^2\theta - 1\right)\left(\hat{I}_{iz}\hat{I}_{jz} - \frac{1}{4}\left(\hat{I}_{i+}\hat{I}_{j-} + \hat{I}_{i-}\hat{I}_{j-}\right)\right)$$

In the foregoing discussion the case of a pair of isolated spins was considered. In a real spin system this is certainly not the case since the dipolar Hamiltonian

links each nucleus to all other nuclei within the system. Thus the interaction is more properly described as a summation;

$$\hat{H}_D = \sum_{l<m}\left(\frac{h}{2\pi}\right)^2\left(\frac{\mu_o}{4\pi}\right)\gamma_l\gamma_m r^{-3} I_l \cdot \underline{D}^{lm} \cdot I_m$$

where *l* and *m* represent all pairs of nuclei. The inequality ensures that each pair is counted once only. Note also that tensor notation is required to describe the system.

2.3 Indirect Spin-Spin Coupling

Indirect spin-spin coupling, otherwise known as J coupling, is an indirect spin coupling effect. This describes the coupling of nuclear spins via the electrons present in the molecular system surrounding them. This interaction cannot act directly. It must be transmitted via electrons - which is in contrast to the dipolar Hamiltonian which is a through space effect.

The Hamiltonian describing indirect (scalar) coupling is given by;

$$\left(\frac{h}{2\pi}\right)^{-1}\hat{H}_J = \sum_{l<m} I_l \cdot \underline{J}_{lm} \cdot I_m$$

where $\underline{J}_{lm}$ is the indirect coupling tensor. It is clear that $\hat{H}_J$ takes the same form as the dipolar Hamiltonian. Thus it can in principle be a source of homogeneous broadening in the same manner as the dipolar interaction. However, the coupling is no larger than ca. 220 Hz for the compounds

studied in this thesis, and is therefore quite small compared to the dipolar or shielding interactions. Any averaging effects that apply to the dipolar interaction also apply to scalar coupling (e.g. MAR and multiple pulse operation).

The nature of the dipolar and scalar coupling tensors themselves are however slightly different. The former is traceless. Thus under conditions of averaging the isotropic part will be zero. In contrast, the indirect coupling will have a non-zero trace, resulting in non-zero scalar coupling.

2.4 Averaging Techniques

In the solution state, rapid molecular tumbling as a result of thermal energy provides averaging of the interactions discussed in the preceding sections. Generally, solution state spectra are highly detailed, with resolution of considerable fine structure. The spectra readily reveal chemical shift and scalar coupling information. However in the case of solid-state studies, the molecules are generally immobile, and consequently there are no rapid isotropic averaging processes taking place.

The aim of solid-state NMR is to apply averaging techniques so that artificial isotropic averaging can take

place, with the ultimate goal of achieving resolution and fine structure comparable to that observed in the solution state.

Three averaging techniques have been applied for the work presented in this thesis, namely magic angle spinning (MAS), high power proton decoupling (HPPD) and multiple pulse (MP) operation. A fourth technique (CRAMPS) which is essentially a combination of the MAS and MP techniques has also been used.

2.4.1 Magic Angle Spinning.

Rapid macroscopic sample rotation was first introduced by Andrew, Bradbury and Eades in 1958 [5], in an investigation of dipole-dipole interactions. It was later recognized independently by Andrew et. al. [6] and Lowe[7] that by careful choice of the angle of rotation, line broadening due to dipole-dipole interactions could be reduced to zero. The angle of the rotation axis with respect to the static Zeeman field which gave complete removal of the interaction was 54.7^{O}, otherwise referred to as the "magic angle". Subsequently it was demonstrated that magic angle rotation would also remove broadening effects due to the anisotropy in chemical shielding[8].

The way in which magic angle rotation operates is best illustrated by way of the example of dipole-dipole broadening. If one considers a pair of spins, i and j,

present in a powdered sample undergoing rotation about an axis inclined at an angle , β, with respect to the applied Zeeman field (Figure 2.1).

Figure 2.1 : Diagram to illustrate the motion of an internuclear vector r_{ij} when rotated about an axis inclined at an angle β to B_o.

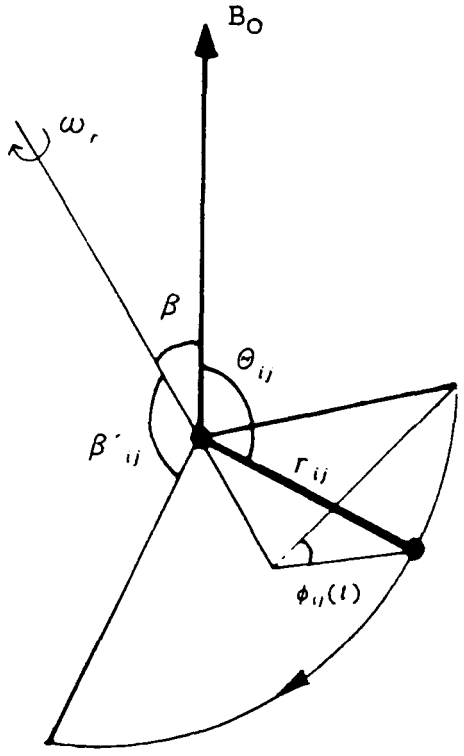

r_{ij} is the internuclear distance, θ_{ij} is the angle between the internuclear vector and B_0, β'_{ij} is the angle between the internuclear vector and the rotation axis, and $\phi_{ij}(t)$ is a phase factor in order to define the starting position of the internuclear vector.

Cos θ_{ij} can be expressed in terms of other angles in the system [9];

$$\cos\theta_{ij} = \cos\beta\cos\beta'_{ij} + \sin\beta\sin\beta'_{ij}\cos(\omega_r t + \phi_{oij})$$

which can be substituted into the geometric term of the truncated dipolar Hamiltonian, which after re-arrangement gives;

$$\hat{H}_D = \sum_{i=1}^{N_I}\sum_{m=1}^{N_S}\left(\frac{h}{2\pi}\right)^2 \gamma_I\gamma_S r^{-3}(\hat{I}_z\hat{S}_z)\{(3\cos^2\beta - 1)(3\cos^2\beta'_{ij} - 1)$$

$$+3\sin 2\beta\sin 2\beta'_{ij}\cos(\omega_r t + \phi_{oij})$$

$$+3\sin^2\beta\sin^2\beta'_{ij}\cos 2(\omega_r t + \phi_{oij})\}\left(\frac{\mu_o}{4\pi}\right)$$

for the heteronuclear case. The homonuclear dipolar Hamiltonian can be obtained in a similar form (the geometric terms will be identical to those for the heteronuclear case).

The important features to note are;

(a) The angle β is under the control of the experimentalist. Selecting β as the magic angle results in the first term going to zero.

(b) The remaining two terms are periodic in ω_r and $2\omega_r$, respectively and give rise to rotational sidebands at multiples of ω_r.

(c) The elimination of the effects of $\hat{H}_D$ by rotation at the magic angle only occurs when $\hat{H}_D$ can be truncated to terms involving $(3\cos^2\theta - 1)$. This is generally true for $\hat{H}_D$ in practice because the Zeeman term dominates in high magnetic fields. However the procedure is not always so simple for the quadrupolar interaction, which may be significant compared to $\hat{H}_Z$.

The net result in high fields is, however, that a centreband resonance free from dipolar broadening flanked by rotational sidebands may be achieved by using magic angle rotation.

It should however be noted by the reader that there is a constraint concerning the MAR technique. Homogeneously and inhomogeneously broadened signals behave differently under the influence of averaging techniques. For a homogeneously broadened line, each nucleus contributes to the full static bandwidth, whereas inhomogeneously broadened lines result from a superposition of a large number of narrow resonances. Consequently, an inhomogeneously broadened line can be

narrowed using NMR provided the rotation rate is greater than the linewidth of each of the constituent "narrow" signals. For the case of a homogeneously broadened line rotation must be at a rate greater than the total static bandwidth in order for averaging to take place. For the work presented in this thesis the maximum rotation rate that could be obtained was 5 kHz. Consequently homogeneous broadening greater than 5 kHz could not be removed by MAR alone. Indeed, even homogeneous interactions as low as 2-3 kHz would be further narrowed by spinning at speeds greater than 5 kHz. Recent developments have seen the advent of spinning systems capable of rotation rates in excess of 15 kHz, enabling high resolution spectra to be obtained for a wider range of homogeneously broadened systems (although apparatus of this type was not available at Durham). For systems containing abundant, high-γ spins e.g. ^{1}H and ^{19}F, homogeneous broadening could be as large as 40 kHz. Clearly an alternative method of line narrowing is required. Multiple pulse techniques (discussed in the section 2.4.3) provide a means of averaging in spin systems of this type.

2.4.2 High Power Proton Decoupling

The effects of heteronuclear dipolar interactions between protons and the nucleus of interest can be removed by the use of a double resonance experiment where HPPD is applied on the second channel. The technique involves irradiation at high power, of the protons in the system.

The irradiation induces time evolution of the proton spin states resulting in time dependence of the heteronuclear dipolar coupling. Thus, averaging of the interaction takes place. Decoupling of this type can be accomplished in two ways, either with a preparation pulse or without. The latter method results in rapid destruction of the proton magnetisation whereas the former corresponds to the so called "spin lock" condition where the proton magnetisation is preserved via a 90^{0} phase shift in the decoupling field. Under spin lock conditions the decay of proton magnetisation is governed by the proton $T_{1\rho}$. The "spin lock" decoupling method is used for cross polarization experiments (see chapter 3).

2.4.3 Multiple Pulse Techniques.

In section 2.4.1 (magic angle rotation) it was demonstrated that the dipolar interaction can be removed via manipulation of the geometric term in the dipolar Hamiltonian. An alternative approach is to manipulate the spin term, i.e. averaging in spin-space. The classical energy for a pair of point magnetic dipoles $\underline{\mu}_i$ and $\underline{\mu}_j$ can be written [10] as;

$$U = 2r_{ij}^{-3}\frac{\mu_o}{4\pi}\left(1-3\cos^2\theta_{ij}\right)\left\{\underline{\mu}_i\cdot\underline{\mu}_j - 3\left(\mu_z\right)_i\left(\mu_z\right)_j\right\}$$

In the case of rapid isotropic molecular motion the term $(3\cos^2\theta - 1)$ will be zero and no dipolar broadening will be observed. In the case of solid samples with large dipolar interactions, manipulation of the geometric term may be insufficient for removal of dipolar interactions. If one now considers the case where the nuclear spins themselves could rotate about the magic angle, U would be zero. Waugh et. al.[11] have demonstrated this can indeed be done using carefully-timed radio frequency pulses. If the following sequence, known as the WAHUHA[11] sequence, is considered in the rotating frame;

$$\left[90_{x'} - 2\tau - 90_{-x'} - \tau - 90_{y'} - 2\tau - 90_{-y'} - \tau - \right]$$

one can imagine the magnetisation **M** which possesses the same frequency as the rotating frame is initially along the z' axis. The first pulse along x' will flip the magnetisation to the y' plane for a period of time 2τ. The second pulse will send **M** back to the z' direction for a period of time τ. The sequence of events then repeats but with the magnetisation being flipped into the x' direction and then back into the z' direction. Once the cycle is completed, **M** is back in its original position having spent one third of its time in each of the directions x', y' and z'. The sequence of events just described will only strictly be true if the pulses were of a duration small compared to τ. A

further requirement is that the cycle time 6τ is much less than T_2 in order that the magnetisation does not decay during the multiple pulse cycle.

If the effect of the WAHUHA sequence on the dipolar interaction energy is now considered there are two terms of importance namely $\underline{\mu}_i \cdot \underline{\mu}_j$ and $(\mu_z)_i(\mu_z)_j$. The former is simply a scalar product of the two magnetic moments and therefore depends only on the relative orientations of $\underline{\mu}_i$ and $\underline{\mu}_j$. The latter is a product of the z-components of the magnetic moments $\underline{\mu}_i$ and $\underline{\mu}_j$. This term must be averaged over the three orientations described previously. Since the magnetisation spends an equal amount of time (2τ) in each of the directions x', y' and z' the average will be;

$$\langle (\mu_z)_i (\mu_z)_j \rangle = \frac{1}{3}\left\{ (\mu_{x'})_i (\mu_{x'})_j + (\mu_{y'})_i (\mu_{y'})_j + (\mu_{z'})_i (\mu_{z'})_j \right\}$$

$$= \frac{1}{3} \underline{\mu}_i \cdot \underline{\mu}_j$$

thus U will be zero. The WAHUHA sequence has indeed been demonstrated to give a substantial reduction in U. In practice, a series of consecutive pulse cycles of the type just described are applied, with single point data sampling taking place in appropriate windows within each of the cycles. Fourier transformation of the resulting free induction decay leads to a frequency domain spectrum of the type obtained in a conventional NMR experiment. The

multiple pulse sequence does however act on the other internal Hamiltonians also. This results in the chemical shift, shielding anisotropy and heteronuclear scalar coupling being scaled by a factor dependent on the multiple pulse sequence used. In the case of the WAHUHA sequence the scaling factor is approximately $1/\sqrt{3}$.

Although the WAHUHA sequence should in principle reduce the dipolar Hamiltonian to zero, complete removal does not actually occur for a number of reasons including;

(i) inhomogeneities in B_1 fields

(ii) inaccuracies in pulse angles and timings.

These problems have been addressed by a number of workers. The radio frequency field inhomogeneity has been improved by the use of flat wire coils together with a spherical sample volume to eliminate bulk susceptibility effects[12]. The consequences of pulse errors have been minimised by the proposal of more complex multiple pulse sequences[13]. For the multiple pulse work presented in this thesis the MREV-8 eight-pulse sequence[14] has been used. Pulse sequences of 16 and 24 pulses evaluated[15] for the spectrometer system used for this work and were demonstrated as offering in practice no measurable improvement in resolution or ease of implementation compared to the MREV-8 sequence.

As mentioned earlier in this section the shielding anisotropy is scaled but not fully removed by multiple pulse sequences. Thus, the use of multiple pulse techniques alone will generally give spectra in which detailed isotropic chemical shift information (from chemically inequivalent environments for example) is obscured by shielding anisotropy effects. If however magic angle rotation and multiple pulse operation are combined, isotropic chemical shift information can be obtained. The combination of the two techniques is usually referred to as CRAMPS (combined rotation and multiple pulse spectroscopy).

The description of multiple pulse and CRAMPS techniques given here has been at a very superficial level in order to demonstrate the way in which they operate. Detailed rigorous treatments can be found elsewhere[4,16].

2.5 Cross-polarization

The polarization transfer technique[17] is a powerful method of acquiring spectra of rare spin systems. However, the technique is not limited to dilute spin systems only. It can indeed be applied to isotopically abundant spin systems. For example, the CP spectra presented in this thesis result from polarization transfer from ^{1}H to ^{31}P, both of which are present in 100% natural abundance.

A number of benefits are offered when using cross-polarization which include;

(a) Potential gains in sensitivity compared to conventional single-pulse excitation.

(b) More rapid pulse repetition rates are often possible as a result of protons having significantly shorter relaxation times compared to ^{31}P nuclei within the same sample.

(c) Cross-polarization offers a technique of spectral editing. Efficient polarisation transfer will only take place between ^{1}H and ^{31}P nuclei which are in very close proximity.

The cross-polarization (CP) experiment relies on the transfer of spin order from one spin system to the other. The state of the spin system in the presence of perturbing fields H_{1I} and H_{1S} for spins I and S respectively may be described as follows[17];

$$H_{tot} = H_Z + H_{DII} + H_{DSS} + H_{DIS} + H_{1I}(t) + H_{1S}(t)$$

where H_Z is the Zeeman interaction, H_{DII} and H_{DSS} are the homonuclear spin interactions for spins of types I and S respectively. H_{DIS} is the heteronuclear dipolar interaction term.

From the above equation it is evident that the the interaction linking the two spin reservoirs is the heteronuclear dipolar interaction term, $\hat{H}_{DIS}$, which has the following truncated form;

$$\hat{H}_{DIS} = \frac{\mu_o}{4\pi}\left(\frac{h}{2\pi}\right)^2 \frac{\gamma_I \gamma_S}{r^3} \sum_{i=1}^{N_I} \sum_{m=1}^{N_S} \left(1 - 3\cos^2\theta_{im}\right)\left\langle \hat{I}_z \hat{S}_z \right\rangle$$

Efficient polarization transfer will only take place between I and S spins within close proximity of each other as a consequence of the r^{-3} dependence of $\hat{H}_{DIS}$.

If we now transfer the total Hamiltonian, $\hat{H}_{tot}$ to the doubly rotating frame under the transformation[17];

$$\hat{H}_{tot}(\mathrm{ROT}) = R\hat{H}_{tot}(LAB)R^{-1}$$

where;

$$R = \exp\left\{-it\left(\omega_{oI}\hat{I}_z + \omega_{oS}\hat{S}_z\right)\right\}$$

it is possible to transform both spin reservoirs such that they both lie along the same axis in the doubly rotating frame (by the choice of an appropriate phase correction factor). It is now possible to picture the two spin system as reservoirs of Zeeman energy which communicate through dipolar coupling. If the I spins are given a high degree of spin order (low spin temperature) and the S spins (infinite spin temperature initially) are brought into thermodynamic contact, then polarization transfer will occur until

thermal equilibrium has been reached. Equilibrium will be established at the most rapid rate when the Hartmann-Hahn condition[18] is satisfied such that;

$$\gamma_I B_{1I} = \gamma_S B_{1S}$$

The rate of polarization transfer is governed by the time constant T_{IS}, where;

$$(T_{IS})^{-1} = C_{IS} < \Delta\omega^2 >_{IS} < \Delta\omega^2 >_{II}^{-\frac{1}{2}}$$

$< \Delta\omega^2 >_{II}$ is the normal high-field truncated second moment and C_{IS} depends upon geometrical factors. The consequence of the form of T_{IS}, is that high rates of polarization transfer will occur when the {H-H} bandshape is narrow and the {P-H} bandshape is broad.

Having undergone cross-polarization the S spins have magnetisation of their own and can be observed directly. An enhancement in sensitivity proportional to the ratio of the γ's can be achieved over conventional SPE techniques. Clearly when potential reductions in pulse repetition times are also accounted for, the gains may be substantially greater. The selectivity of the CP technique results from the strong dependence of the heteronuclear dipolar interaction on the I, S internuclear distance.

REFERENCES

[1] J. Herzfeld and A. E. Berger,
J. Chem. Phys. 73, (1980), 6021.

[2] M. M. Maricq and J. S. Waugh,
J. Chem. Phys. 70, (1979), 3300.

[3] R. K. Harris,
"Nuclear Magnetic Resonance Spectroscopy",
Pitman Books Ltd., London (1983).

[4] U. Haeberlen
"High-resolution NMR in Solids: Selective Averaging"
Academic Press, New York (1976).

[5] E. R. Andrew, A Bradbury and R. G. Eades,
Nature, Lond., 182, (1958), 1659.

[6] E. R. Andrew, A Bradbury and R. G. Eades,
Nature, Lond., 183 (1959), 1802.

[7] I. J. Lowe,
Phys. Rev. Lett, 2, (1959), 285.

[8] E. R. Andrew and R. G. Eades,
Disc. Faraday Soc., 34, (1962), 38.

[9] E. R. Andrew
Phil. Trans. R. Soc. Lond., A299, (1981), 505.

[10] T. C. Farrar and E. D. Becker,
"Pulse and Fourier Transform NMR",
Academic Press, New York (1971).

[11] J. S. Waugh, L. M. Huber and U. Haeberlen
Phys. Rev. Lett., 20, (1968), 180.

[12] G. J. Nesbitt,
Ph.D. Thesis, University of Durham (1986)

[13] M. Mehring,
"High-Resolution NMR Spectroscopy in Solids: Basic Principles and Progress",
Springer, Berlin, 1976, VOL 11.

[14] P. Mansfield,
J. Phys., C4, (1971), 1444.
W. K. Rhim, D. D. Elleman and R. W. Vaughan,
J. Chem. Phys., 58, (1973), 1772.

[15] P. Jackson,
Ph.D. Thesis, University of Durham (1987).

[16] B. C. Gerstein and C. R. Dybowski,
"Transient Techniques in NMR of Solids: An Introduction to Theory and Practice"
Academic Press, New York (1971).

[17] A. Pines, M. Gibby and J. S. Waugh,
J. Chem. Phys., 59, (1973), 569.

[18] S. R. Hartmann and E. L. Hahn,
Phys. Rev., 128, (1962), 2042.

CHAPTER 3 - EXPERIMENTAL CONSIDERATIONS

3.1 Spectrometer System

The spectrometer system used for the majority of the investigations presented in this thesis was a Bruker CXP-200 equipped with a 4.7 Tesla wide-bore (89.5 mm) magnet. The spectrometer was dual-channel covering a wide range of operating frequencies, making multinuclear operation possible. The nuclei considered in this thesis are ^{1}H, ^{31}P and ^{79}Br. Their relevant properties are summarised in Table 3.1.

Table 3.1 : NMR Parameters of Relevant Nuclei

Nucleus	Spin	% Natural Abundance	Sensitivity (relative to protons)	Frequency /MHz
^{1}H	1/2	100	1.0	200.13
^{31}P	1/2	100	0.0665	81.014
^{79}Br	3/2	50.5	4.01 E-2	50.155

The details of the spectrometer construction are well known[1]. A number of probe systems were available for use with the spectrometer. Those relevant to the investigations presented in this thesis will each be considered in turn;

(a) ^{1}H high-power wide-line probe (Static Samples).

Capable of delivering 90^{O} pulse lengths ca. 1 μs, whilst offering very short pulse recovery times. The probe was used for the acquisition of wideline spectra and T_1 data. The sample (volume ca. 20 mm^3) was contained in cylindrical sample cavity in a glass tube with glass end stops.

(b) ^{1}H CRAMPS probe.

The construction and design of this probe has been described elsewhere[2]. It enables the sample to be irradiated with intense, highly homogeneous pulses, with rapid electronic recovery of the probe following the pulse, thus preventing the signal of interest being obscured by probe ring-down. These criteria must be satisfied if CRAMPS (combined rotation and multiple pulse spectroscopy) operation is to be successful. Samples were spun in "broomstick" style rotors which contained ca. 15 mm^3 of sample in a spherical cavity.

(c) Broadband high-resolution MAS probes.

For the study of ^{31}P there were two probes of this type available. The first was of the Andrew-Beams design, and was available throughout the duration of the studies presented in the thesis. Secondly, there became available a more modern probe of the double-bearing

design. This probe offered superior power handling and sample spinning characteristics. Consequently, wherever possible the double-bearing probe was used. However situations did arise where it was necessary to revert to using the Andrew-Beams probe, for example when only a small amount of sample was available. (The double-bearing spinning system required the sample rotor to be full and evenly packed in order to achieve stable spinning). The two types of spinning system used rotors of similar sample capacity (ca. 0.7 cm^3).

3.2 Pulse Sequences

A variety of pulse sequences have been applied to the samples investigated in this thesis and are summarised diagrammatically in Figure 3.1. In this section the pulse sequences will be reviewed, with brief comments upon their implementation.

The single-pulse and single-pulse-decoupled sequences Figure 3.1(a) and 3.1(b) were used both to acquire spectra and in the tune-up procedure for other sequences. A 90^{O} pulse excites nuclei of the resonance frequency of interest. The decay is then observed either with or without HPPD depending on the requirements of the experiment. These experiments yield signals which are quantitative provided that the delay between repetition of the pulse sequence is sufficient for the

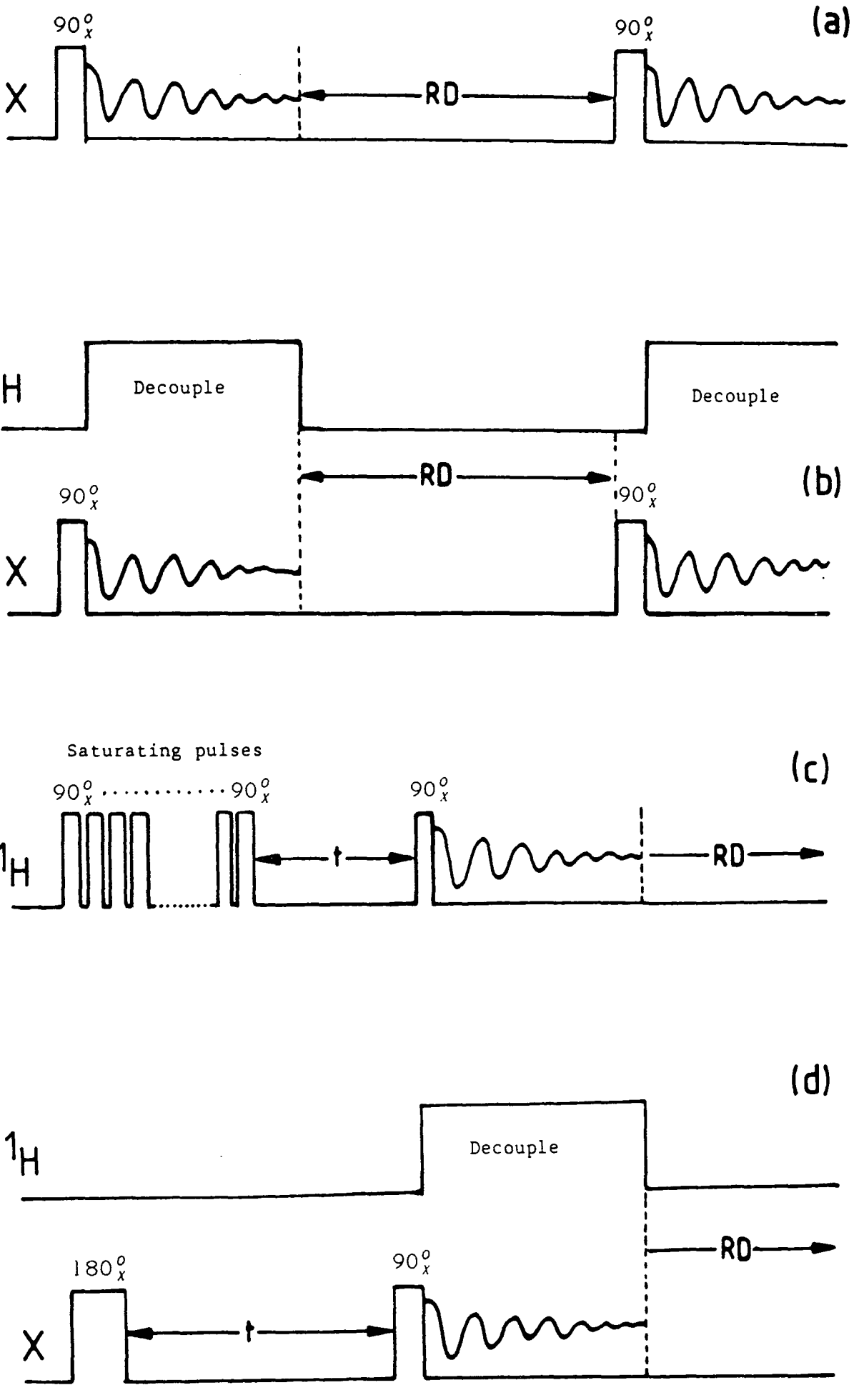
(a)
90°x
90°x
X
RD
(b)
1H
Decouple
Decouple
RD
90°x
90°x
X
(c)
Saturating pulses
90°x ..... 90°x
90°x
1H
t
RD
(d)
1H
Decouple
RD
180°x
90°x
X
t

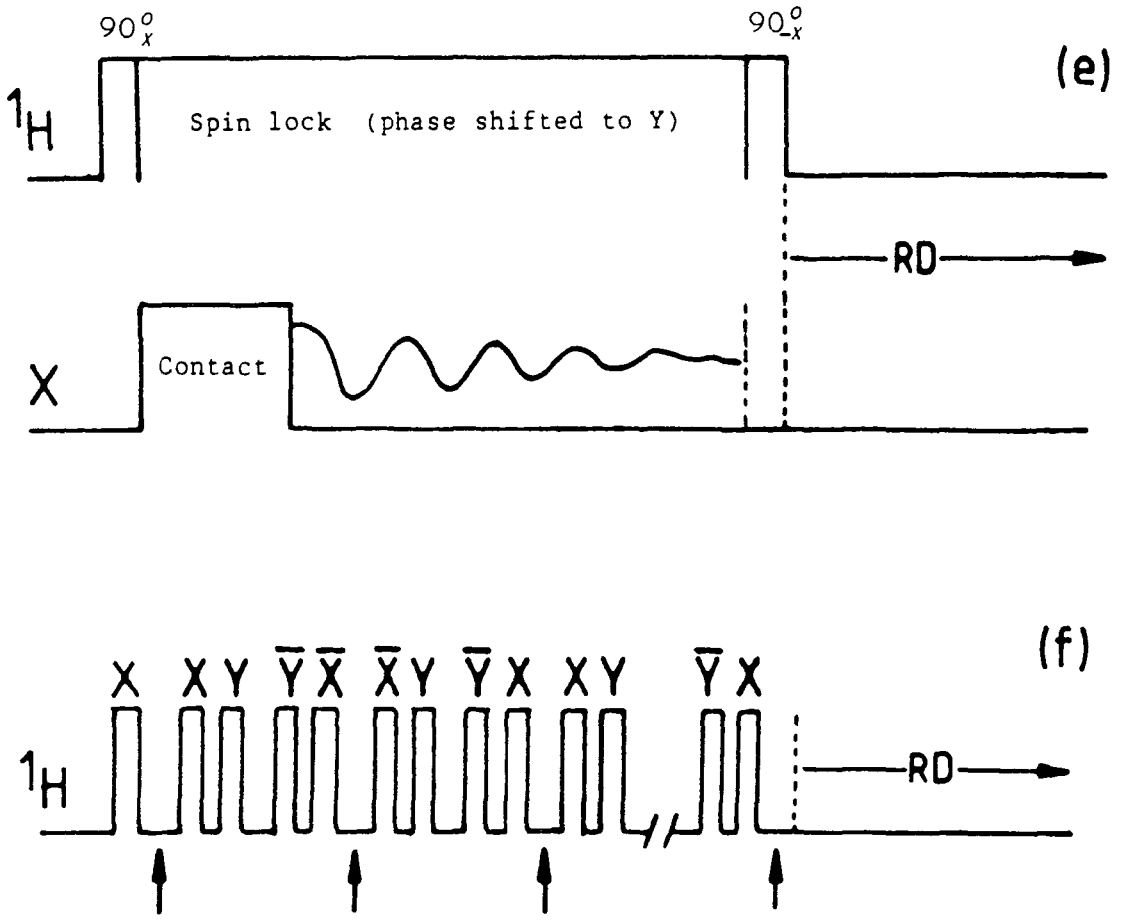

Figure 3.1 : Pulse sequences used in this study

(a) Single Pulse Excitation
(b) Single Pulse Excitation with High Power Proton Decoupling
(c) Saturation Recovery
(d) Inversion Recovery
(e) Cross-Polarization (Flip-back pulse included)
(f) MREV-8 (Sampling points indicated by arrows)

RD = Recycle Delay
t = Variable delay

NB : Diagrams are not to scale

nuclei to fully relax (relaxation measurements will be discussed later in this section). Mis-setting of the pulses has no effect other than to cause a lower signal intensity than can theoretically be achieved. All the pulse sequences detailed in this section benefited from accurate setting of the 90^{O} pulse duration. Sequences 3.1(a) and 3.1(b) could be used to achieve this by setting the excitation pulse duration to twice that required for a 90^{O} pulse. The relevant transmitter power output could then be adjusted from zero until a maximum in the signal intensity was obtained, and the power output could be increased further until the signal reached a minimum i.e. a 180^{O} null signal. Halving the excitation pulse duration back to its intended value gave rise to an accurate 90^{O} pulse length and hence maximum signal intensity.

Direct T_1 relaxation measurements were made using either the saturation-recovery sequence, Figure 3.1(c), or by inversion recovery with decoupled acquisition, Figure 3.1(d). The saturation-recovery sequence irradiates the sample with a series of 90^{O} pulses in rapid succession thus saturating the signal. There is then a delay before observation of the recovered signal. By acquiring data at increasing recovery delays the T_1 can be calculated. The inversion-recovery sequence, as its name suggests, inverts the magnetisation using a 180^{O} pulse and then allows the recovery to be monitored. A delay is allowed before application of a 90^{O}

read pulse followed by data acquisition whilst decoupling. Once again, from the recovery data the T_1 can be calculated. It is important to note that in the inversion-recovery sequence HPPD only takes place during the acquisition (the power handling characteristics of the probe and spectrometer electronics will not allow decoupling throughout the entire sequence). Consequently it should be appreciated that any relaxation effects resulting from heteronuclear interactions will contribute to the measured value of T_1.

The cross-polarization sequence, Figure 3.1(e) used spin-temperature inversion[3] and flip-back[4] to reduce instrumental artifacts and to reduce the recycle time respectively. Proton magnetisation is brought into the x-y plane using a 90^0 pulse, and this is immediately followed by a phase shift of 90^0 resulting in the protons being spin-locked in the y direction. Immediately following the phase shift on the ^1H channel, a "contact" pulse is applied on the phosphorus channel with the ratio of proton to ^{31}P power levels satisfying the Hartmann-Hahn matching condition[5]. At this stage magnetisation transfer takes place between the proton and phosphorus spin reservoirs. Upon equilibration of spin temperatures the contact pulse ends and data acquisition takes place whilst the protons remain spin-locked. The optimum contact time (which depends upon the rate of magnetization transfer between the spin reservoirs) for phosphorus in phosphate systems was found

almost universally to be ca. 1 ms. Beyond the optimum contact time the signal intensity observed is dependent on the ^{1}H $T_{1\rho}$ (the proton spin lattice relaxation time in the rotating frame). Thus the CP technique using variable contact times can be used to determine proton $T_{1\rho}$ values. All ^{31}P $T_{1\rho}$ values reported in this thesis were determined by this method.

The MREV-8 sequence 3.1(f) was used in the CRAMPS experiments and included a spin-temperature phase alternation step. The series of pulses of changing r.f. phase result in windows where the effect of the dipolar Hamiltonian on the magnetisation is zero whilst the magic-angle rotation removes shielding anisotropy effects. At each sampling window (indicated by arrows) a single data point is acquired. The cycle is repeated anything up to 4000 times per transient, resulting in a free induction decay which must be smoothed (as a consequence of sampling twice per cycle) before Fourier transformation is carried out. The frequency domain of the resulting spectrum will be scaled by a factor determined (in principle) by the multiple-pulse sequence used. For the MREV-8 sequence the theoretical scaling factor is $\sqrt{2}/3$ which corresponds to compression of the chemical shift by a factor of 2.1. The scaling factor was determined experimentally by co-addition of signals from the reference sample at a number of frequency offsets differing by 1.0 kHz. Fourier transformation of the resulting FID gave a spectrum of equally spaced signals (which should be 1 kHz apart) from which the

actual scaling factor could be determined, generally the value obtained was close to 0.5. The tune-up procedure for multiple-pulse operation requires very accurately set pulse phases and amplitudes. The method of spectrometer adjustment for CRAMPS operation has been documented in detail elsewhere[6]. In order to optimise the resolution achieved by this technique the irradiation frequency should be set close to the signal(s) of interest. Since the data are in non-quadrature form, the irradiation frequency has to be chosen carefully such that resolution is optimised, whilst folding back of the spectrum is avoided. Also it should be realised that if the irradiation frequency is to low frequency of the signals under observation the entire spectrum obtained will be reversed.

3.3 Tune-up samples and procedures

In order to make efficient use of the spectrometer, and to obtain reproducible, meaningful results it was necessary to set up the above mentioned pulse sequences accurately and consistently. Thus the same tune-up sample was used each time the spectrometer was used to perform a particular type of experiment. Brushite was chosen for all phosphorus tune-up procedures apart from the ^{31}P MREV-8 experiments presented later in this thesis. In dual-channel experiments the proton 90^{O} pulse duration was set using the proton signal from brushite itself. Typical 90^{O} pulse lengths were 5 μs (or less, if the double bearing-probe was used) giving an

effective proton decoupler power of 50 kHz. At a modest spinning speed (ca. 2.5 kHz) brushite should give a signal of linewidth less than 100 Hz provided that the sample achieved stable spinning , on angle, and that efficient HPPD is taking place. When accurately tuned, the SPE experiment should yield a signal in a single transient requiring 20 dB of receiver attenuation. For CP experiments the Hartmann-Hahn match was set by observing single transients and varying the low-frequency transmitter output to obtain maximum signal intensity. When optimised a single scan required 40 dB of receiver attenuation.

For CRAMPS experiments the sample used in the tune-up procedure was liquid H_2O sealed in a glass sphere. Having completed the tune-up procedure the efficiency of the MREV-8 sequence was assessed by observation of the proton signal from adamantane. The scaled linewidth obtained should be less than 50 Hz if the MREV-8 sequence is optimised.

3.4 Referencing

All phosphorus spectra were referenced with respect to 85% H_3PO_4 in aqueous solution ($\delta_P = 0 ppm$). The referencing procedure was however modified as work on this thesis progressed to provide a more accurate and convenient method. Initially, referencing was done by replacement of the sample rotor by a sealed vial containing 85% phosphoric acid. This method presented two problems. Firstly the sample vial was in contact with the coil, which could result in mis-alignment of

the coil resulting from rough probe handling, combined with the prospect of contamination being left behind on the coil subsequently resulting in severe arcing problems. Secondly, the resolution obtained from the liquid phosphoric acid was rather poor as a consequence of the sample being static rather than spun (as in conventional solution state studies). The former problem was overcome by carrying out referencing of all samples relative to spinning samples of solid brushite, which has a chemical shift of 1.2 ppm. with respect to phosphoric acid. However, the linewidth of brushite was ca. 100 Hz, resulting in still relatively poor resolution of the referencing procedure (bearing in mind the small differences in chemical shifts that we are aiming to detect). In later studies ammonium dihydrogen phosphate (ADP) was found to routinely give a linewidth of less than 35 Hz and a chemical shift of 0.8 ppm. with respect to phosphoric acid. Subsequently all samples were referenced relative to ADP and then the values converted to the phosphoric acid scale.

The ^{1}H CRAMPS technique was found to require very accurate referencing in order to yield reproducible chemical shifts. There was also the added complication of scaling of the chemical shift. The problems were overcome by internal referencing of the samples being run. This was done by adding two or three small crystals of adamantane to the sample compartment of the rotor following the acquisition of a spectrum without added adamantane. All the manipulation of

the data was carried out to give correctly scaled spectra. The adamantane signal was then referenced as +1.74 ppm. with respect to TMS. (N.B. The two signals from adamantane were not resolved.) From the adamantane reference the chemical shifts of the signals of interest could be measured and noted. The spectrum without added adamantane could then be plotted out with complete confidence in the chemical shift scale (without any of the signals of interest being obscured or distorted by the adamantane resonance).

Internal referencing for the ^{31}P CRAMPS experiments was not carried out since a suitable reference sample could not be found. Referencing was done by replacement of the sample rotor with one containing 85% H_3PO_4 and then a spectrum acquired at the frequency offset used for the sample of interest (N.B. Phosphoric acid was seen to attack Delrin sample rotors causing them to explode within a matter of minutes. Consequently KEL-F rotors were used.).

3.5 Rotor Angle Adjustment

In magic-angle spinning experiments accurate setting of the rotor angle is essential for optimum resolution (the consequences of rotor angle mis-set are considered in chapter 4). The rotor angle was set using the procedure outlined by Frye and Maciel [7]. The method relies on the maximisation of the spinning sideband pattern obtained for the ^{79}Br resonance in KBr. In practice, the extent of the spinning sideband

pattern in the transformed spectrum is evident from the form of the free induction decay (FID) itself. An extended spinning sideband pattern manifests itself as a series of "spikes" in the FID. Adjustment of the rotation angle is carried out until the "spikes" are seen to fill as much of the length of the FID as possible. This has been shown [7] to be accurate to within +/- 0.1^{O}. However, it is believed by the author that this method is accurate to better than +/- 0.05^{O}. The rotor-angle setting procedure was different for the two types of MAS probe. The Andrew-Beams probe required setting of the magic angle for every single sample studied and whenever the spinning speed was changed. This was done by including a few grains of KBr in addition to the sample itself in the rotor. If it was necessary for the sample to remain uncontaminated with KBr, PTFE tape was used to segregate the sample from the KBr. The probe was then placed in the magnet bore and the rotor spun. The spectrometer and probe were then retuned for observation of ^{79}Br. The desired spinning rate was selected and accurately determined from the spinning sideband pattern from the KBr. Having selected the desired rotation rate the angle setting procedure could commence. Owing to the very small quantity of KBr present it was necessary to accumulate at least 64 transients in order for the FID to be well defined above the noise level. This was not a major problem since a recycle delay of just 0.1 s between transients was sufficient.

Angle adjustment for the double-bearing probe was verified at the beginning and end of every spectrometer session. Provided the probe had not been removed from the magnet bore during the session, the rotor angle was noted to have remained constant regardless of the spinning rate used. Consequently angle setting/verification could be carried out using a rotor filled with KBr. All samples were spun in rotors free from KBr when the double bearing probe was used.

3.6 Tensor Component Determination

Tensor components for the various samples studied in this thesis were determined by one or both of the methods detailed below. Throughout this thesis the same conventions with regard to shielding tensor information have been followed. The convention chosen is as used by Haeberlen[8]. The isotropic shielding is given by;

$$\bar{\sigma} = \frac{1}{3} Tr \underline{\sigma} = \frac{1}{3}(\sigma_{11} + \sigma_{22} + \sigma_{33}) \qquad 3.1$$

The three tensor components are assigned as follows;

$$|\sigma_{33} - \bar{\sigma}| \geq |\sigma_{11} - \bar{\sigma}| \geq |\sigma_{22} - \bar{\sigma}| \qquad 3.2$$

The anisotropy and asymmetry are defined respectively as;

$$\delta = \sigma_{33} - \bar{\sigma} \qquad 3.3$$

and

$$\eta = \frac{(\sigma_{22} - \sigma_{11})}{\delta} \qquad 3.4$$

3.6.1 Moments Analysis of Spinning Spectra

This method of tensor component determination was proposed by Maricq and Waugh[9]. The technique relies on the determination of the second and third moments, where the m^{th} moment is given by;

$$M_m = \omega_r^m \sum_{N=N-}^{N+} \frac{N^m A_N}{\sum A_N} \qquad 3.5$$

A_N is the intensity of the N^{th} sideband and ω_r is the spinning rate expressed in Hz. The numbering scheme used corresponds to the centreband being taken as band zero and the sidebands to high frequency being numbered sequentially (increasingly positive). Likewise the bands to low frequency are numbered increasingly negative going further away from the centreband. The second and third moments can be expressed in terms of η and δ;

$$M_2 = \left(\frac{\delta^2}{15}\right)(3 + \eta^2) \qquad 3.6$$

$$M_3 = \left(\frac{2\delta^3}{35}\right)(1 - \eta^2) \qquad 3.7$$

From the above equations it is clear that solutions to the cubic equation in δ may be determined. The value of η is then calculated by substitution of the determined value of δ in one of the moments equations. From the values of η and δ the shielding tensor components can be determined using the relations;

$$\sigma_{11} = \bar{\sigma} - \left(\frac{\delta}{2}\right)(1+\eta) \qquad 3.8$$

$$\sigma_{22} = \bar{\sigma} - \left(\frac{\delta}{2}\right)(1-\eta) \qquad 3.9$$

$$\sigma_{33} = (\bar{\sigma} + \delta) \qquad 3.10$$

It should be noted that there are three solutions to the equation and hence three possible sets of tensor components. Each set of components corresponds to a possible permutation of the σ values. The correct set of σ values were selected bearing in mind the convention $|\sigma_{33} - \bar{\sigma}| \geq |\sigma_{11} - \bar{\sigma}| \geq |\sigma_{22} - \bar{\sigma}|$. A simple BASIC program was written to carry out the calculations when given the chemical shift, spinning rate and the band intensities.

When using this method of tensor component determination it is important to include all sideband intensities, especially the weak high-order sidebands. The sensitivity of this method to the high-order sideband intensities is evident from equation 3.5 where there is a weighting factor N^m, where

N is the sideband number and m the moment. Clearly this factor will have a significant effect, especially in the determination of the third moment. The effect of neglecting weak, high-order spinning sidebands from the analysis has been considered by Clayden et. al.[10]. In order to minimise errors, excellent signal-to-noise is required to ensure all sidebands are evident above the noise level. A good level of signal-to-noise was relatively easily achieved for the majority of the spectra presented in this thesis. Intensities were generally measured using peak heights rather than integration. This method is fully acceptable provided that there is very stable rotor spinning (and consequently an identical lineshape for the centreband and sidebands alike). Any variation in spinning rate would manifest itself as a broadening of spinning sidebands whilst the centreband linewidth remains unchanged. If this situation arose it would be necessary to integrate the intensities rather than use peak heights.

An alternative method does exist, and was proposed by Herzfeld and Berger[11]. The method is a little less critical in terms of the number of spinning sidebands required in order to determine values for the shielding tensor components. A graphical method is used, where in principle, just two spinning sidebands are needed in order to define a unique crossing corresponding to a particular set of shielding tensor components. The method of moments was favoured by the author

since it was found to be rather easier to implement and all solutions were unambiguous. Hence the graphical method has not been used for the results presented in this thesis.

3.6.2 Fitting of Static Spectra.

Tensor components can also be determined from static spectra by fitting to a calculated bandshape. Diagrams indicating the form of axially symmetric and non-symmetric shielding tensor patterns are given in Figure 3.2. In the axially symmetric case σ_{11} and σ_{22} coincide. Several computer programs have been written to perform the fitting operation [12,13]. A limitation of this method is that the spinning (high-resolution) spectrum should have only one signal, otherwise fitting of the static bandshape for several signals becomes rather complicated.

The program written by Groombridge[13] has been used for the results presented in this thesis. This program operates by assuming that broadening effects are superimposed over the unbroadened powder pattern. These broadening effects are assumed to be gaussian in nature and are thought to result from residual dipolar interactions, scalar coupling, bulk magnetic susceptibility effects and inhomogeneity in both B_0 and B_1 magnetic fields. The program numerically combines a gaussian function with the unbroadened powder pattern and then iterates over the tensor components and the width of the

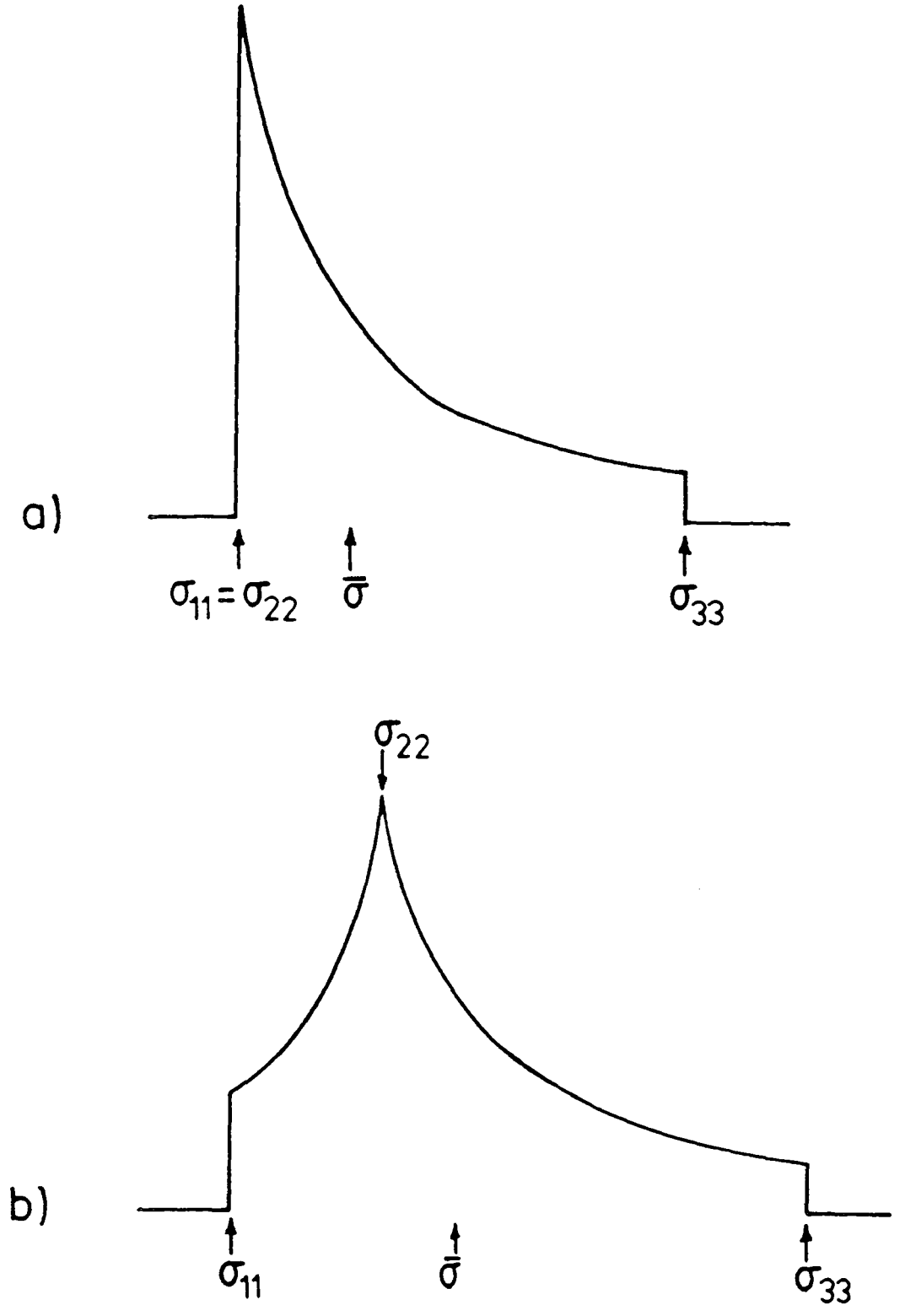

Figure 3.2 : Representation of characteristic shielding tensor patterns

(a) Axially symmetric
(b) General non-symmetric

gaussian function. A simplex fitting routine is used. The fitted spectrum can then be visually inspected and the quality of fit assessed. Often it was necessary to modify the guessed values of the gaussian broadening and the tensor components in order to get a good fit. Generally the fitted values for the first pass of the program were good initial guesses for the second run of the program, and so on. A typical fitted spectrum is shown in Figure 3.3.

3.7 Sample Sources

3.7.1 Model Phosphate Compounds

BDH Chemical Co. Ltd.:

$CaHPO_4$

$CaHPO_4.2H_2O$

$NaH_2PO_4.2H_2O$

$Na_2HPO_4.12H_2O$

NH_4NaHPO_4

KBr

Aldrich Chemical Co. Ltd.:

$NH_4H_2PO_4$

$(NH_4)_2HPO_4$

$(NH_4)_3PO_4$

$Na_4P_2O_7.10H_2O$

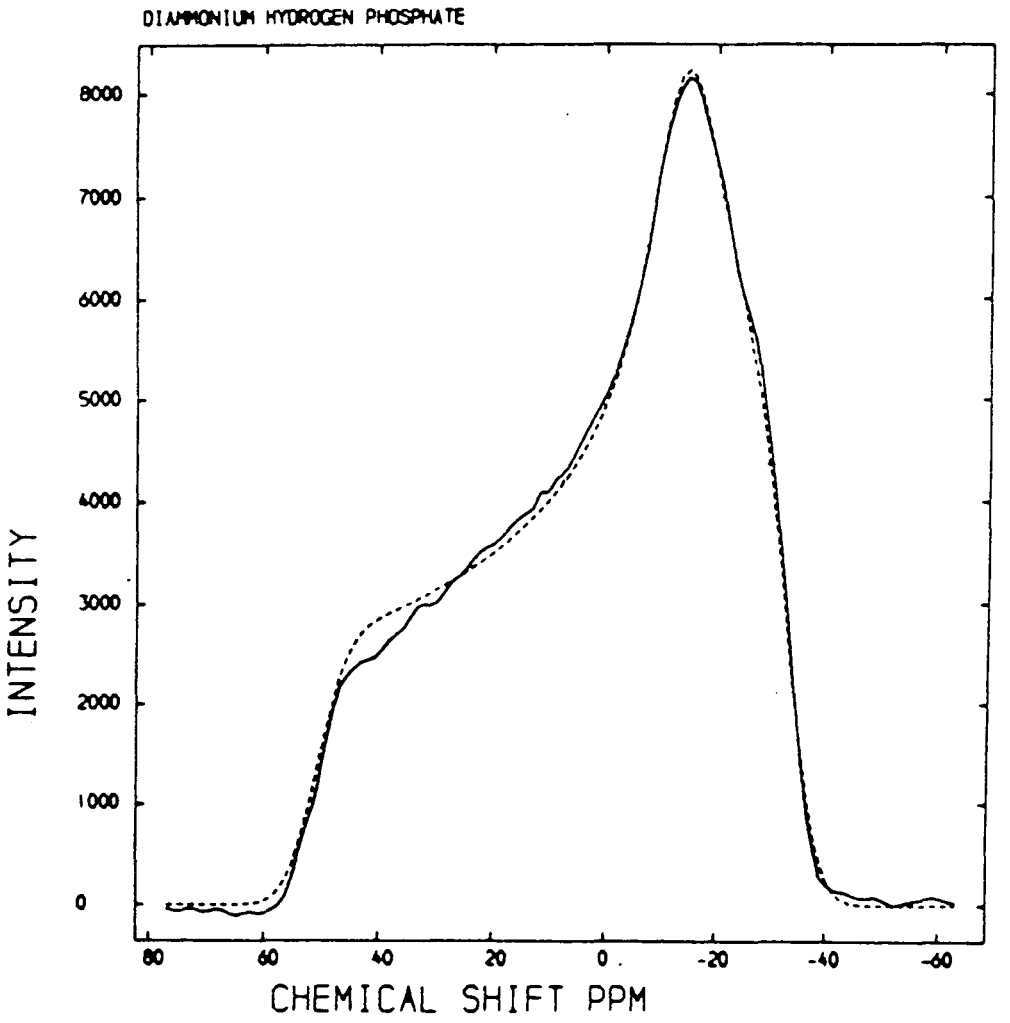

Figure 3.3 : Static powder pattern for $(NH_4)_2HPO_4$

Solid line ; Experimentally acquired spectrum

Dotted Line ; Best fit to experimental data using computer fitting routine

$Na_3PO_4.12H_2O$

Na_2HPO_4

$NaH_2PO_2.H_2O$

3.7.2 Amorphous Calcium Phosphate Samples.

The series of ACP compounds and samples of HAP were prepared and supplied by D. W. L. Hukins and J. E. Harries, Department of Medical Biophysics, University of Manchester. Details of the preparation of the ACP compounds are given in chapter 5.

3.7.3 Phosphorus-Sulphur Compounds.

The series of phosphorus-sulphur compounds were purified/synthesized and supplied by D. Woollins and P. Wood, Department of Chemistry, Imperial College, London.

REFERENCES

[1] Bruker Spectrospin Ltd.,
"Pulse NMR Spectrometer CXP Users Manual"

[2] G. J. Nesbitt,
Ph.D. Thesis, University of Durham (1986).

[3] E. O. Stejskal and J. Schaefar,
J. Magn. Reson. 18, (1975), 560.

[4] U. Haeberlen and N Tegenfeld,
J. Magn. Reson. 36, (1979), 453.

[5] S. R. Hartmann and E. L. Hahn,
Phys. Rev. 128, (1962), 2042.

[6] P. Jackson,
Ph.D. Thesis, University of Durham (1987).

[7] J. S. Frye and G. E. Maciel,
J. Magn. Reson. 48, (1982), 125.

[8] U. Haeberlen,
"High Resolution NMR in Solids", Academic Press
(1976).

[9] M. M. Maricq and J. S. Waugh,
J. Chem. Phys. 70, (1979), 3300.

[10] N. J. Clayden, C. M. Dobson, Lu-Yun Lian and D. J. Smith,
J. Magn. Reson. 69, (1986), 476.

[11] J. Herzfeld and A. E. Berger,
J. Chem. Phys. 73, (1980), 6021.

[12] P. D. Murphy and B. C. Gerstein,
"Analysis and computerised Fitting of the Lineshape of the NMR Powder Pattern", Iowa State University Report IS-4516 (1978).

[13] C. J. Groombridge,
Ph.D. Thesis, University of East Anglia (1983).

CHAPTER 4 - MODEL INORGANIC PHOSPHATES

4.1 Introduction

Phosphate systems in the solid state are of interest to a wide range of scientists including geochemists, biochemists, physical chemists and industry. The kind of phosphate systems encountered often occur in the form of mixtures or are otherwise unsuitable for X-ray investigation. Thus we require a technique which will enable us to study such systems non-destructively. Clearly solution-state NMR techniques are unsuitable because the materials often have poor solubility and because they do not give rise to distinctive phosphate units in solution.

High-resolution solid-state phosphorus-31 NMR has particular advantages over conventional structural techniques because of its versatility and the specialised information it can reveal. Firstly NMR monitors short range order : thus amorphous phases can be studied. Secondly multicomponent systems can be examined, and thirdly a range of NMR experiments are possible and can be used to selectively detect certain types of phosphate species.

In this chapter a number of solid-state NMR experiments will be evaluated, and in particular, their suitability for studies of phosphate-containing systems. Both wide-line and high-resolution techniques will be considered. Results will be presented for a selection of representative phosphates which are readily available in the laboratory.

The phosphate systems which are of interest in this study generally contain two readily observable NMR nuclei namely ^{1}H and ^{31}P. The following techniques will be considered here : ^{1}H and ^{31}P relaxation, ^{31}P SPE, CP, variable contact time and dipolar suppression experiments, and also ^{1}H wide-line spectra and ^{1}H CRAMPS. The compounds available for study are listed in Table 4.1.

4.2 Literature Survey

The systems considered in this chapter are orthophosphates (i.e. phosphates in which each oxygen atom is linked to only one phosphorus). Solid-state ^{31}P NMR studies of inorganic phosphates have covered two main areas to date, namely mineralised tissue (e.g. teeth and bone), and synthetic model compounds. The model compounds are often of interest in their own right. For example, sodium phosphates are a major constituent of washing powders, and are used as coatings for colour pigments.

In this survey, literature covering solid-state NMR studies of inorganic calcium phosphates will be discussed first, since they fall into the subject area of mineralised phosphates, and have been of particular interest in the work presented in this thesis. Secondly, publications

Table 4.1 : Phosphates Compounds Available for Study.

Compound	Chemical Formula	Abbreviation	Crystal structure reference number
Monetite	$CaHPO_4$	MON	1
Brushite	$CaHPO_4.2H_2O$	BRUS	2
Hydroxyapatite	$Ca_{10}(OH)_2(PO_4)_6$	HAP	3
Amorphous calcium phosphate	Unknown	ACP	---
Ammonium dihydrogen phosphate	$NH_4H_2PO_4$	ADP	4
Diammonium hydrogen phosphate	$(NH_4)_2HPO_4$	DAHP	5
Triammonium phosphate trihydrate	$(NH_4)_3PO_4.3H_2O$	TAP	6
Ammonium sodium hydrogen phosphate	$NH_4NaHPO_4.4H_2O$	----	7
Sodium pyrophosphate	$Na_4P_2O_7$	----	8
Trisodium phosphate dodecahydrate	$Na_3PO_4.12H_2O$	----	9
Disodium hydrogen phosphate	Na_2HPO_4	----	---
Disodium hydrogen phosphate dodecahydrate	$Na_2HPO_4.12H_2O$	----	10
Sodium dihydrogen phosphate dihydrate	$NaH_2PO_4.2H_2O$	----	11

associated with other inorganic phosphates will be reviewed; data for a selection of such compounds will be presented later in this chapter.

4.2.1 Inorganic Calcium Phosphates

Inorganic calcium phosphates have been studied using high-resolution solid-state ^{31}P NMR techniques by a number of workers[12-29]. Interest mainly concerns the formation, structure and maturation of calcium phosphates which are of importance in the study of biological systems such as mineralised tissues and milk solids.

Herzfeld *et al.* made use of magic-angle spinning and high-power proton decoupling techniques in the study of inhomogeneously broadened biological systems[12]. The phosphate systems considered were hydroxyapatite, brushite and bone. The choice of the two model phosphate compounds was governed by the results of earlier X-ray studies. Spinning sideband intensities in ^{31}P SPE/HPPD/MAS spectra indicated that high-density (mature) bone had a predominantly hydroxyapatite-like character whereas low density (young) bone was most like brushite. On the basis of this and other non-NMR evidence it was proposed that in the maturation of bone tissue, the first mineral phase deposited was brushite, and that on maturing brushite persists but the main phase present becomes hydroxyapatite. Chemical shifts were difficult to measure accurately in the

bone samples because the resonances were broad. However a shift difference of 1.5 ppm was observed between low and high density bones. A similar shift difference between brushite and hydroxyapatite signals was also noted. Spectra of bone tissues at increasing stages of development were compared with spectra from various brushite/hydroxyapatite mixtures, enabling estimates of the brushite:hydroxyapatite ratios of the various bone samples to be made. In the case of the most mature sample, similar ^{31}P solid-state NMR spectra could be obtained from a carbonated HAP sample. Linewidths observed for the bone samples were noted to be significantly broader than for the synthetic calcium phosphates. This was thought to be due to a dispersion of chemical shifts resulting from a number of sources such as strains, impurities and lack of long-range order.

Rothwell, Waugh and Yesinowski made variable temperature measurements on a range of solid calcium phosphates[13]. It was noted that ^{31}P chemical shifts tended to move to low frequency upon protonation of the phosphate. The chemical shift anisotropy was found to be small for $(PO_4)^{3-}$ groups, but significantly larger for $(HPO_4)^{2-}$ and $(H_2PO_4)^-$ groups, as would be expected. Low temperature measurements (-165^oC) on octacalcium phosphate $Ca_8H_2(PO_4)_6.5H_2O$ showed an apparent increase in the shielding anisotropy of the $(HPO_4)^{2-}$ groups suggesting that some atomic or molecular motion had been frozen out.

Spectra of a number of non-stoichiometric hydroxyapatites (Ca:P < 1.67) showed little difference to the ^{31}P spectra of stoichiometric HAP (Ca:P = 1.67). It was therefore proposed that the non-stoichiometry of the samples did not result from the presence of additional compounds with Ca:P ratios of less than 1.67. Instead a scheme involving Ca^{2+} vacancies in a HAP lattice with an accompanying loss of OH^- ions and addition of protons seemed most consistent with the NMR data. Low temperature spectra (-187^{o}C) for the non-stoichiometric hydroxyapatites again gave some evidence for the freezing out of molecular motion. Phosphorus-31 solid-state NMR of dental enamel were also discussed and shown to resemble that for HAP at room temperature, however at low temperature significant enhancement of the spinning sideband intensity indicated the presence of protonated phosphate units. Phosphorus relaxation times were reported to be approximately 90 s for dental enamel and ranging between 1 and 22 s in the synthetic hydroxyapatite samples.

Williams, Giles and Posner[14] obtained and compared high-resolution solid-state ^{31}P NMR spectra of a soil and several phosphate species. The spectra acquired indicated that the phosphate present in the soil sample was certainly not in the form of $AlPO_4$. The soil phosphate was thought to be quite closely related to hydroxyapatite although the spinning sideband intensities were somewhat different for HAP.

Yesinowski reported the acquisition of high-resolution ^{31}P NMR spectra from solids in colloidal suspensions[15]. This technique eliminated the need for MAS in order to obtain a high resolution ^{31}P spectrum of solid hydroxyapatite. The resonance attributed to HAP occurred at 2.8 ppm with a linewidth of 36 Hz. It was noted that the HAP linewidth was not solely due to magnetic field inhomogeneity since a solution phosphate resonance observed in the spectrum was considerably narrower. Later work (Yesinowski and Benedict) used a similar method to monitor the precipitation of $CaHPO_4.2H_2O$ via ^{31}P NMR[16].

Tropp *et al.*[17] carried out a detailed study of amorphous calcium phosphate. Both CP and SPE experiments were performed at temperatures between 25 and -120^{o}C. ACP was reported to have the same chemical shift as HAP. With CP the spinning sidebands of ACP were noted to be more intense than for HAP but weaker than those of either brushite or monetite. SPE spectra of HAP/dibasic calcium phosphate mixtures were shown to mimic the spectra of ACP quite well when appropriate proportions of each were chosen. However, CP experiments showed a differential enhancement of sideband intensities, in contrast to results for experiments on ACP which gave identical CP and SPE spectra over the temperature range 25 to -120^{o}C. Vacuum drying of the ACP at 450^{o}C was used to remove tightly bound water. The sideband intensities in the SPE spectrum of ACP were

undiminished, but it was no longer possible to obtain a CP signal. It was suggested that tightly bound water was probably not of intrinsic importance in the structure of ACP. Heat treatment of HAP did not affect the CP signal. It was concluded that ACP is a unique calcium phosphate compound with the observed sidebands being due to structural distortion of unprotonated phosphate units rather than a mixture of protonated and unprotonated phosphates.

An extensive study of the solid-state phosphorus-31 NMR of phosphate systems was made by Cox[18]. Chemical shift, linewidth and shielding tensor data were presented for a wide range of inorganic phosphate systems including calcium, sodium and ammonium phosphates. Biological systems such as milk solids, soil and seeds were also considered. It was found that model calcium phosphate compounds gave distinctive spectra, with spinning sidebands being indicative of protonated or non-protonated phosphate units. Spectra were in most cases rationalised in terms of known crystal structures. A substantial portion of the work considered the nature of phosphate within milk solids, in particular casein micelles. A number of samples were studied and although other techniques revealed little difference in the composition between the samples, ^{31}P NMR indicated clear differences in the phosphate environments present. At least two signals could be detected for each casein sample. Assignments were made indicating whether the

phosphate species present were organic or inorganic, and if inorganic, whether or not the species was protonated. Static proton spectra of selected phosphate species were also presented.

A pair of papers by Aue *et al.*[19] and Roufosse *et al.*[20] considered ^{31}P NMR of some synthetic calcium phosphates as potential models of bone mineral in the former and then went on to apply the results to a number of chick bone samples in the latter. The model compounds included crystalline HAP, carbonated HAP, ACP, monetite, brushite and octacalcium phosphate. Each sample was studied using SPE, CP, and dipolar dephasing experiments with two different decoupling window times of 0.5 and 1.0 ms. Standard spectra against which comparisons of the ^{31}P NMR data from bone samples could be made were obtained. The importance of carrying out a number of selective NMR experiments was emphasised since in systems with both an apatite phase and a protonated phosphate phase, the protonated species cross-polarized most efficiently and were more easily suppressed in a dipolar dephasing experiment. The investigation of bone mineral phases and comparison with the spectra of model compounds resulted in the proposal of a model structure for the major calcium phosphate phase in bone being hydroxyapatite containing ca. 5-10 % $(CO_3)^{2-}$ and ca. 5-10 % $(HPO_4)^{2-}$ groups in brushite-like configuration.

Like Herzfeld *et al.*[12] it was noted that $(HPO_4)^{2-}$ content was highest in the youngest bone and decreased progressively with increasing age of the specimen.

4.2.2 Other Inorganic Phosphates

Inorganic phosphates other than calcium phosphates have been studied using ^{31}P solid-state NMR in some detail in recent years. Published literature has concentrated on purely structural studies rather than applied work.

Andrew *et al.*[26] made use of magic-angle spinning ^{31}P NMR in the study of polycrystalline sodium triphosphate, $Na_5P_3O_{10}$. Two resonances were observed with approximate ratio 2:1. Theoretical chemical shifts for the two types of phosphorus atoms were calculated based on π-bond character for each type of phosphorus. The absolute values of the calculated chemical shifts showed poor agreement with the measured values. However, the difference between the values was reasonably close to that observed. Increased π-bonding to the terminal P atoms was thus used to account for the shift of one resonance with respect to the other. More recently, Burlinson *et al.*[22] have published refined NMR data for this compound. More accurate chemical shifts along with shielding tensor components for terminal and middle phosphorus nuclei were presented. Based on the assumption that the shielding tensor is a sum of tensors

associated with the individual P-O bonds in the $(P_3O_{10})^{5-}$ ion an approximate assignment of the principal components to specific directions in the ion were made.

Grimmer and Haubenreisser[23] carried out a detailed study of some potassium phosphates $P_2O_5.xK_2O$ $(0 \leq x \leq 3)$ using both static and magic angle spinning methods. These compounds had four basic structural units; PO_4 tetrahedra, PO_4 end groups, PO_4 middle groups and PO_4 branching groups. It was shown that the measured chemical shift and tensor data were sensitive to the kind of PO_4 group present. It was noted that ^{31}P chemical shifts move to low frequency on successive protonation for the potassium orthophosphates, in agreement with the earlier findings of Rothwell *et al.*[13] who observed the same trend for calcium orthophosphates.

Duncan and Douglass carried out ^{31}P solid-state NMR experiments with and without magic-angle spinning for a number of condensed phosphates[24]. In systems showing more than one resonance, static powder patterns were simulated using a summation of calculated powder patterns for each type of phosphorus present. The individual patterns were obtained using tensor components determined from analysis of spinning spectra. Calculated shielding tensor components were found to be of use as an unambiguous means of assigning resonances to either end, middle or branching phosphate groups.

Griffiths *et al.*[25] presented chemical shift and tensor data for a range of solid sodium ortho-, pyro-, poly- and meta-phosphates. The multiplicity of resonances indicated structural inequivalences in agreement with X-ray data. Again an overall trend in chemical shifts was noted, i.e. lower frequency with increased hydrogen levels. Exceptions to this trend were observed and it was suggested that a change in hydration state could be responsible. Observed linewidths were somewhat broader than expected. Also, linewidth measurements on anhydrous sodium pyrophosphate at different field strengths did not follow the ratio of observation frequencies. It was proposed that observed linewidths may in part be due to the second order effect of dipolar coupling to the sodium cation.

Clayden *et al.*[26] in a discussion of chemical shift tensor analyses and simulation of slow-spinning MAS and static spectra, carried out careful analysis of shielding tensors for sodium dihydrogen orthophosphate.

Turner *et al.*[27] obtained high-resolution NMR data for a variety of orthophosphates including some calcium, ammonium and sodium phosphates. Chemical shifts were shown to correlate reasonably well with electronegativity, Z/r and $z/\sqrt{r}$ where Z is the cation charge and r is the cation radius. It was also demonstrated that isotropic chemical shifts can be used to determine π-bond order around the

phosphorus atom. Shielding anisotropy was also related to P-O bond length and shown to correlate well with the average deviation of the O-P-O angle from the tetrahedral value.

Cheetham *et al.*[28] reported correlations between ^{31}P chemical shifts and summed bond strengths at the phosphate oxygen atoms for a range of inorganic phosphates. An example was given where the correlation could be used as a means of assigning the two ^{31}P resonances observed for α -$CaZn_2(PO_4)_2$.

Harris *et al.*[29] demonstrated how residual broadening in solid-state phosphorus-31 CP/MAS spectra could be reduced by the application of multiple pulse sequences of the MREV-8 type. Examples of increased resolution at modest spinning speeds and improved definition of static powder bandshapes were given for several inorganic phosphates. This work will be discussed and extended in chapter 6.

Having considered phosphorus NMR studies in some detail, a brief mention will be given to the high resolution NMR technique, ^{1}H CRAMPS[30-33]. A discussion of this technique is given in chapter 2. Scheler *et al.*[32] are the only workers who have published results for inorganic phosphates. Data were presented for $NH_4H_2PO_4$, $(NH_4)_2HPO_4$ and KH_2PO_4. In the case of the ammonium salts, ^{1}H CRAMPS was shown to effectively distinguish between NH_4^+ protons and P-OH protons. Protons in NH_4^+ appear in the region +6.7

to +7.8 ppm whereas P-OH protons were seen to give signals in the range +10.3 to +14.2 ppm because of hydrogen bonding. In the case of NH_4^+ protons, some of the residual linewidth is thought to be a consequence of unresolved heteronuclear ^1H-^{14}N coupling.

4.3 Results and Discussion

4.3.1 Relaxation Time Measurements.

Phosphorus T_1 and $T_{1\rho}$ measurements were made on a selection of phosphate samples at field strengths of 4.7 and 7.04 T. Spin-lattice relaxation (T_1) values were determined by direct observation of the nucleus of interest using the spin-inversion recovery method in the single pulse excitation mode. In contrast ^1H $T_{1\rho}$ measurements were obtained indirectly from plots of log{^{31}P signal intensity} against contact time. The methods used, are discussed more fully in chapter 3. In Table 4.2 a summary of the relaxation parameters obtained is given. Estimated errors in the last digit are shown in brackets. Typical fits to ^{31}P and ^1H T_1 data are illustrated in Figure 4.1, using brushite as an example. Phosphorus T_1 values are in all cases significantly longer than for protons, differing by

Table 4.2 : Phosphorus and proton relaxation time data for selected phosphate species.

Compound	T_1 / seconds[a]			^1H $T_{1\rho}$/ms
	$\lvert^{31}P$ (4.7 T)$\rvert$	$\lvert^{1}H$ (4.7 T)$\rvert$	$\lvert^{1}H$ (7.04 T)$\rvert$	(4.7 T)
$CaHPO_4$	3.8(1)	0.49(1)	0.50(4)	31(1)[b]
$CaHPO_4.2H_2O$	9.3(2)	0.48(1)	0.55(2)	3.6(1)
$Ca_{10}(OH)_2(PO_4)_6$	13.5(1)	0.63(1)	0.57(5)	--------
$NH_4H_2PO_4$	100.6(1)	0.63(1)	0.40(10)	86(1)
$(NH_4)HPO_4$	7.0(1)	0.20(1)	--------	8.7(1)
$NaH_2PO_4.2H_2O$	59(5)[c] 129(8)[d]	2.4(1)	--------	64(2)[e] 6.5(2)[e]
$NaHPO_4$	241(1)	58(1)	--------	16(1)
$NaHPO_4.12H_2O$	-----	0.68(2)	--------	---------
$NaNH_4HPO_4.4H_2O$	17.6(1)	0.17(1)	--------	12(1)

(a)Uncertainty in last digit shown in brackets
(b)Both signals gave the same $T_{1\rho}$ value
(c)Value for ^{31}P resonance at 1.9 ppm
(d)Value for ^{31}P resonance at 0.9 ppm
(e)Two $T_{1\rho}$ components were determined for this sample.

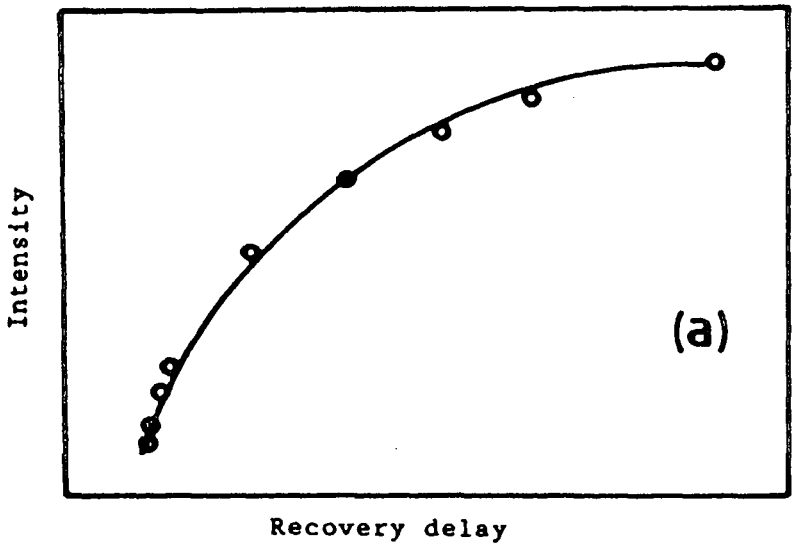

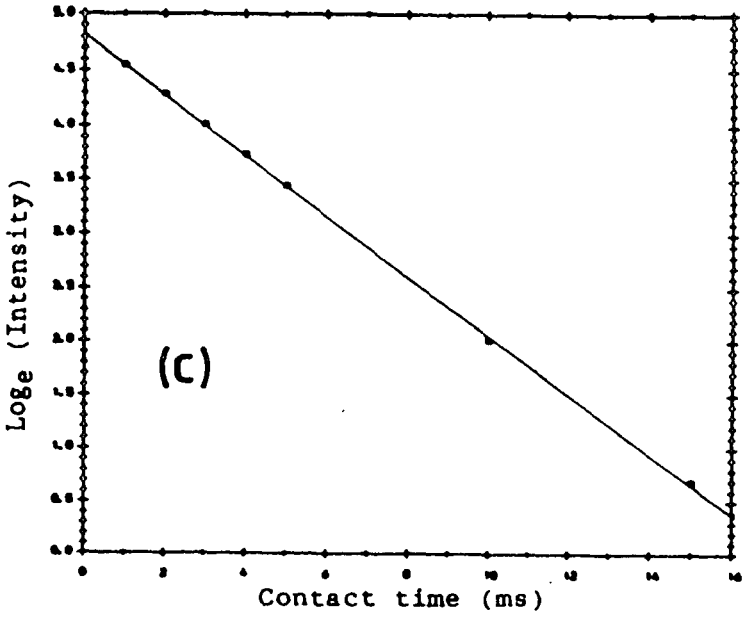

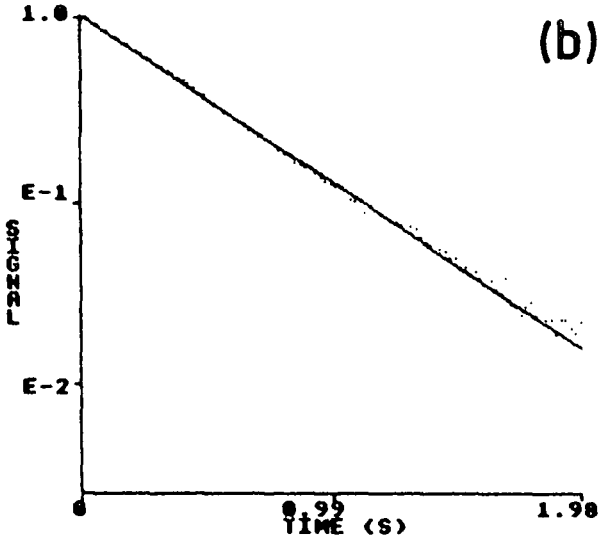

Figure 4.1 : Typical fits to ^{31}P and ^{1}H Relaxation Data for $CaHPO_4.2H_2O$

(a) ^{31}P T_1 data (Inversion recovery sequence with HPPD)
Fitted line produced by the CXP 200 software for T_1 determination.
Line Represents best fit to $Y = A - 2\exp(-T/T_1)$
where A = normalised intensity of largest point

(b) ^{1}H T_1 data (saturation recovery sequence)
Fitted line indicates single exponential behaviour
(multi-exponential data can be dealt with using the fitting routine)

(c) ^{1}H $T_{1\rho}$ data (via ^{31}P variable contact time experiment)

factors ranging from as small as 4.1 to as large as 160. Clearly this implies significant time savings can often be made by using cross-polarization rather than single pulse excitation. However, it is often important to perform both types of experiment on a sample in the first instance, in order to determine whether CP and SPE techniques give identical spectra, otherwise valuable information may be overlooked.

The measured $T_{1\rho}$ values (Table 4.2) cover a wide range from 3.6 ms to 86 ms. For the sample of $NaH_2PO_4.2H_2O$ studied, the two phosphorus signals showed somewhat different behaviour with CP contact time. Figure 4.2 illustrates the centreband for a range of contact times. The lower frequency resonance disappears more quickly with increasing contact time, reflecting the shorter $T_{1\rho}$ value for the protons from which the magnetisation of this signal is derived.

Clearly the contact time used in a CP experiment must be chosen correctly in order to make observation of all signals possible. Variable contact time experiments can be of particular value when multicomponent systems are studied. Careful choice of an appropriate contact time can enable enhancement or suppression of a particular spectral feature provided it has a suitable ^1H $T_{1\rho}$ value.

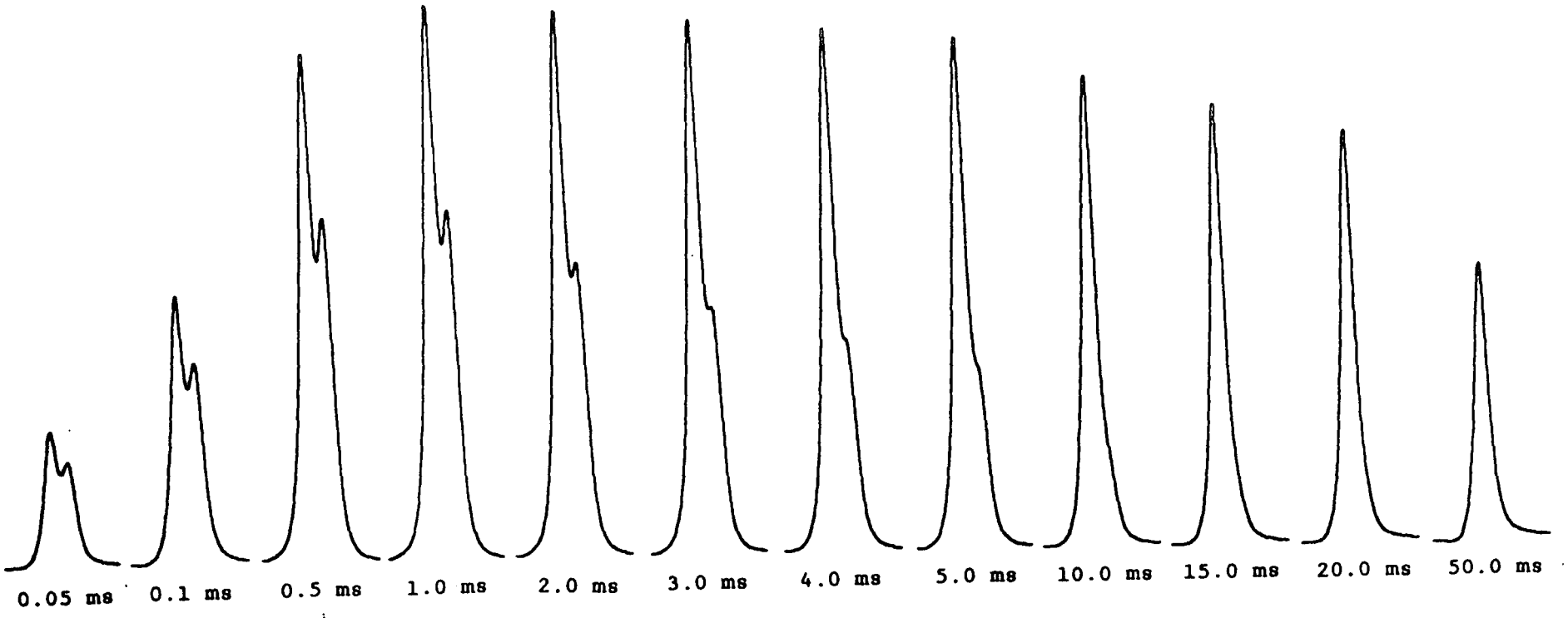

Figure 4.2 : $NaH_2PO_4.2H_2O$, CP variable contact time experiment.

Recycle delay = 20 s, spinning rate 4000 Hz, number of transients = 4
90^0 pulse duration = 4 μs
Centreband only shown. Contact time shown below each centreband.
Absolute intensity scaling.

The relaxation time data presented here are somewhat limited and are intended merely to give the reader a feel for typical relaxation parameters. Clearly a knowledge of such parameters is desirable in order to enable efficient use of spectrometer time, whilst offering further information to characterise phosphate species. Caution should, however, be exercised in the case of directly observed ^{1}H measurements, since one has to be certain that the signal observed is from the protons associated with the phosphate species of interest rather than moisture or impurities.

4.3.2 ^{31}P Cross-polarization and Single Pulse Excitation Spectra

The phosphate compounds considered here were of relatively low molecular weight. Thus in the majority of cases a useful signal could be obtained in a single transient, with up to 50 dB of receiver attenuation being required. In most cases identical spectra were obtained for both CP and SPE experiments. Chemical shift, linewidth and shielding tensor data measured from the spectra of a range of phosphate compound are presented in Table 4.3. As can be noted from Table 4.3, chemical shifts of the phosphate species studied cover a very narrow range (ca. 10 ppm) and in general are not unambiguously characteristic of a particular phosphate species. To add to this problem,

Table 4.3 : Chemical shift, linewidth and shielding tensor data for selected phosphate species.

Compound	δ_P /ppm	$\Delta\nu_{\frac{1}{2}}(min)$ /Hz (at 4.7 T)	Shielding tensor components (ppm)(a) σ_{11} σ_{22} σ_{33}
$CaHPO_4$	-1.7 0.2(b)	not resolved	42 6 -44
$CaHPO_4.2H_2O$	1.2	64	55 5 -64 (52) (2) (-64)
$Ca_{10}(OH)_2(PO_4)_6$	2.7	64	15 0 -23
ACP	2.8	550	not determined
$NH_4H_2PO_4$	0.8	34	-15 -10 22 (-18) (-8) (19)
$(NH_4)_2HPO_4$	1.1	43	36 11 -50 (33) (14) (-51)
$(NH_4)_3PO_4.3H_2O$	3.0 1.4(c) -0.2(c)	19 -- --	not determined
$NH_4NaHPO_4.4H_2O$	4.7	32	31 13 -58 (34) (18) (-62)
$Na_4P_2O_7$	-1.3 -2.8	not resolved	58 21 -70 58 21 -70
$Na_3PO_4.12H_2O$	7.1	68	isotropic
Na_2HPO_4	5.9	96	48 7 -73 (48) (13) (-81)
$Na_2HPO_4.12H_2O$	3.8	64	35 15 -62 (28) (19) (-70)
$NaH_2PO_4.2H_2O$	1.9 0.8(b)	not resolved	-76 -5 75 -50 -23 71

(a)Tensor components determined from static spectra given in brackets (if available)
(b)Shoulder
(c)Weak signal

different workers often report slightly different chemical shifts for a given sample. A comparison of chemical shift values with those of other workers is given in Table 4.4. The variation in reported values is probably a consequence of the reference sample and procedure used. Measured chemical shifts are generally self consistent, but owing to variation of the water content in a nominally 85% solution of phosphoric acid (the reference sample) there are often differences in the shift values relative to H_3PO_4 reported from laboratory to laboratory.

Linewidth data given are minimum values, since for a number of samples, variation of linewidth according to spinning rate was noted. Initially this was suspected to be due to rotor angle variation with spinning rate, but this possibility was ruled out. The double-bearing probe used for these measurements maintained a constant rotor angle throughout the entire spinning speed range. Figure 4.3 shows variable spinning speed data for hydroxyapatite, $NH_4H_2PO_4$, $NH_4NaHPO_4.4H_2O$ and $CaHPO_4.2H_2O$. Graphs 4.3(a) to 4.3(c) show very similar behaviour. Although the data points lie on a smooth curve, it was not possible to fit them to a simple exponential function for example. It would therefore appear that the relationship between linewidth and spinning rate is complex. However it is clear that little benefit would be gained for spinning rates in excess of 5 kHz. Brushite, Figure 4.3(d) shows a different kind of

Table 4.4 : Comparison of chemical shift data obtained in this study with values reported by other workers.

Compound	δ_P /ppm (This work)	δ_P /ppm (Ref 18)	δ_P /ppm (Ref 13)	δ_P /ppm (Ref 19)	δ_P /ppm (Ref 25)	δ_P /ppm (Ref 27)
$CaHPO_4$	-1.7 0.2	-1.8 -0.7	-1.5 0.0	-1.7 -0.3	----- -----	----- -----
$CaHPO_4.2H_2O$	1.2	1.0	1.7	1.4	-----	-----
$Ca_{10}(OH)_2(PO_4)_6$	2.7	2.3	2.8	2.8	-----	-----
ACP	2.8	2.6	-----	3.0	-----	-----
$NH_4H_2PO_4$	0.8	12.9 9.4 5.6	-----	-----	-----	0.9
$(NH_4)_2HPO_4$	1.1	-----	-----	-----	-----	1.5
$(NH_4)_3PO_4.3H_2O$	3.0 1.4 -0.2	----- ----- -----	----- ----- -----	----- ----- -----	----- ----- -----	----- ----- -----
$NH_4NaHPO_4.4H_2O$	4.7	-----	-----	-----	-----	5.1
$Na_4P_2O_7$	-1.3 -2.8	----- -----	----- -----	----- -----	2.9 1.3	----- -----
$Na_3PO_4.12H_2O$	6.9	-----	-----	6.9	7.8	-----
Na_2HPO_4	5.9	-0.2	-----	-----	-0.2	6.6
$Na_2HPO_4.12H_2O$	3.8	-----	-----	-----	-----	-----
$NaH_2PO_4.2H_2O$	1.9 0.8	0.4	----- -----	----- -----	----- -----	----- -----

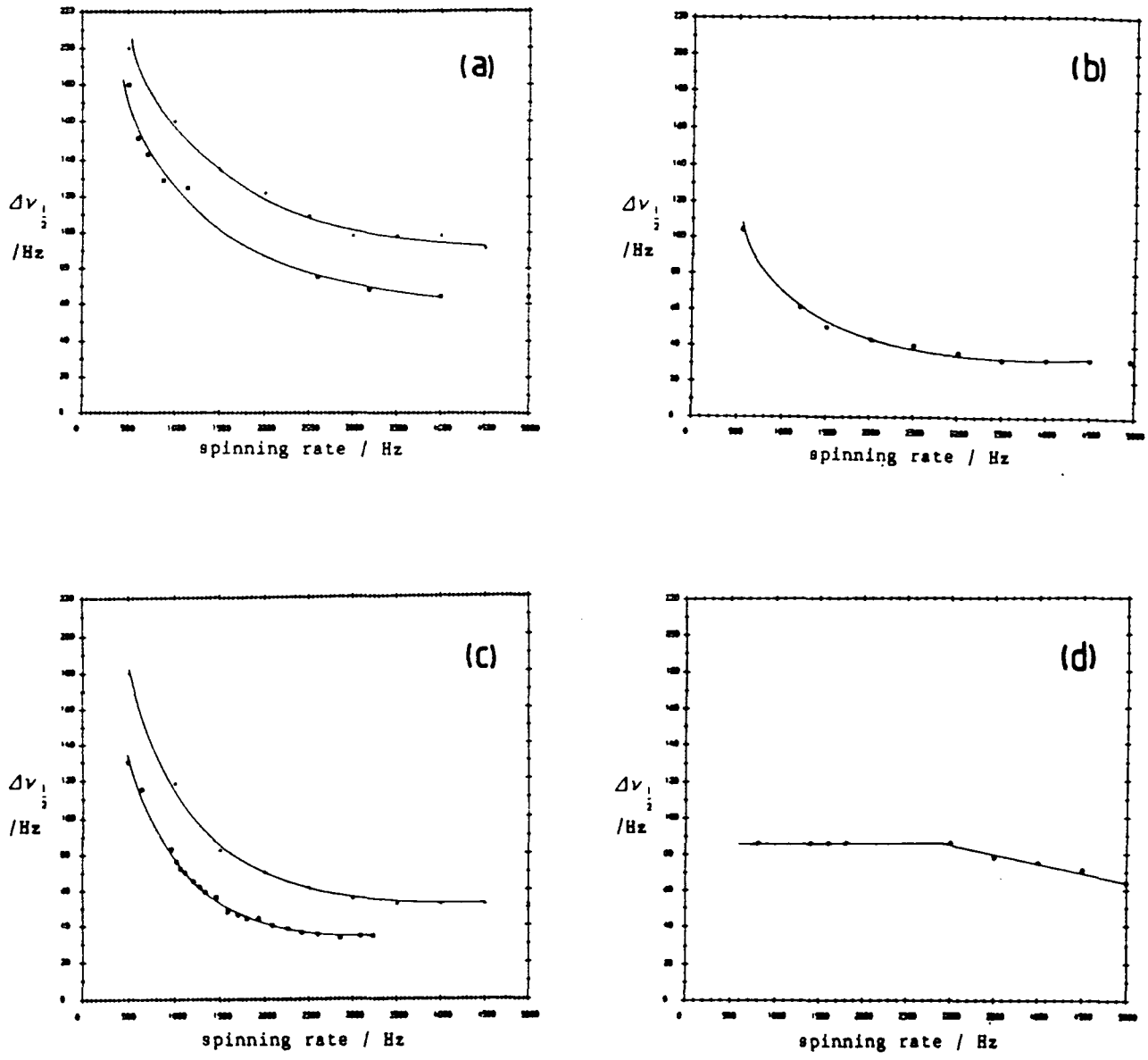

Figure 4.3 : Effect of spinning rate on linewidth for selected phosphates

(a) Hydroxyapatite (b) $NH_4NaHPO_4.4H_2O$

(c) $NH_4H_2PO_4$ (d) $CaHPO_4.2H_2O$

solid lines drawn to demonstrate trends in the data points

boxes ; 4.7 T crosses ; 7.04 T

behaviour with two apparently linear regions. It would appear that further narrowing would be possible if higher spinning rates were attainable. An example of spectral information being concealed at low spinning rates is illustrated in Figure 4.4 for sodium pyrophosphate. At low spinning rates a single resonance is observed, but on moving to a higher spinning rate a pair of resonances is resolved. The multiplicity of the resonances is consistent with the crystal structure[8] which indicates that the phosphorus nuclei in the pyrophosphate group are not equivalent. The exact origins of the line-broadening observed at lower spinning rates are not entirely clear, but will be discussed in more detail in chapter 6. It may be that {P-P} homonuclear broadening and/or molecular motion are factors of importance. It is also interesting to note that in the cases when data were acquired at both 4.7 T and 7.04 T the limiting linewidth was always greater in the high-field case, indicating that the residual interactions responsible for the minimum linewidth are field dependent. It is also interesting to note that the ratios of linewidths; 3.06:2 and 2.84:2 for HAP are close to the ratio of field strengths (3:2).

Shielding tensor components were extracted from the spectra using the method of Maricq and Waugh[34]. Wherever possible the values were refined by computer fitting of the static powder pattern (see chapter 3). Clearly, tensor

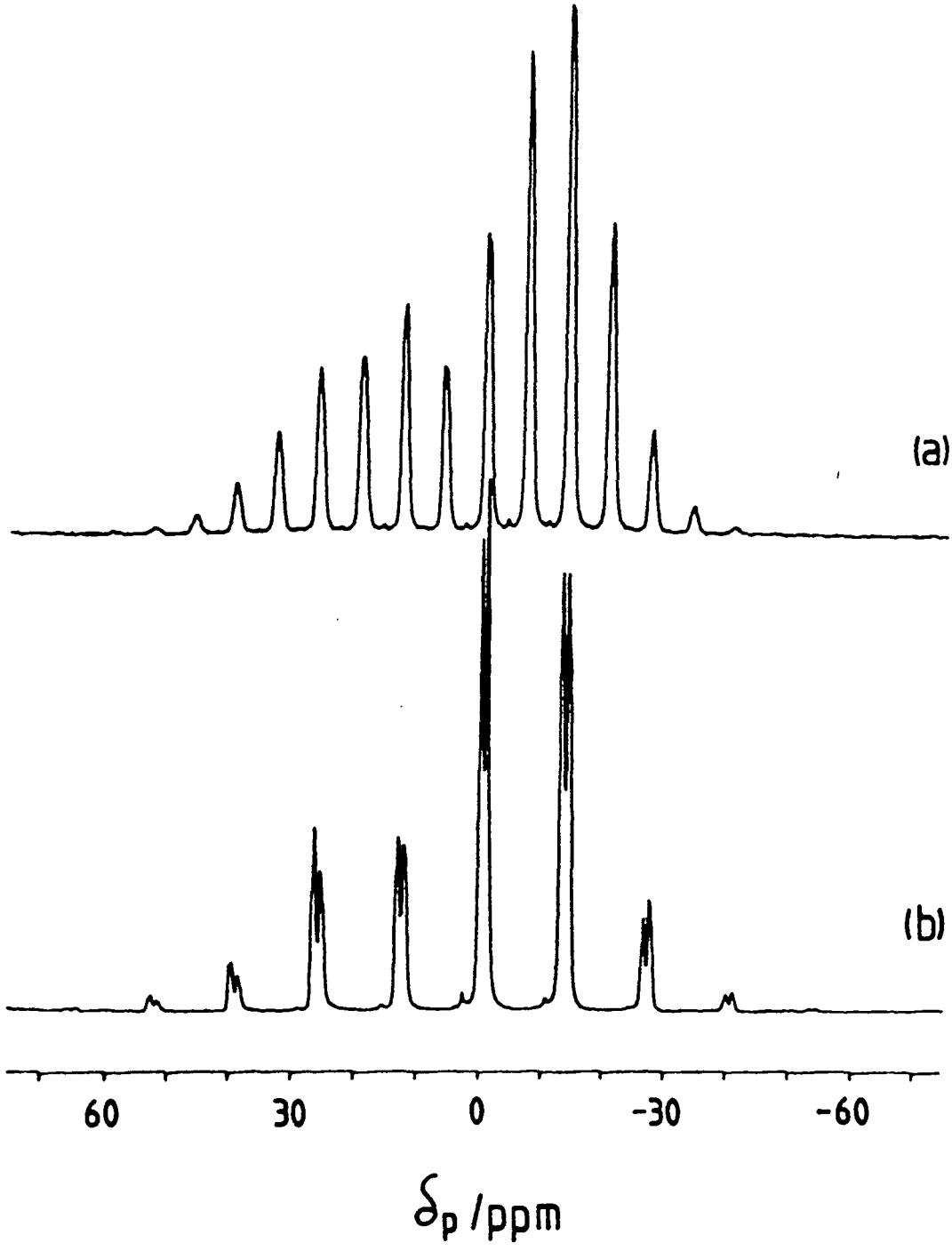

Figure 4.4 : $Na_4P_2O_7$ SPE spectra at two different spinning rates

Recycle delay = 10 s, Number of transients = 32,
90^0 pulse duration = 4 μs

(a) spinning rate = 1075 Hz (b) spinning rate = 2150 Hz

data obtained from static spectra are meaningful only when there is a single phosphate signal. Two additional parameters can be calculated from the shielding tensor component namely the asymmetry parameter η and the shielding anisotropy $\Delta\sigma$. The values of η and $\Delta\sigma$ are given by;

$$\eta = \frac{(\sigma_{22} - \sigma_{11})}{(\sigma_{33} - \bar{\sigma})}$$

$$\Delta\sigma = \sigma_{33} - \frac{\sigma_{11} + \sigma_{22}}{2}$$

with $|\sigma_{33} - \bar{\sigma}| > |\sigma_{11} - \bar{\sigma}| > |\sigma_{22} - \bar{\sigma}|$ and $\bar{\sigma} = \frac{1}{3}(\sigma_{11} + \sigma_{22} + \sigma_{33})$.

The shielding anisotropy reflects the symmetry of the electron cloud around the NMR nucleus of interest. The addition of a substituent to the symmetrical $(PO_4)^{3-}$ ion results ~~results~~ in a significant increase in the shielding anisotropy experienced by the phosphorus-31 nucleus. In the cases studied here the substituent of interest is always H^+. An example of the way in which shielding anisotropy is affected by the addition of H^+ is afforded by a comparison of the spectra of hydroxyapatite and brushite acquired under identical conditions, Figure 4.5. The $(PO_4)^{3-}$ ion in hydroxyapatite has a small anisotropy and shows a weak spinning sideband manifold. Brushite contains $(HPO_4)^{2-}$ units and shows an intense pattern. Thus an indication as to whether or not the phosphate units responsible for a particular signal are protonated or not, can often be

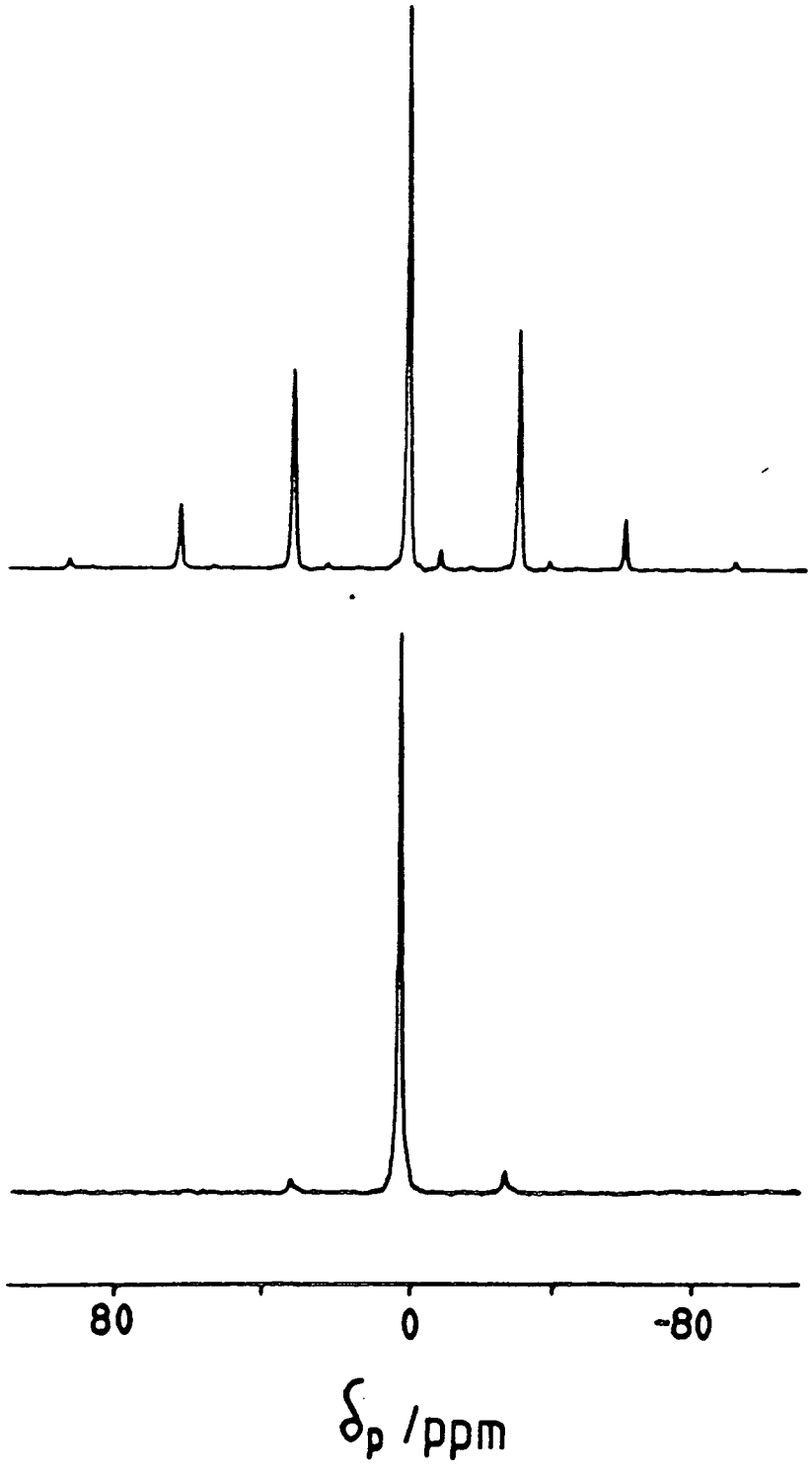

Figure 4.5 : SPE/HPPD spectra of Brushite (top) and hydroxyapatite (bottom) acquired under identical operating conditions.

Recycle delay = 30 s, 90^0 pulse duration = 3.5 μs,
spinning rate = 2.3 kHz, number of transients = 16.

obtained by simply looking at the intensity of the spinning sideband manifold. Sometimes the distinction between weak or strong sidebands is not clear cut. In these cases the $(PO_4)^{3-}$ units may either be significantly distorted and/or have weakened bonding to nearby protons.

Having considered the general features of the phosphorus NMR spectra obtained for a range of phosphate species, the spectra of each compound will now be considered in some detail. Wherever possible comparisons with the crystal structure will be made.

Monetite, $CaHPO_4$, gives essentially identical CP and SPE spectra with resonances being observed at 0.2 ppm and -1.7 ppm. The CP spectrum is shown in Figure 4.6(a). Both resonances have an intense spinning sideband pattern although the sidebands associated with the high frequency resonance are largely lost in the spinning sidebands of the low frequency resonance. The crystal structure[1] indicates space group $P\bar{1}$ with two types of phosphate unit in the asymmetric unit. The first type is covalently bonded to a single hydrogen. The other phosphate shares half each of two other types of proton. The fact that two signals are observed is consistent with the crystal structure, with each signal being due to a different phosphate type. At first sight the intensity ratio of the two resonances does not appear to be 1:1 until it is realised that the high frequency resonance is somewhat broader. The difference in

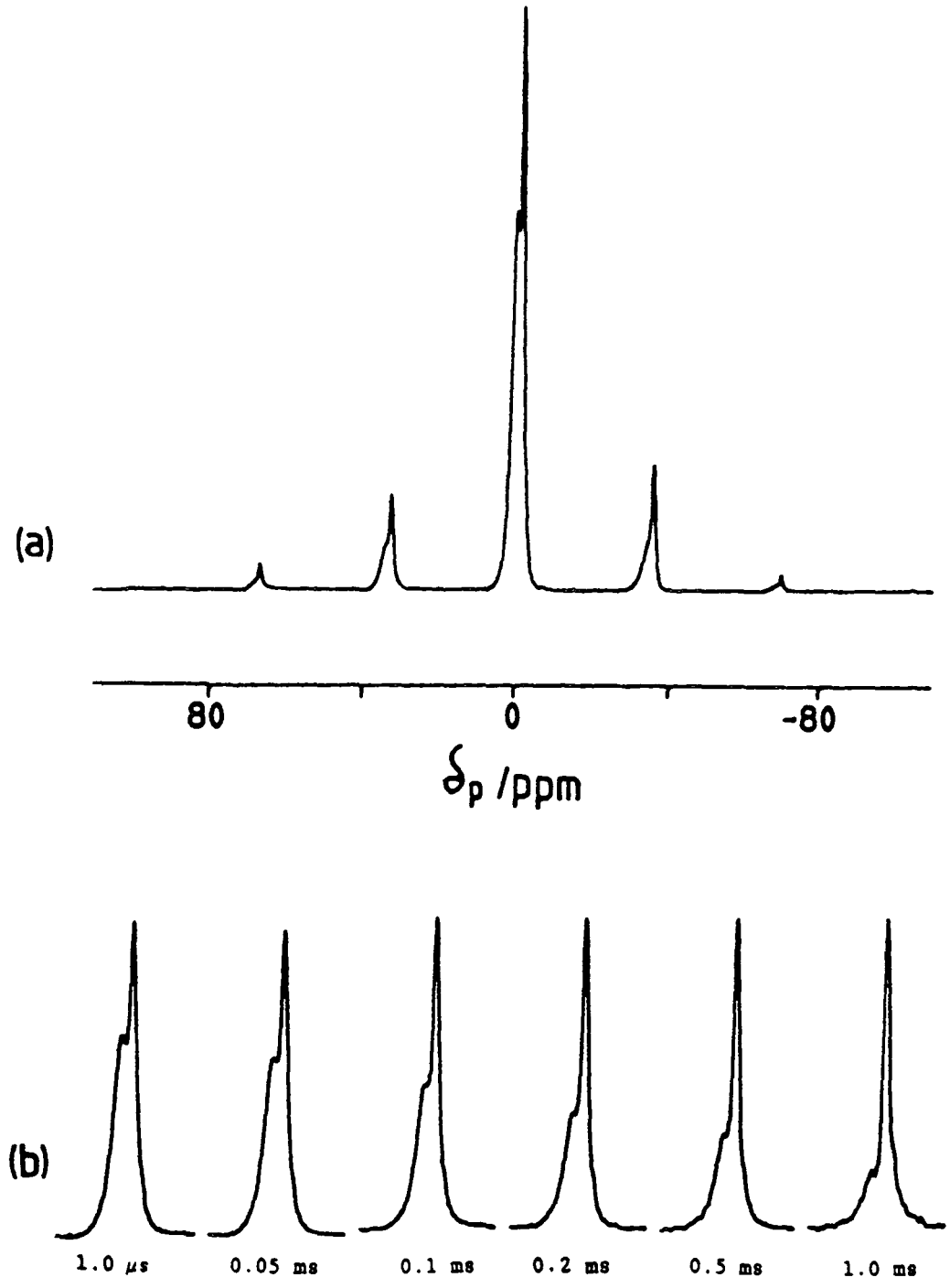

Figure 4.6 : $CaHPO_4$

(a) CP/MAS, contact time = 1 ms , number of transients = 16, 90^0 pulse duration = 5 μs, recycle delay = 10 s, spinning rate = 2300 Hz

(b) Dipolar suppression experiment, centrebands only shown. Decoupling window time indicated below each centreband other operating conditions as for Fig 4.6(a). All spectra scaled to same height.

linewidth for the two signals may be due to insufficient proton decoupling, and/or incomplete removal of {P-P} dipolar interactions. Molecular motion may also affect the relative widths of the signals observed. Confirmation of the inequivalence of the phosphate units being due to differences in bonding to protons was found by performing dipolar suppression experiments. Figure 4.6(b) shows a series of spectra for decoupling window times ranging between 1 μs and 1 ms. Clearly the high frequency resonance is suppressed the most easily indicating it is more closely coupled to protons.

Brushite, $CaHPO_4.2H_2O$, shows a single resonance at 1.2 ppm with a linewidth as narrow as 65 Hz being observed. The spectrum was consistent with the crystal structure[2] which indicates space group $I_a(C_h^6)$ with one phosphorus atom in the asymmetric unit. There is an intense spinning sideband pattern (recall Figure 4.5) owing to the presence of non-symmetrical $(HPO_4)^{2-}$ units. The shielding tensor is non-axial with principal components of 55 ppm, 5 ppm and -64 ppm.

Hydroxyapatite shows a single resonance at 2.7 ppm with a minimum attainable linewidth of 64 Hz. A poor cross-polarization efficiency was noted, with the CP signal being approximately 25 times weaker than the SPE signal. The two types of experiment gave essentially identical spectra. The cross-polarization efficiency reported by

different workers varies quite considerably although the chemical shifts and spinning sideband intensities show reasonable agreement. The variation of cross-polarization efficiency is probably as a result of varying moisture content as a consequence of different sample origins. The linewidth reported here is somewhat narrower than reported by Cox[18]. The difference can be attributed to the lower spinning speed used, 1.9 kHz vs. 4.0 kHz in this study. From Figure 4.3(a) it can be seen that at 1.9 kHz a linewidth of 95 Hz would be expected for HAP, which agrees well with the reported value of 100 Hz by Cox[18]. The crystal structure[3] reports space group $P6_3/m$, with half a phosphate group (as a consequence of the mirror plane) in the asymmetric unit. The single NMR signal observed for hydroxyapatite indicating one phosphate species is therefore in agreement with the crystal structure. Dipolar $\{^1H\text{-}^{31}P\}$ coupling is noted to be small, since , in the absence of HPPD the linewidth is just 143 Hz. This is further evidence of the remoteness of protons from the phosphate group. The observation of weak sidebands results from minor distortion of the $(PO_4)^{3-}$ group. The crystal structure indicates a variation in P-O bond lengths between 1.529 and 1.552 Å, and O-P-O bond angles between 111.3^O and 107.8^O.

Amorphous calcium phosphate has an unknown structure. It shows a single broad resonance at 2.8 ppm with weak spinning sidebands. Both CP and SPE experiments were

performed, with the amorphous nature of the sample being reflected in the linewidths of 550 and 530 Hz respectively. Detailed discussion of the structure and NMR spectra of ACP will be given in chapter 5.

A series of three ammonium phosphates was studied, namely $NH_4H_2PO_4$, $(NH_4)_2HPO_4$ and $(NH_4)_3PO_4.3H_2O$ Slow spinning spectra of the three compounds are illustrated in Figure 4.7.

$NH_4H_2PO_4$ gave the spectrum illustrated in Figure 4.7(a). A single resonance at 0.8 ppm was observed, a linewidth as narrow as 34 Hz was observed when spinning rates in excess of 3.0 kHz were used. The crystal structure[4] indicates space group $I\bar{4}2d$ with a single phosphate group in the asymmetric unit. From the empirical formula of ammonium dihydrogen phosphate, one would expect a high shielding anisotropy as a consequence of protonated phosphate units. However, the spinning sideband pattern in Figure 4.7(a) is rather weak (bearing in mind the slow spinning rate), thus casting some doubt over the extent of protonation. The crystal structure indicates that each hydrogen is equally shared between oxygens of different phosphate units, allowing half a proton per oxygen. This can be seen in the perspective view of the unit cell, as shown in Figure 4.8(a). The P-O bond lengths are all 1.537(1) Å and O-P-O angles are $111.17(4)^{O}$ in four cases and $108.63(4)^{O}$ in the remaining two. Thus the phosphorus nucleus is in a

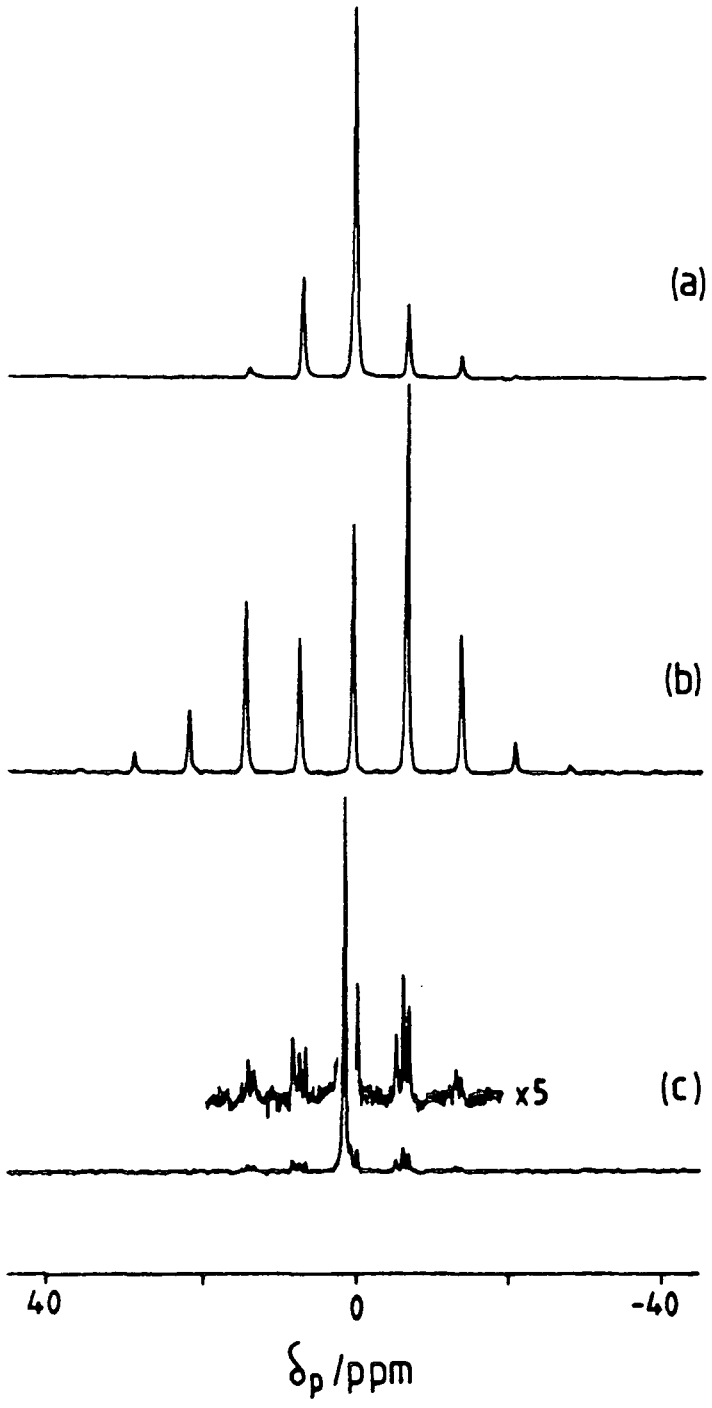

Figure 4.7 : ^{31}P CP/MAS spectra of $NH_4H_2PO_4$, $(NH_4)_2HPO_4$ and $(NH_4)_3PO_4.3H_2O$

Recycle delay = 10 s, contact time = 1 ms, spinning rate = 1100 Hz
90^0 pulse duration = 4 μs,

(a) $NH_4H_2PO_4$, number of transients = 80

(b) $(NH_4)HPO_4$, number of transients = 80

(c) $(NH_4)_3PO_4.3H_2O$, number of transients = 300

(Low capacity rotor used in order to achieve optimum resolution)

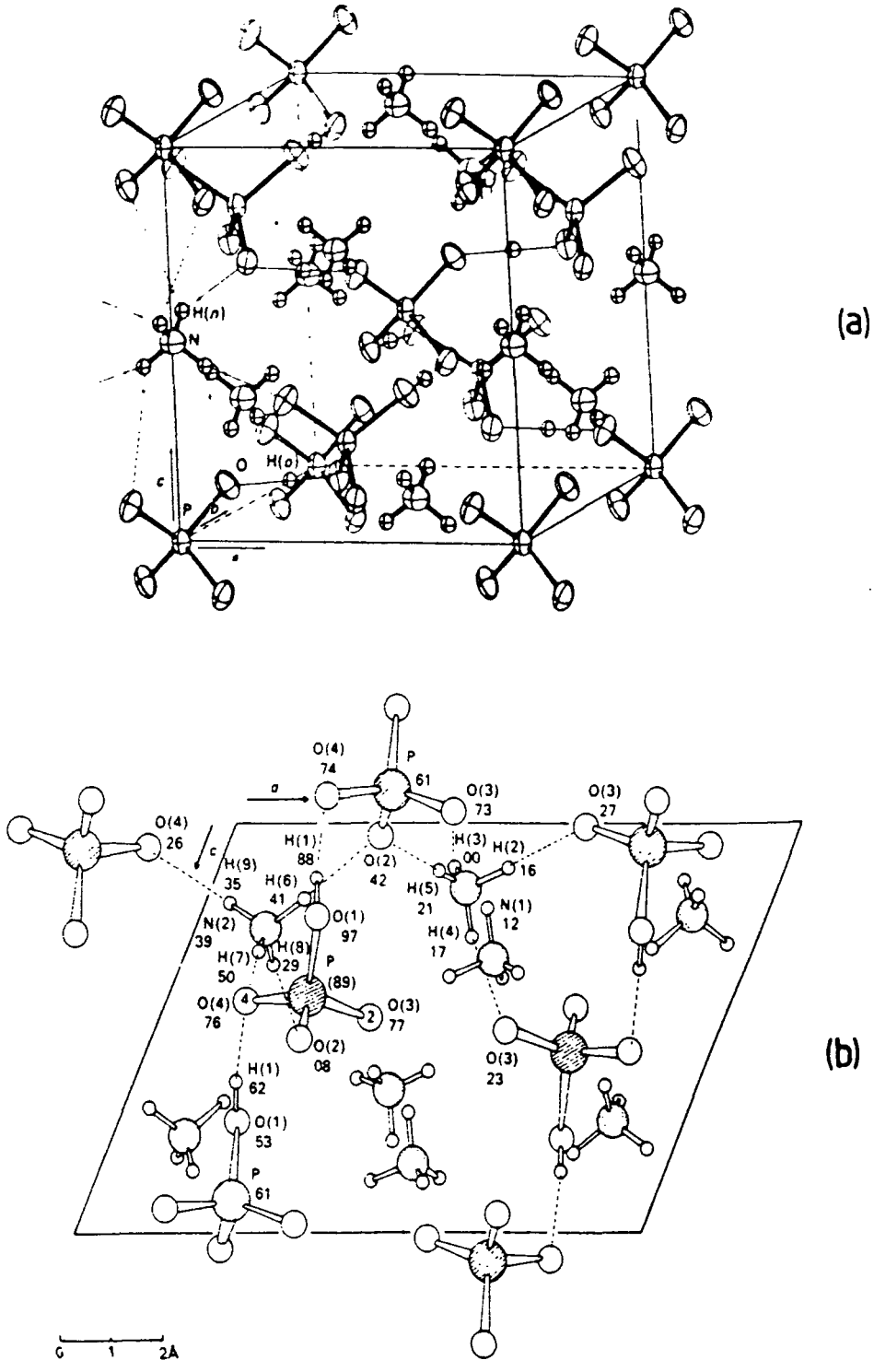

Figure 4.8 : Illustration of crystal structures of $NH_4H_2PO_4$ and $(NH_4)_2HPO_4$

(a) $NH_4H_2PO_4$: Perspective view taken from Ref. [4]

(b) $(NH_4)_2HPO_4$: Taken from Ref. [5]

surprisingly symmetrical environment with the shielding anisotropy of the phosphorus signal resulting from a relatively minor distortion of the bond angle rather than a substituent effect.

$(NH_4)_2HPO_4$ shows a single resonance at 1.1 ppm with a minimum linewidth of 43 Hz. The CP spectrum acquired at a spinning rate of 1.1 kHz is shown in Figure 4.7(b). The crystal structure[5] indicates space group $P2_1/c$ with P-O bond lengths ranging between 1.519 and 1.587 Å, and O-P-O bond angles between 103.61^O and 113.19^O. In contrast to ADP, a particular oxygen in each phosphate unit is clearly protonated (see Figure 4.8(b)). The protonation of the phosphate group is clearly responsible for the marked distortion of the phosphate units, which is reflected in the large shielding anisotropy responsible for the intense sideband pattern.

The spectrum acquired for triammonium phosphate trihydrate is illustrated in Figure 4.7(c). Three signals are observed. The most intense resonance occurs at 3.0 ppm and has very weak spinning sidebands. The two remaining signals are approximately a factor of sixteen weaker. They occur at 1.4 ppm and -0.2 ppm and show moderately intense sidebands. The crystal structure[6] indicates space group $P2_1/c$ with a single molecule in the asymmetric unit. Thus only a single resonance would be expected in the ^{31}P NMR spectrum. The three resonances can therefore only be

explained in terms of some level of decomposition of the compound having taken place. The sample had a damp appearance and smelt of ammonia. Of the three resonances it was not possible to identify which one was from $(NH_4)_3PO_4.3H_2O$. The crystal structure indicates that P-O bond lengths vary between 1.533 and 1.541 Å and O-P-O bond angles between 108.7^{O} and 110.1^{O}. These are only minor distortions of the $(PO_4)^{3-}$ group and thus it would seem likely that the phosphate signal of pure $(NH_4)_3PO_4.3H_2O$ would have a small shielding anisotropy. Thus the most intense resonance is the most likely candidate since it is almost isotropic whereas the low intensity resonances appear to have significant shielding anisotropy.

Static and spinning spectra of $NaNH_4HPO_4.4H_2O$ are shown in Figure 4.9. A single resonance is observed at 4.7 ppm with a linewidth as narrow as 32 Hz being attained. An intense spinning sideband pattern is found with the shielding tensor approaching axial symmetry. The crystal structure[7] indicates space group $P\bar{1}$ with one molecule in the asymmetric unit, which is consistent with the single ^{31}P resonance observed. The P-O bond lengths vary between 1.515 and 1.598 Å and O-P-O bond angles between 103.8^{O} and 112.8^{O}. The large variation of the bond lengths and angles indicates highly distorted phosphate units, which is in accordance with the large shielding anisotropy, $\Delta\sigma$, of 88

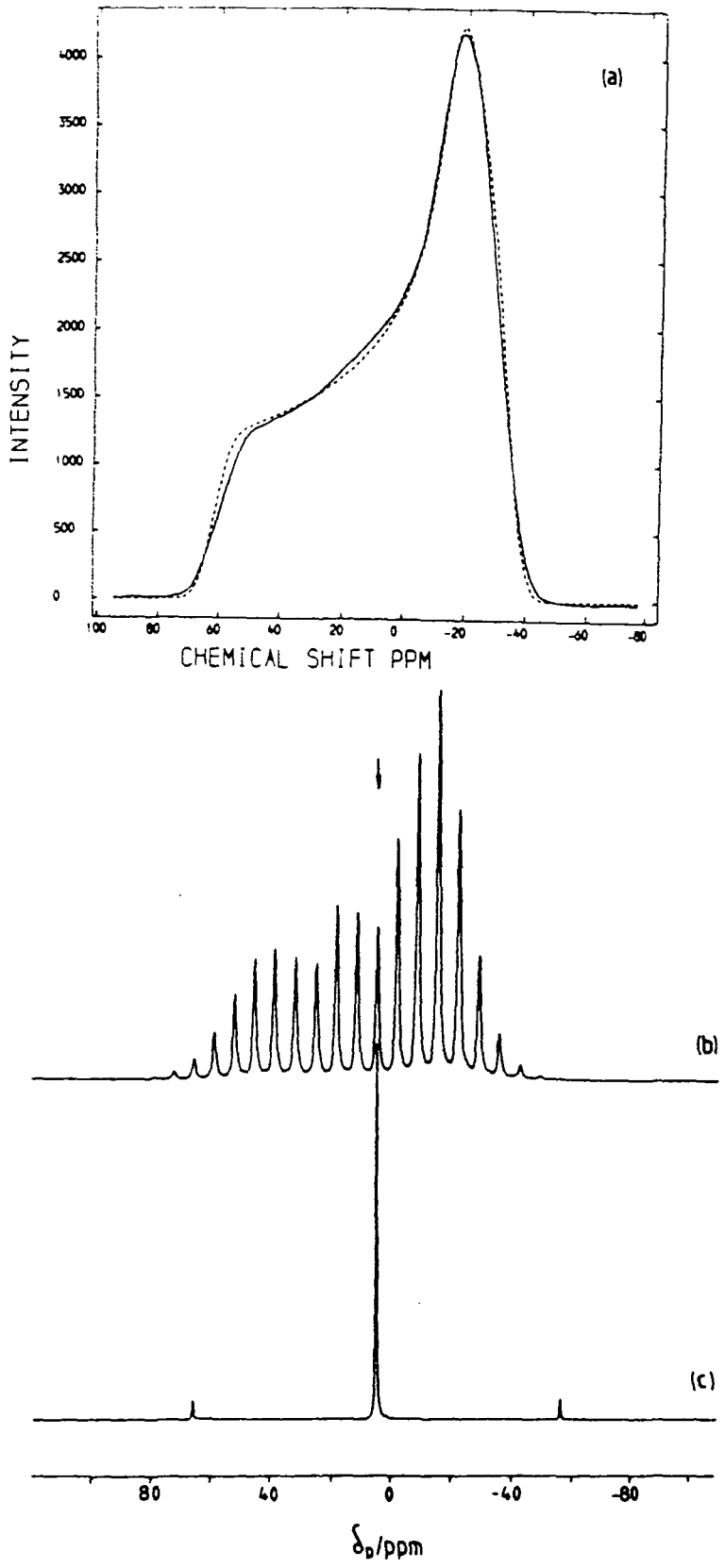

Figure 4.9 : ^{31}P CP Spectra of $NH_4NaHPO_4.4H_2O$
Recycle delay = 10 s, contact time = 1 ms,
90^0 pulse duration = 3.5 μs, Number of transients = 32
(a) Static. Solid line ; acquired spectrum, dotted line ; fitted
(b) MAS, spinning rate = 550 Hz (c) MAS, spinning rate = 4950 Hz

ppm. From the NMR spectra it is possible to conclude that the phosphate groups are protonated, rather than protons being shared (for example).

$Na_3PO_4.12H_2O$ gave a single resonance at 7.1 ppm with a linewidth of 68 Hz. The resonance was almost isotropic, with only very weak spinning sidebands. This compound should be more correctly known as $Na_3PO_4(NaOH)_{0-0.25}.12H_2O$, since it is not possible to obtain it without some sodium hydroxide being present. The crystal structure[9] indicates space group $P\bar{3}c1$ with a single molecule in the asymmetric unit. The P-O bond lengths range from 1.512 to 1.531 Å with O-P-O bond angles between 109.3^{O} and 109.6^{O}. Thus the phosphate units are hardly distorted, consistent with the virtually isotropic resonance observed.

Static and spinning ^{31}P NMR spectra of anhydrous Na_2HPO_4 are illustrated in Figure 4.10. The shielding tensor is highly anisotropic with $\Delta\sigma$= 111 ppm. The spinning spectrum gives a single resonance at 5.9 ppm with a linewidth of 96 Hz. There are no crystal data available for this compound. On the basis of the NMR data alone it can be proposed that there is a single phosphate group in the asymmetric unit, and that the phosphate groups are protonated.

The ^{31}P NMR static and spinning spectra of $Na_2HPO_4.12H_2O$ are illustrated in Figure 4.11. A single resonance at 3.8 ppm with a linewidth of 64 Hz was observed in the high

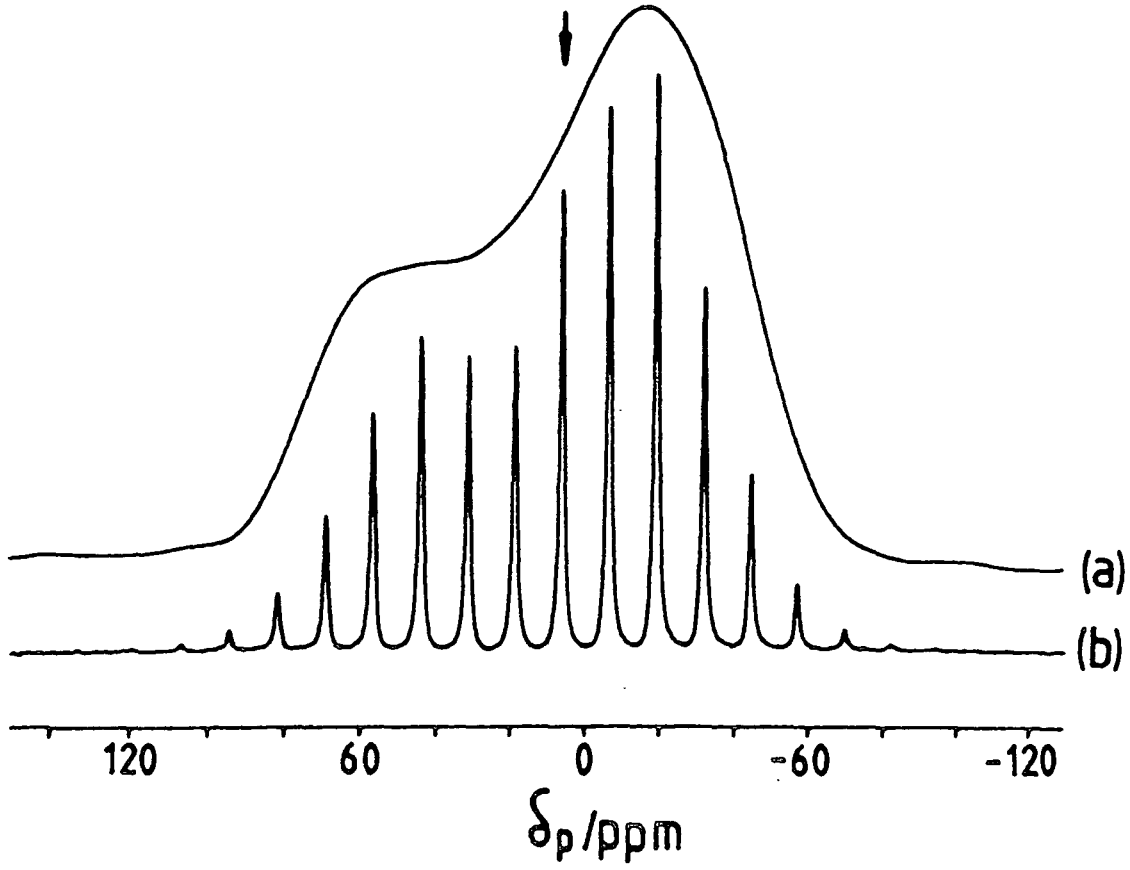

Figure 4.10 : ^{31}P CP Spectra of Na_2HPO_4 (anhydrous)
Recycle delay = 120 s, contact time = 1 ms
90^0 pulse duration = 3.5 μs, Number of transients = 24

(a) Static
(b) MAS, spinning rate = 1000 Hz
(Centreband indicated by arrow)

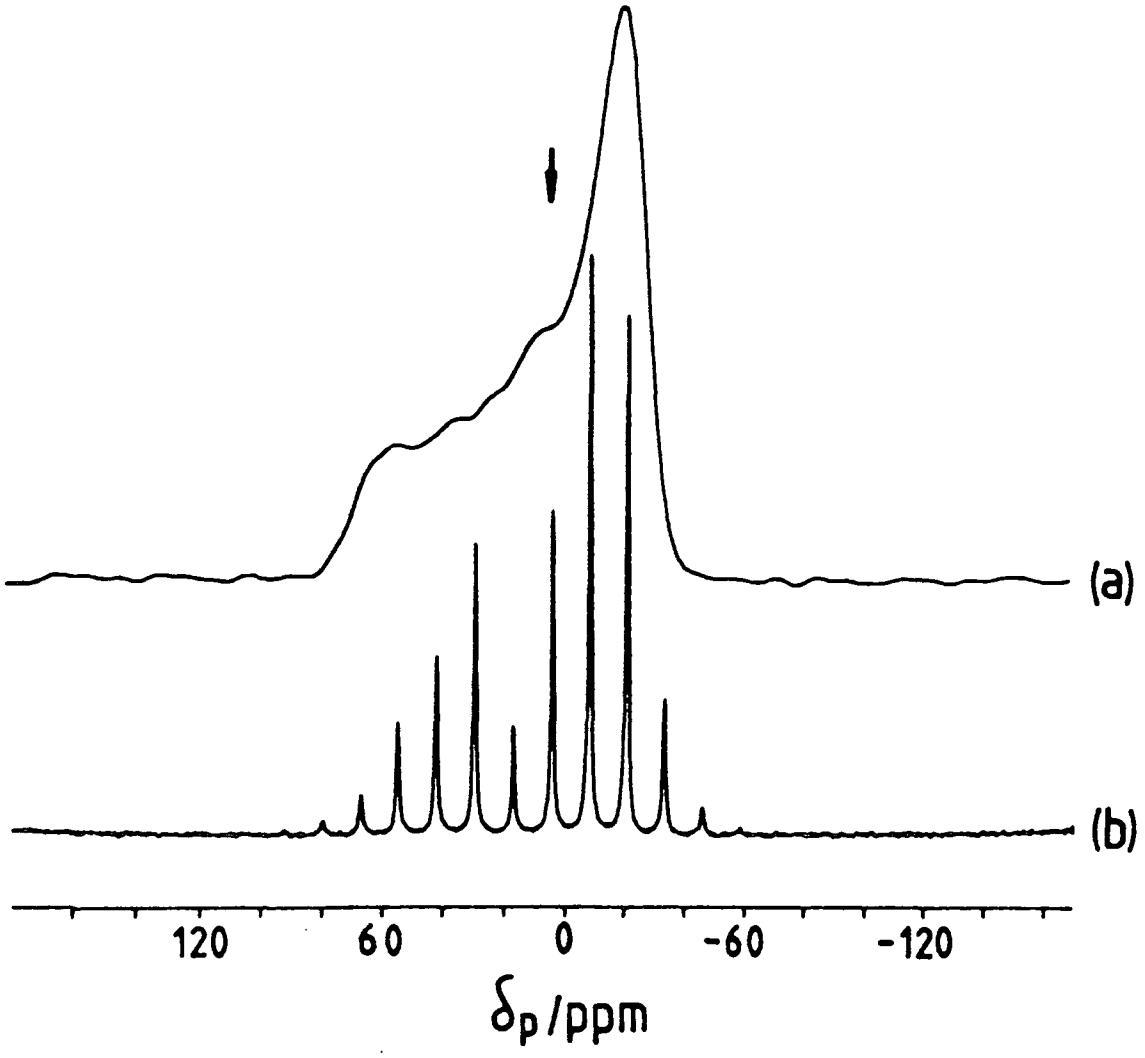

Figure 4.11 : ^{31}P CP Spectra of $Na_2HPO_4.12H_2O$
Recycle delay = 10 s, contact time = 1 ms
90^0 pulse duration = 3.5 μs

(a) Static, number of transients = 16
(b) MAS, spinning rate 1000 Hz, number of transients = 8
(Centreband indicated by arrow)

resolution spectrum. The crystal structure paper[10] pointed out that two phases of this compound exist, and that the commercially available product was always in the β -form. The space group of β-$Na_2HPO_4.12H_2O$ is $C2/c$ with P-O bond lengths between 1.510 Å and 1.594 Å and O-P-O angles between 104.3^{O} and 112.2^{O}. The large shielding anisotropy ($\Delta\sigma$=93 ppm) confirms that the phosphate units are protonated, consistent with the considerable distortion of the phosphates groups noted in the crystal structure. The static spectrum indicates that the shielding tensor has approaching axial symmetry in contrast to anhydrous form (Figure 4.10(a)).

Figure 4.12 illustrates the CP spectrum of $NaH_2PO_4.2H_2O$. As discussed earlier (section 4.3.1) the phosphorus spectrum shows two resonances with rather different ^1H $T_{1\rho}$ characteristics for the protons in contact with them. The signals occur at 1.9 ppm and 0.8 ppm with shielding anisotropies, $\Delta\sigma$ of 116 and 108 ppm for high and low frequency resonances respectively. The crystal structure[11] of $NaH_2PO_4.2H_2O$ indicated space group $P2_12_12_1$ with one molecule in the asymmetric unit. The two signals are therefore inconsistent with the crystal structure. However there are crystallographic data[11,35] which gave strong evidence that $NaH_2PO_4.2H_2O$ easily loses water if left open to the atmosphere, according to the equation;

Figure 4.12 : ^{31}P CP/MAS spectrum of $NaH_2PO_4.2H_2O$

Recycle delay = 10 s, contact time = 1 ms, 90^0 pulse duration = 4 μs
Spinning rate = 4000 Hz, number of transients = 4
(Centrebands indicated by arrows)

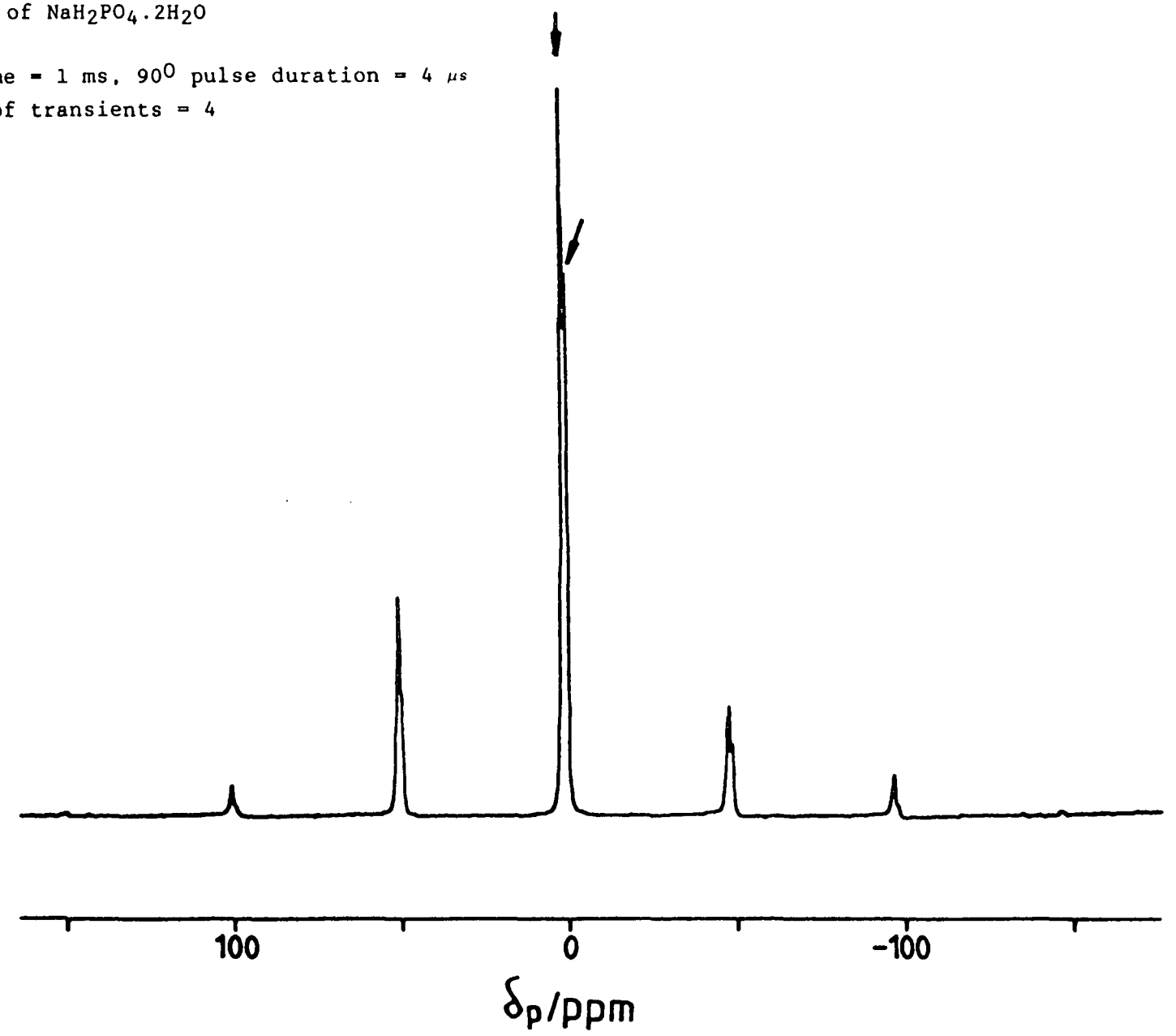

$$NaH_2PO_4.2H_2O \rightleftharpoons NaH_2PO_4.H_2O + H_2O$$

The monohydrate crystalises in space group $Pna2_1$ [35] with a single molecule in the unit cell. It is therefore likely that the two resonances observed for our sample were from a mixture of the di- and mono-hydrate. Supporting evidence came from Turner *et al.*[27] and Griffiths *et al.*[25]. The former reported δ_ρ=2.3 ppm and $\Delta\sigma$=119.4 ppm for $NaH_2PO_4.H_2O$, and the latter δ_ρ=0.4 pm and $\Delta\sigma$=108 ppm from $NaH_2PO_4.2H_2O$. Bearing in mind the possible differences in referencing in going from one laboratory to another the chemical shifts and anisotropy values compare favourably with the values reported for the two resonances observed here. On the basis of these comparisons it is proposed that the sample studied here was in fact a mixture of the mono-hydrate and di-hydrate of sodium dihydrogen phosphate.

In an attempt to summarise the ^{31}P data obtained for the samples studied in this thesis, efforts were made to correlate chemical shifts/shielding anisotropies with bond lengths/angles. No significant correlations could be found for the chemical shift data, probably due in part to the lack of spread in values compared to the potential errors in their measurement. The situation was rather more encouraging for the shielding anisotropy data, which showed a high correlation with the mean deviation of the O-P-O angle from the tetrahedral value (correlation coeff. =

0.97). A correlation of this type had been previously reported for a number of phosphate species by Turner *et al.*[27]. The data presented in Table 4.5 reproduces and extends the findings of Turner *et al.* (a larger number of phosphate compounds were considered in this study).

Figure 4.13 illustrates the quality of the linear correlation. The solid line represents a function of the form;

$$|\Delta\sigma| = 32.00\left(\sum^{n} |109.5 - \theta_{O\text{-}P\text{-}O}|/n\right) - 1.18$$

where $\Delta\sigma$ is the shielding anisotropy, n is the number of angles (in the case of a Tetrahedron n=5) and $\theta_{O\text{-}P\text{-}O}$ is the O-P-O bond angle. The fit determined for the work presented in this thesis is in close agreement with that determined by Turner *et al.* which gave coefficients of 30.90 and -1.22 respectively in an equation of the same form. The slight difference between the two equations probably results from minor differences between the methods of shielding tensor determination and referencing procedures.

Table 4.5 : Mean Bond-Angle Deviations and Shielding Anisotropy Data for The Compounds Studied in this Thesis.

Compound	$\sum^{n} \lvert 109.5 - \theta_{O\text{-}P\text{-}O} \rvert / n$	$\lvert \Delta\sigma \rvert$ / ppm
$CaHPO_4$	2.08	61.0
$CaHPO_4.2H_2O$	2.95	94.0
$NH_4H_2PO_4$	1.17	34.5
$(NH_4)_2HPO_4$	2.38	73.5
$NH_4NaHPO_4.4H_2O$	2.73	80.0
Na_2HPO_4	3.17	100.5
$Na_2HPO_4.12H_2O$	2.51	87.5
$NaH_2PO_4.2H_2O$[a]	3.02	107.5
$NaH_2PO_4.H_2O$[a]	3.87	115.5

(a) Shielding anisotropy data for $NaH_2PO_4.H_2O$ and $NaH_2PO_4.2H_2O$ are included assuming that the sample studied was indeed a mixture of the monohydrate and dihydrate.

Figure 4.13 : Graph of Shielding Anisotropy against Mean Deviation of the Bond Angle from the Tetrahedral Value for the Series of Data Listed in Table 4.5.

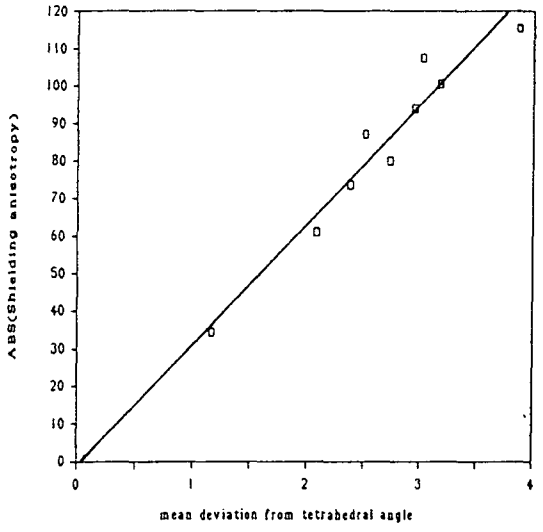

In conclusion, high-resolution solid-state ^{31}P spectra of low molecular weight inorganic phosphates can be readily obtained using both CP and SPE techniques. Chemical shifts cover a small range ca. 10 ppm, with shielding anisotropies/tensor components having a considerably wider range of values. The phosphorus spectra give a direct insight into the nature of the phosphate environment in the solid state, revealing information regarding molecular symmetry and the crystallographic environment. The intensity of spinning sidebands (which can be quantified in terms of the shielding anisotropy) give information

regarding whether or not phosphate units are protonated. In the case of non-protonated phosphate units any spinning sidebands result from distortion of the phosphate unit itself. Linewidths of certain species are strongly dependent on magic angle spinning rate, thus for optimum resolution, high rotation rates should be used. Typically, crystalline species give linewidths of less than 100 Hz.

4.3.3 ^{1}H Wide-line and ^{1}H CRAMPS Spectra

Proton wide-line spectra were acquired for a number of phosphate species and are illustrated in Figure 4.14.

The proton spectrum of brushite shows a central resonance ($\Delta\nu_{\frac{1}{2}}$ =14 kHz) which is assignable to the proton bound to the phosphate group, and a broad doublet (J = ca. 52 kHz) which can be attributed to the tightly bound water group. The spectrum duplicates almost exactly the results obtained by Cox[18]. Hydroxyapatite showed a single sharp resonance ($\Delta\nu_{\frac{1}{2}}$=1.1 kHz) in contrast to the two resonances reported by Cox. The difference almost certainly being due to different sample origins. The signal observed here is probably due to OH^- groups in the HAP lattice. The presence of mobile water cannot be ruled out, but the poor cross-polarization efficiency of this sample (see previous section) does suggest that the water content of this particular sample is small. Ammonium dihydrogen phosphate

Figure 4.14 : ^{1}H SPE/Static Wide-line spectra for selected phosphates.
Recycle delay = 10 s, number of transients =16
90^{0} pulse duration = 1.5 μs

(a) $CaHPO_4.2H_2O$
(b) $Ca_{10}(OH)_2(PO_4)_6$
(c) $NH_4H_2PO_4$
(d) $(NH_4)_2HPO_4$
(e) $(NH_4)_3PO_4.3H_2O$
(f) $NaH_2PO_4.2H_2O$
(g) $Na_2HPO_4.12H_2O$

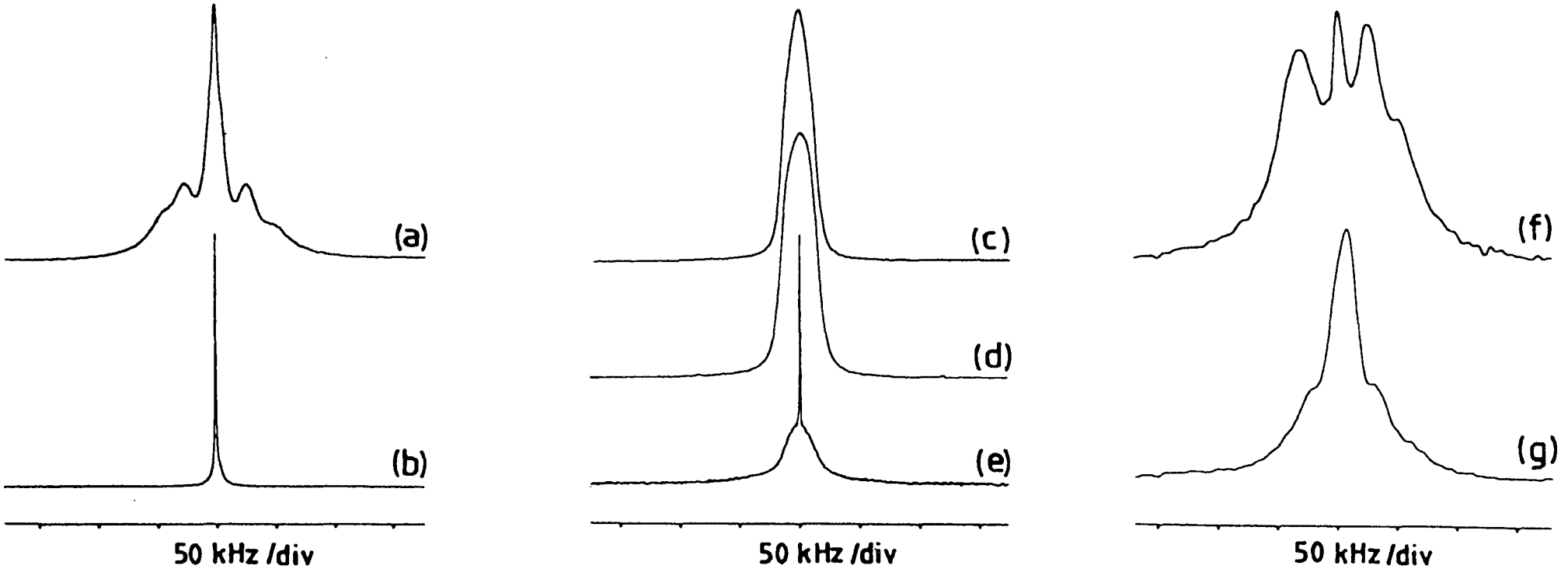

and diammonium hydrogen phosphate gave virtually identical spectra with linewidths of 28 kHz and 31 kHz respectively. The signal being almost entirely due to protons in NH_4^+. Tri-ammonium phosphate tri-hydrate gave a somewhat different spectrum, with a sharp resonance ($\Delta\nu_{\frac{1}{2}}$=1 kHz) superimposed over a broad resonance ($\Delta\nu_{\frac{1}{2}}$=30 kHz). As discussed in the previous section the tri-ammonium phosphate tri-hydrate had a damp appearance, thus the sharp resonance is almost certainly due to mobile water. The broader resonance being due to NH_4^+ protons, as for $NH_4H_2PO_4$ and $(NH_4)_2HPO_4$. No evidence for a doublet due to tightly bound water was found. Di-sodium hydrogen phosphate dodecahydrate gave a complicated spectrum with a sharp central resonance (due to the proton bound to phosphate), a broad doublet (J = ca. 57 kHz) which is probably due to tightly bound water, and a shoulder to low frequency which cannot be assigned. It is probable that the shoulder is an artifact since it is a long way from the resonance frequency for protons. The doublet is of a similar kind to that observed for brushite but in this case has a higher intensity relative to the central resonance owing to the ratio of PO-H:H_2O being a factor of twelve less. Sodium dihydrogen phosphate dihydrate gave a broad central resonance ($\Delta\nu_{\frac{1}{2}}$ =31 kHz) and evidence for a doublet splitting (J = ca. 48 kHz). The central resonance is assignable to the $(H_2PO_4)^-$ protons and the doublet to tightly bound water. As discussed in the previous section

this sample is thought to be a mixture of the di-hydrate and mono-hydrate, although it is not possible to confirm or disprove the proposal from the ^1H wideline spectrum.

From these ^1H wideline results it is clear that this kind of experiment although not high resolution, does yield some useful information regarding the general characteristics of the sample under investigation. In particular, the spectra indicate the presence of tightly bound water particularly well, provided a significant proportion of the protons in the sample under investigation are present in this form. Protons bound to phosphate or in the form of NH_4^+ appear to give broad resonances (> 10 kHz) in the centre of the spectrum whereas mobile water (or OH^-) give significantly narrower signals.

The ^1H CRAMPS technique although not routine, is becoming more commonly used. The practical aspects of the technique have been discussed in chapter 3. Protons in phosphate systems have not been subject to CRAMPS investigation previously, although a considerable amount of ^1H NMR work on other hydrogen bonded systems has been carried out[36-39]. These studies indicated that the proton chemical shift was sensitive to the nature of hydrogen bonding, in particular the $r_{OH....O}$ distance. Hydrogen bonding in phosphate systems is of considerable importance,

thus a ^{1}H CRAMPS study of a number of phosphates was undertaken. A summary of ^{1}H CRAMPS results for a number of phosphate compounds is given in Table 4.6. Figure 4.15 shows ^{1}H CRAMPS spectra for monetite, brushite and hydroxyapatite. Monetite shows three signals at 15.4 ppm, 14.0 ppm and 13.1 ppm. Consultation of the crystal structure[1], revealed three different $r_{OH....O}$ distances of 2.549(1) Å, 2.560(1) Å and 2.658(1) Å consistent with the three signals observed. The signals have an intensity ratio reasonably close to 1:1:2 in accordance with the crystal structure. A single proton is covalently bonded to one phosphate unit and half each of the other two types of proton are shared by the second phosphate group in the asymmetric unit. If a large frequency offset was used in the ^{1}H CRAMPS experiment a large spectral width could be observed without folding back of the spectrum occurring. The spectrum of monetite showed spinning sidebands (Figure 4.15(b)) indicating considerably anisotropy of the ^{1}H shielding tensor. The poorer resolution is a consequence of the larger frequency offset used. There was no evidence of spinning sidebands in the ^{1}H CRAMPS spectra of the other phosphate samples. Brushite showed a broad resonance at 5.2 ppm due to bound water and a somewhat sharper resonance at 9.9 ppm due to the P-OH proton. The $r_{OH....O}$ distance associated with the acidic proton was 2.678(5) Å[2]. The spectrum of hydroxyapatite (Figure 4.15(d)) shows two resonances at 0.2 and 6.5 ppm respectively. The high

Table 4.6 : ^{1}H CRAMPS Chemical shift data (and coupling constant data where appropriate) for selected phosphates and ammonium nitrate.

Compound	^{1}H Chemical Shift /ppm (relative to TMS) POH	H_2O	OH^-	NH_4^+	J_{N-H} / Hz
$CaHPO_4$	15.4	---	---	---	---
	14.0	---	---	---	---
	13.1	---	---	---	---
$CaHPO_4.2H_2O$	9.9	5.2	---	---	---
$Ca_{10}(OH)_2(PO_4)_6$	---	6.5[a]	0.2[a]	---	---
$NH_4H_2PO_4$	14.5	---	---	6.8	46
	(13.9)[b]	---	---	(6.7)[b]	---
$(NH_4)_2HPO_4$	10.6	---	---	8.2	---
	---	---	---	7.9	---
	(10.3)[b]	---	---	(7.8)[b]	---
$(NH_4)_3PO_4.3H_2O$	---	5.9	---	8.0	---
$^{14}NH_4{}^{14}NO_3$	---	---	---	6.5	45
$^{15}NH_4{}^{14}NO_3$	---	---	---	6.4	71

[a] Tentative assignment

[b] Taken from Reference 32 (for comparison).

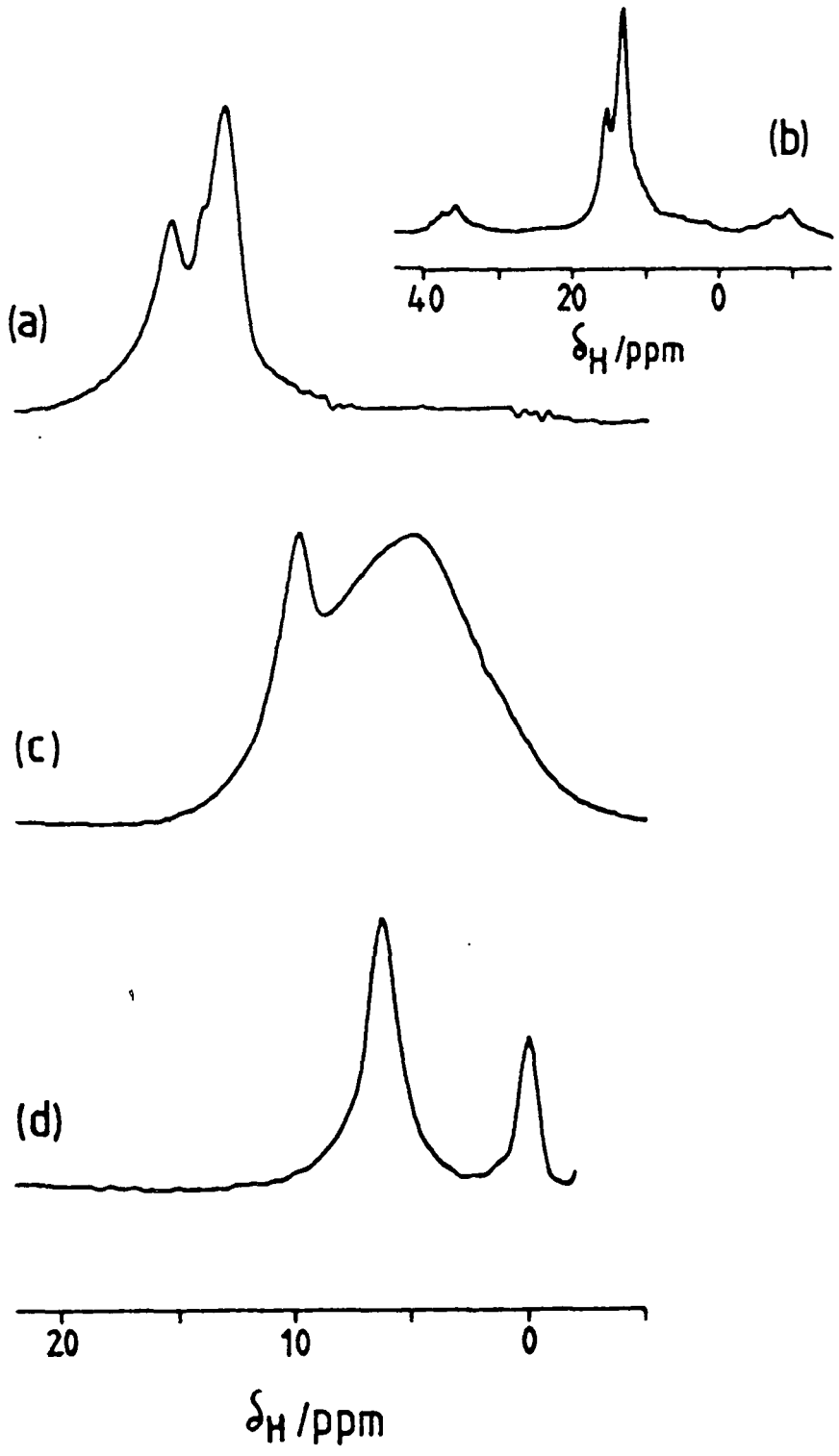

Figure 4.15 : ^1H CRAMPS Spectra of monetite, brushite and hydroxyapatite. Recycle delay = 10 s, 90^0 pulse duration = 2 μs, spinning rate = 2400 Hz, number of transients = 32

(a) $CaHPO_4$, frequency offset = -1000 Hz
(b) $CaHPO_4$, frequency offset = -3000 Hz
(c) $CaHPO_4.2H_2O$, frequency offset = -1000 Hz
(d) $Ca_{10}(OH)_2(PO_4)_6$, frequency offset = -1000 Hz

frequency resonance is believed to be due to water since it occurs in the same spectral region as the water resonance for brushite and tri-ammonium phosphate tri-hydrate. The resonance at 0.2 ppm has tentatively been assigned to OH^-. $NH_4H_2PO_4$, $(NH_4)_2HPO_4$ and $(NH_4)_3PO_4.3H_2O$ gave the ^1H CRAMPS spectra illustrated in Figure 4.16. The P-OH resonance for the ammonium and di-ammonium salts occurs at 14.5 and 10.6 ppm respectively with their corresponding $r_{OH....O}$ distances being 2.490(1) and 2.615(1) Å. The NH_4^+ signals of these two compounds show some fine structure. In the case of $NH_4H_2PO_4$ the band closely resembles a 1:1:1 triplet probably due to $\{^1H-^{14}N\}$ J-coupling. In an attempt to verify this assignment, spectra of $^{14}NH_4NO_3$ and $^{15}NH_4NO_3$ were acquired using ^1H CRAMPS and are illustrated in Figure 4.17. In the ^{14}N case a triplet is seen with J = 46 Hz and for ^{15}N a doublet was seen with J = 71 Hz, consistent with ^1H coupling to I = 1 and I = ½ nuclei respectively. The coupling constants measured compare favourably with solution state values[40] of 52.6 +/- 0.1 Hz and 73.7 +/- 0.1 Hz for $^{14}NH_4NO_3$ and $^{15}NH_4NO_3$ respectively. On the basis of these results it became clear that the splitting observed for $NH_4H_2PO_4$ was indeed J-coupling with J_{N-H} = 46 Hz. In the case of di-ammonium hydrogen phosphate the fine structure in the NH_4^+ region is clearly more complicated than a simple triplet. The crystal structure[5] indicated that the two NH_4^+ groups are in fact crystallographically inequivalent, thus the structure seen in the ^1H CRAMPS spectrum is due to

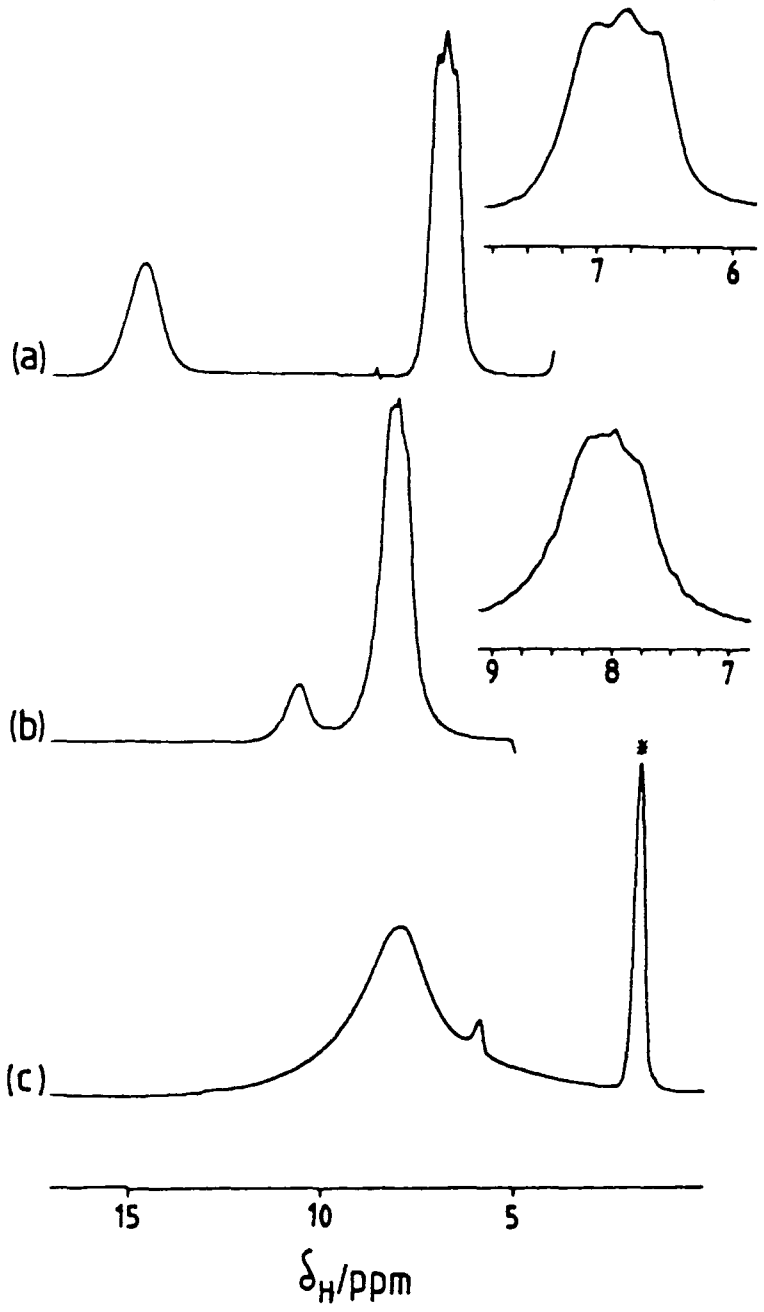

Figure 4.16 : ^1H CRAMPS Spectra of $NH_4H_2PO_4$, $(NH_4)_2HPO_4$ and $(NH_4)_3PO_4.3H_2O$
Recycle delay = 10 s, 90^0 pulse duration = 2 μs
spinning rate = 2400 Hz

(a) $NH_4H_2PO_4$: frequency offset = -600 Hz, number of transients = 12
(NH_4^+ band inset)

(b) $(NH_4)_2HPO_4$: frequency offset = -400 Hz, number of transients = 32
(NH_4^+ band inset)

(c) $(NH_4)_3PO_4.3H_2O$: frequency offset = -1500 Hz, number of transients = 32
*adamantane reference

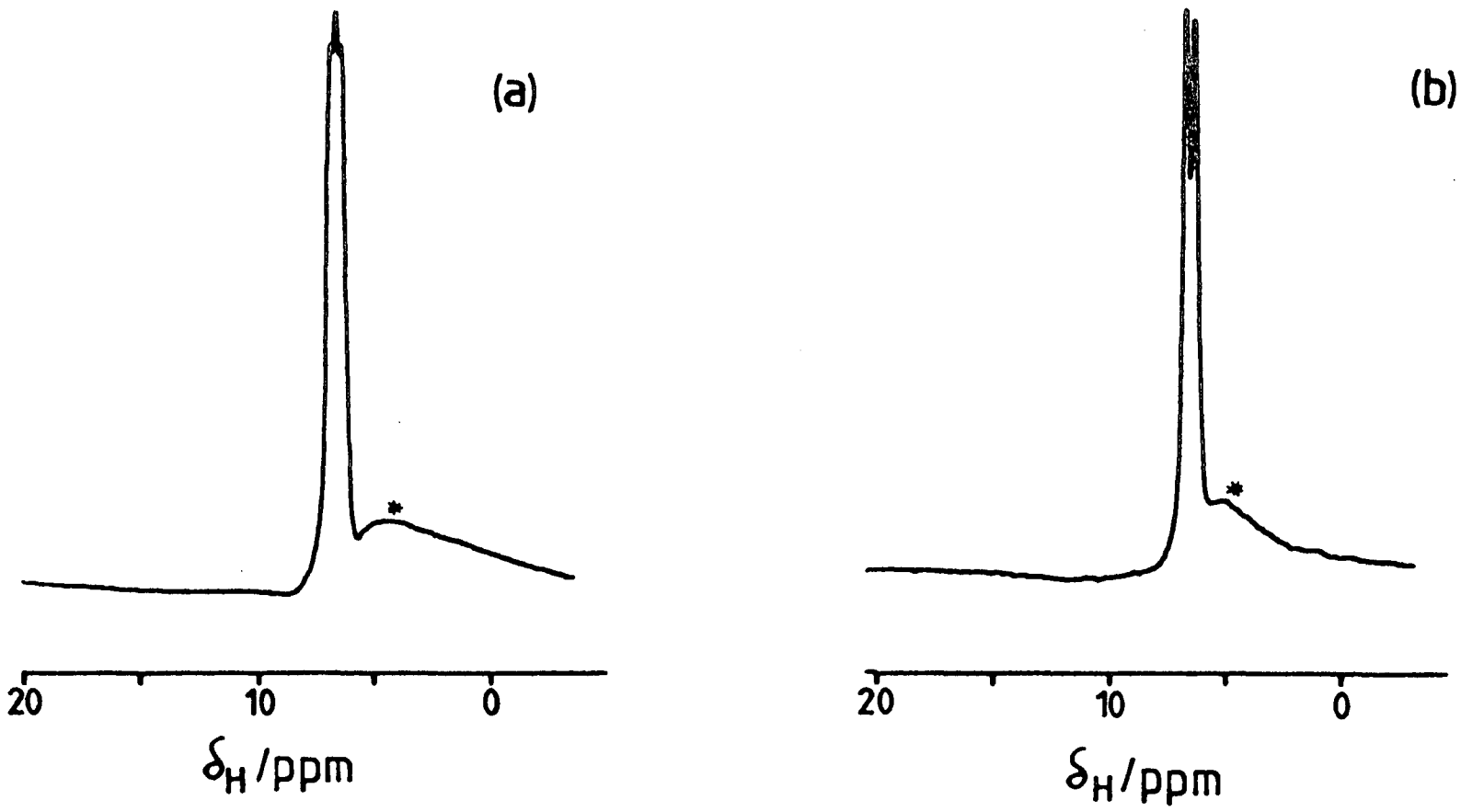

Figure 4.17 : ^1H CRAMPS Spectra of $^{14}NH_4{}^{14}NO_3$ and 98 atom % $^{14}NH_4{}^{15}NO_3$
Recycle delay = 10 s, 90^o pulse duration = 2 μs
spinning rate = 2400 Hz, frequency offset = -1000 Hz, number of transients = 32
*broad baseline artifact

(a) $^{14}NH_4{}^{14}NO_3$ (b) $^{15}NH_4{}^{14}NO_3$

the overlap of two NH_4^+ triplets. Tri-ammonium phosphate tri-hydrate showed a broad resonance at 8.0 ppm due to NH_4^+ and a somewhat weaker but sharper resonance at 5.9 ppm due to water. The phosphorus spectra of this sample indicated that it was impure, probably due to decomposition. The NH_4^+ region appears rather broad with no fine structure probably as a consequence of a range of NH_4^+ species being present in the impure sample. The water resonance appears to be quite narrow (compared to brushite for example) suggesting that it may well be mobile.

As mentioned earlier in this section correlations between hydrogen-bond length and chemical shift had been reported for a number of hydrogen-bonded systems. It was hoped that the data reported in this thesis would follow trends consistent with the previously published work. A plot of $\bar{\sigma}_H$ $(=-\delta_H)$ against hydrogen-bond distance (defined as $r_{O....O}$) is shown in Figure 4.18. The data appear to follow an approximately linear trend. However, Berglund and Vaughan[36] reported a curved correlation based on the calculations of Ditchfield[41] (represented by the solid curve on Figure 4.18). The shape of the curve is unchanged from that reported previously[36], although it was necessary to offset the curve by a few ppm in order to achieve the best fit. The need to offset the curve can be attributed to differences in the proton donating group (compared to the carboxyl groups considered by Berglund and

Vaughan). Clearly it is difficult to define any clear-cut correlations when only a few data points are used in the analysis. A larger data set would allow a more rigorous (and conclusive) analysis to be carried out.

Figure 4.18 : Plot of Observed Proton Shielding Against Hydrogen-Bond Length for a Selection of Phosphate Compounds.

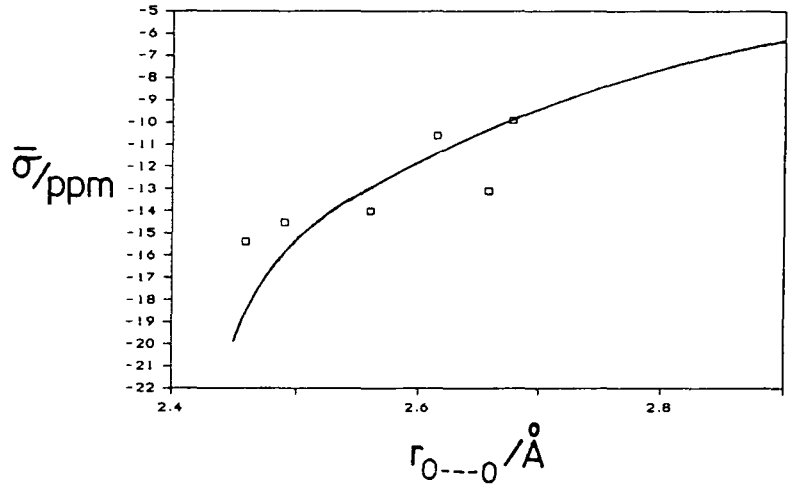

solid curve represents the results of theoretical calculations based on the $(H_2O)_2$ dimer from reference 36, and has been offset to higher frequency (downwards) by 6 ppm.

Despite being unable to define precisely the form of the correlation between hydrogen-bond length and shielding, it is obvious from Figure 4.18 that the overall trend is for shielding to increase as hydrogen-bond length increases. ^1H CRAMPS shifts can be measured to within an accuracy of +/- 0.2 ppm so the deviations from the theoretical correlation

are due to additional effects (not accounted for in the theory), rather than errors in the measurement of the chemical shift itself.

While this thesis was in the final stages of typing a paper was published[42] reporting ^{1}H high-speed MAS spectra for a number of phosphate species including monetite, brushite and hydroxyapatite. Spinning rates in excess of 7 kHz were used to obtain the spectra. The chemical shift data reported were in good agreement with the results presented in this thesis. However, the published spectra were of slightly lower resolution than the ^{1}H CRAMPS spectra presented here (only two signals were observed for monetite). Also of relevance to the variable spinning speed data presented in this thesis for ^{31}P, was a plot showing the behaviour of ^{1}H linewidth for HAP as a function of spinning rate. The graph followed a similar trend to those presented in Figs. 4.3(a) to 4.3(c).

In conclusion, wideline ^{1}H NMR of phosphates is a particularly simple technique which should not be overlooked, since it can give valuable information regarding protons in the system. Linewidths are characteristic, i.e. ca. 1 kHz for mobile species, > 10 kHz for bound protons, and a broad doublet (J = ca. 50 kHz) is seen for tightly bound water. ^{1}H CRAMPS is a difficult technique to implement but gives pleasing results for

phosphate systems. The results obtained allow assignment of particular spectral regions to particular proton types namely, 5-7 ppm to water, 6-8 ppm to NH_4^+ and 10-15 ppm to P-OH. The technique is sensitive to $r_{OH....O}$ for the P-OH protons with three signals being resolved for the three proton types in monetite, thus crystallographic information is accessible via ^1H CRAMPS.

REFERENCES

[1] M. Catti, G. Ferraris and A. Filhol,
Acta Cryst. B33, (1977), 1223.

[2] N. A. Curry and D. W. Jones,
J. Chem. Soc. A. (1971), 3275.

[3] M. I. Kay, R. A. Young and A. S. Posner,
Nature 204, (1964), 1050.

[4] A. A. Kahn and W. H. Baur,
Acta Cryst. B29, (1973), 2721.

[5] A. A. Kahn, J. P. Roux and W. J. James,
Acta Cryst. B28, (1972), 2065.

[6] D. Mootz and H. Wunderlich,
Acta Cryst. B26, (1970), 1826.

[7] G. Ferraris and M. Franchini-Angela
Acta Cryst. B30, (1974), 504.

[8] K. Y. Leung and C. Calvo,
Canad. J. Chem. 50, (1972), 2519.

[9] E. Tillmanns and W. H. Baur,
Acta Cryst. B27, (1971), 2124.

[10] M. Catti, G. Ferraris and G. Ivaldi,
Acta Cryst. B34, (1978), 369.

[11] H. Bartl, M. Cattiand G. Ferraris,
Acta Cryst. B32, (1976), 987.

[12] J. Herzfeld, A. Roufosse, R. A. Haberkorn, R. Griffin and M. J. Glimcher.
Phil. Trans. R. Soc. Lond. B289, (1980), 459.

[13] W. P. Rothwell, J. S. Waugh and J. P. Yesinowski. *J. Am. Chem. Soc.* 102, (1980), 2637.

[14] J. P. Williams, R. G. F. Giles and A. M. Posner, *J. Chem. Soc. Chem. Comm.* (1981), 1051.

[15] J. P. Yesinowski, *J. Am. Chem. Soc.* 103, (1981), 6266.

[16] J. P. Yesinowski and J. J. Benedict, *Calcif. Tissue Int.* 35, (1983), 284.

[17] J. Tropp, N. C. Blumenthal and J. S. Waugh, *J. Am. Chem. Soc.* 105, (1983), 22.

[18] I. J. Cox, *Ph.D. Thesis*, University of East Anglia, (1984).

[19] W. P. Aue, A. H. Roufosse, M. J. Glimcher and R. G. Griffin, *Biochemistry* 23, (1984), 6110.

[20] A. H. Roufosse, W. P. Aue, J. E. Roberts, M. J. Glimcher and R. G. Griffin, *Biochemistry* 23, (1984), 6115.

[21] E. R. Andrew, D. J. Bryant, E. M. Cashell and B. A. Dunell, *Chem. Phys. Lett.* 77, (1981), 614.

[22] N. E. Burlinson, B. A. Dunell and J. A. Ripmeester, *J. Magn. Reson.* 67, (1986), 217.

[23] A. R. Grimmer and U Haubenreisser, *Chem. Phys. Lett.* 99, (1983), 487.

[24] T. M. Duncan and D. C. Douglass, *Chem. Phys.* 87, (1984), 339.

[25] L. Griffiths, A. Root, R. K. Harris, K. J. Packer, A. M. Chipperdale and F. R. Tromans,
J. Chem. Soc. Dalton Trans. (1986), 2247.

[26] N. J. Clayden, C. M. Dobson, Lu-Yun Lian, and D. J. Smith
J. Magn. Reson. 69, (1986), 476.

[27] G. L. Turner, K. A. Smith, R. J. Kirkpatrick and E. Oldfield
J. Magn. Reson. 70, (1986), 408.

[28] A. K. Cheetham, N. J. Clayden, C. M. Dobson and R. J. B. Jakeman,
J. Chem. Soc. Chem. Comm. (1986), 195.

[29] R. K. Harris, P. Jackson, P. J. Wilkes and P. S. Belton,
J. Magn. Reson. 73, (1987), 178.

[30] L. M. Ryan, R. E. Taylor, A. J. Paff and B. C. Gerstein,
Chem. Phys. Lett. 52, (1977), 508.

[31] L. M. Ryan, R. C. Wilson and B. C. Gerstein,
Chem. Phys. Lett. 52, (1977), 341.

[32] G. Scheler, U. Haubenreisser and H. Rosenberger,
J. Magn. Reson. 44, (1985), 134.

[33] R. K. Harris, P. Jackson, G. J. Nesbitt and B. J. Say. Poster presented to B.R.S.G. Oxford, April 1986.

[34] M. M. Maricq and J. S. Waugh,
J. Chem. Phys. 70, (1979), 3300.

[35] M. Catti and G. Ferraris,
Acta Cryst. B32, (1976), 359.

[36] B. Berglund and R. W. Vaughn,
J. Chem. Phys. 73, (1980), 2037.

[37] C. McMichael Rohlfing, L. C. Allen and R. Ditchfield,
J. Chem. Phys. 79, (1983), 4958.

[38] G. A. Jeffrey and Younghee Yeon,
Acta Cryst. B42, (1986), 410.

[39] R. K. Harris and P. Jackson,
"NMR Studies of Hydrogen-bonding in Solids by the CRAMPS Technique"
In Press.

[40] J. D. Baldeschwieler,
J. Chem. Phys. 36, (1962), 152.

[41] R. Ditchfield
J. Chem. Phys. 65, (1976), 3123.

[42] J. P. Yesinowski and H. Eckert
J. Am. Chem. Soc. 109, (1987), 6274.

CHAPTER 5 - SYNTHETIC CALCIUM PHOSPHATES

5.1 INTRODUCTION

Several types of solid calcium phosphate, exhibiting distinct X-ray diffraction patterns, can be obtained by precipitation from aqueous solutions at normal pressures. Their chemical nature is summarised in Table 5.1. The table also includes the commonly obtained amorphous form of calcium phosphate, the nature of which is ill-defined and probably variable. These phosphates are of considerable importance in both geochemistry and biochemistry, but they often occur in intimate admixture or otherwise are unsuitable for X-ray investigation. Therefore it is important to have methods of characterising calcium phosphates (and substances such as milk solids, which contain them) non-destructively and of studying their formation and interconversion. Clearly solution-state NMR techniques are unsuitable, both because of the very low solubility of the materials in water and because they do not give rise to distinctive phosphate units in solution. Solid-state methods are therefore required.

In Chapter 4, solid-state NMR was demonstrated to be a powerful technique for use in the study of inorganic phosphate systems. Although phosphorus chemical shifts alone are not particularly distinctive of a given phosphate species, solid-state NMR spectra contain a great deal of information in addition to the chemical shift. Spinning sidebands are very sensitive to the symmetry of the phosphate unit. For example $(PO_4)^{3-}$ in hydroxyapatite shows a very weak pattern whereas

$(HPO_4)^{2-}$ in brushite shows a very strong pattern. NMR is dependent on short-range interactions and is thus applicable regardless of long range order or not. However, it is not insensitive to order. Since disordered compounds contain a range of environments they result in a dispersion of chemical shifts and hence broad lines. Compounds with long-range order have few environments and therefore give rise to a discrete range of chemical shifts and hence give narrow lines. Linewidths are thus a measure of order, which offers a means of monitoring the maturation of an amorphous solid to a crystalline phase. Crystalline solids have phosphorus NMR linewidths <100 Hz in contrast to a truly amorphous phase which has linewidths in the region of 500 Hz.

In addition to phosphorus NMR techniques, use has also been made of proton measurements including relaxation time data, wideline and CRAMPS spectra. The wideline technique has been shown to be a useful method of detecting tightly bound water. Mobile and bound protons can be distinguished according to the linewidths observed for the central resonances. CRAMPS proved very informative for the pure model compounds discussed in chapter 4. The technique has been evaluated further using the samples discussed in this chapter.

A particularly interesting area of calcium phosphate chemistry encompasses the formation and structural nature of the precipitated hydroxyapatites. When hydroxyapatite (HAP) is precipitated from a supersaturated solution of calcium

phosphate, an unstable amorphous calcium phosphate (ACP) is observed as a precursor phase[1]. This precursor, which is non-crystalline, can be stabilised by dehydration in a freeze-drying apparatus[2]. As usually prepared, ACP has a Ca/P ratio of 3:2 rather than 5:3 for HAP.

Table 5.1 : Solid Calcium Phosphates

Compound	Formula	Ca:P
Anhydrous monocalcium phosphate	$Ca(H_2PO_4)_2$	0.5
Monocalcium phosphate monohydrate	$Ca(H_2PO_4)_2.H_2O$	0.5
Monetite (anhydrous dicalcium phosphate)	$CaHPO_4$	1.0
Brushite (dicalcium phosphate dihydrate)	$CaHPO_4.2H_2O$	1.0
Octacalcium phosphate	$Ca_8H_2(PO_4)_6.5H_2O$	1.33
β-Tricalcium phosphate (anhydrous)	$Ca_3(PO_4)_2$	1.5
Hydroxyapatite	$Ca_{10}(OH)_2(PO_4)_6$	1.67
Amorphous calcium phosphate	unknown	---

The basic structural unit of ACP has been proposed to be $Ca_9(PO_4)_6$ in the form of clusters 9.5 Å in diameter[3]. These clusters are thought to close-pack randomly, forming spheres 300-1000 Å in diameter (as seen by electron microscopy). The freeze-dried solid is also thought to contain 15% to 20% water, which is assumed not to be an essential part of the $Ca_9(PO_4)_6$ structure but to reside in the interstices between clusters. The transformation from ACP to microcrystalline hydroxyapatite is thought to take place by solubilisation of the ACP followed by renucleation as hydroxyapatite[4]. The role of carbonate in poorly crystalline HAP has received a good deal of attention[5]. Introduction of carbonate is seen to reduce the degree of order or crystallinity. On the basis of evidence from infrared spectroscopy[6] the planar $(CO_3)^{2-}$ ion is thought to substitute in some random way for the tetrahedral $(PO_4)^{3-}$ ion.

The series of ACP samples studied here were prepared in the hope, *inter alia*, of using NMR to monitor the transition from ACP to a moderately crystalline HAP and of studying the influence of carbonate incorporation. This work has been carried out as part of a collaborative study involving J. E. Harries and D. W. L. Hukins (Department of Medical Biophysics, University of Manchester, England), who prepared the samples and wherever possible carried out infra-red, X-ray and EXAFS measurements on them.

Information on ^{31}P chemical shifts and linewidths for a number of the forms of calcium phosphate were available to us from previous work[7] in our research group (see Table 5.2) and from the more recent data presented in chapter 4. However, some caution should be exercised in considering the chemical shifts because of the difficulty in obtaining a consistently accurate referencing procedure in relation to some of the small differences between species.

5.2 Sample Preparations

Samples 1 to 4 were prepared with the aim of determining the most suitable method of obtaining ACP, and to evaluate the potential of solid-state NMR for use in studies of systems of this type.

Sample 1 was prepared at $37^{o}C$ by the simultaneous addition of equal amounts of 0.34 mol dm^{-3} $CaCl_2$ and 0.2 mol dm^{-3} Na_2HPO_4 whilst stirring continuously. The pH of both solutions was initially brought to pH 10 with 1 mol dm^{-3} NH_3. A rapid drop of pH was noted on mixing. A sample was extracted immediately after addition of the reactants.

Sample 2 was prepared with the aim of preventing the pH drop noted during the preparation of sample 1. The same concentrations were used and the following procedure was adopted. 200 cm^3 of $CaCl_2$ initialised at pH 10 was placed in

Table 5.2 : Phosphorus Chemical Shift and Linewidth Data for Selected Calcium Phosphates[7]

Compound	Linewidth $\Delta\nu_{\frac{1}{2}}/Hz$	Chemical Shift δ_p/ppm	Sideband Intensity
Monocalcium phosphate monohydrate	150	-0.6 (-0.1) -5.0 (-4.6)	intense intense intense intense
Monetite	250	-0.7 -1.8	intense intense
Brushite	85	+1.0 (+1.7)	intense intense
Octacalcium phosphate	---	+2.6 (+3.4) +1.2 -0.8 (-0.1) (-2.2)	weak weak weak medium medium weak
β-Tricalcium phosphate	200	+9.2 +5.2 +4.2	 weak weak
Hydroxyapatite	100	+2.3 (+2.8)	weak weak
Amorphous calcium phosphate	350 480	+2.6 (+1.7)	weak weak

a beaker, continuously stirred and 200 cm^3 of 0.2 mol dm^{-3} Na_2HPO_4 added dropwise, whilst maintaining the pH at 10 with 1M NH_3. The sample was extracted immediately after addition.

Sample 3 was taken from the reaction mixture from which sample 1 was obtained, but was extracted 24 h after the solution was prepared.

Sample 4 was prepared in an identical manner to sample 2 but with the reactant concentrations halved.

In the light of i.r., X-ray, EXAFS and NMR evidence (discussed in the next section) an improved method for the preparation of ACP was devised. Consequently the sample codes for all subsequent preparations are preceded by ACP because they were believed to originate from an initially amorphous calcium phosphate.

The ACP samples were prepared at room temperature in a helium atmosphere. An equal amount of 3.75 mM ammonium phosphate solution was added dropwise to continuously stirred 6.25 mM calcium chloride. Both solutions were preadjusted to pH 10 with 0.880 ammonia, and the pH was kept constant by the addition of further amounts of ammonia. The precipitates formed were extracted after various time periods by centrifugation and then freeze dried overnight. Sample ACP was extracted from the solution immediately after mixing was

completed. ACP19H, ACP22H, ACP26H and ACP5D were extracted from solution after 19 h, 22 h, 26 h, and 5 days, respectively.

Carbonated ACP samples were prepared in the same manner as the other ACP samples except for added carbonate. Samples ACPCO3-1, ACPCO3-2 and ACPCO3-3 were each allowed to mature in 800 ml of solution for 22 h in the presence of 0.1, 0.2 and 0.5 g of ammonium carbonate respectively.

All samples were stored at $0^{o}C$ in the presence of anhydrous silica gel.

5.3 RESULTS AND DISCUSSION

5.3.1 Preliminary Examination of Samples 1 to 4

5.3.1.1 Phosphorus-31 NMR Study

Cross-polarization and single-pulse excitation spectra were acquired for all samples. Identical spectrometer parameters were used for all samples, so the spectra are directly comparable. A summary of the NMR data for samples 1 to 4 is given in Table 5.3. The NMR spectra obtained for each sample will now be considered in some detail.

Table 5.3 : Summary of NMR data for samples 1 to 4

Sample	Cross-polarization		Single-Pulse-Excitation	
	Shift/ppm	Linewidth/Hz	Shift/ppm	Linewidth/Hz
1	---	---	2.4	215
	1.2	114	---	---
2	2.8	450	2.7	370
3	---	---	2.1	150
	1.1	150	---	---
			-1.7	nm*
4	2.8	420	2.8	370

* not measured (shoulder)

Sample 1 gave rise to the CP and SPE spectra illustrated in Figure 5.1. The two types of NMR experiment gave very different spectra. The CP spectrum shows a single resonance at 1.2 ppm. with a linewidth of 114 Hz and a rich sideband manifold. These features are indicative of a crystalline phase with protonated phosphate units. The SPE spectrum shows a resonance at 2.4 ppm. with weak spinning sidebands. The

species responsible for this signal is phosphate which is not protonated. Clearly there are at least two phosphate species in this sample which are very different. Bearing in mind the significant pH drop during preparation, the presence of protonated phosphate is only to be expected. The absence of signal from protonated phosphate in the SPE spectrum indicates that the non-protonated phosphate is the dominant phase, but since there is only one resonance observed in the CP experiment it must have a poor relative cross-polarization efficiency.

The CP and SPE spectra obtained for sample 2 are illustrated in Figure 5.2. The CP spectrum shows a broad resonance, linewidth 450 Hz, at 2.8 ppm with a weak spinning sideband pattern. A similar spectrum was observed for the SPE experiment with a resonance at 2.7 ppm with linewidth 370 Hz. The chemical shift is in both cases close to that of hydroxyapatite although the resonances are significantly broader and the sideband intensities a little higher. The relatively broad lines observed indicate a lack of crystallinity. In going from SPE to CP experiments the linewidth increases by 80 Hz and a slight enhancement of the spinning sidebands is observed, indicating the presence of at least two different phosphate environments.

Sample 3 gave rise to the CP and SPE spectra illustrated in Figure 5.3. The spectra are very different, particularly in the intensity of the spinning sidebands, and since the

Figure 5.1 : ^{31}P Spectra of Sample 1

Recycle delay = 30 s,
spinning rate = 2.5 kHz,
90^{0} pulse duration = 4 μs
number of transients = 100

(a) SPE/HPPD/MAS
(b) CP/HPPD/MAS : contact time = 1 ms

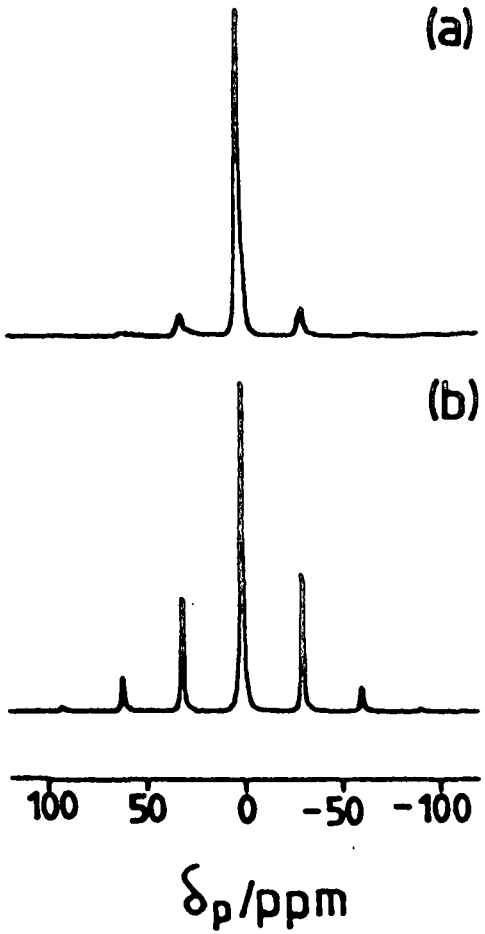

Figure 5.2 : ^{31}P Spectra of Sample 2

Recycle delay = 30 s,
spinning rate = 2.5 kHz,
90^{0} pulse duration = 4 μs
number of transients = 100

(a) SPE/HPPD/MAS
(b) CP/HPPD/MAS : contact time = 1 ms

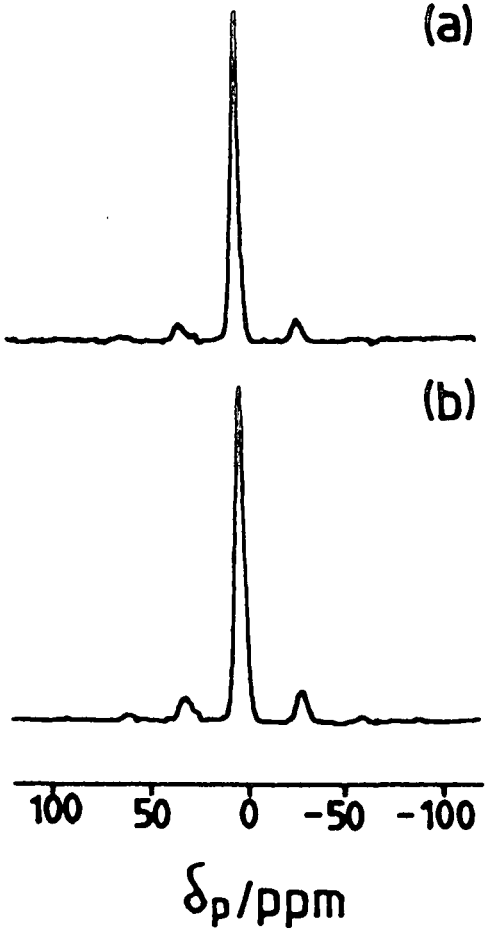

Figure 5.3 : ^{31}P Spectra of Sample 3

Recycle delay = 30 s,
spinning rate = 2.5 kHz,
90^{0} pulse duration = 4 μs
number of transients = 100

(a) SPE/HPPD/MAS
(b) CP/HPPD/MAS : contact time = 1 ms

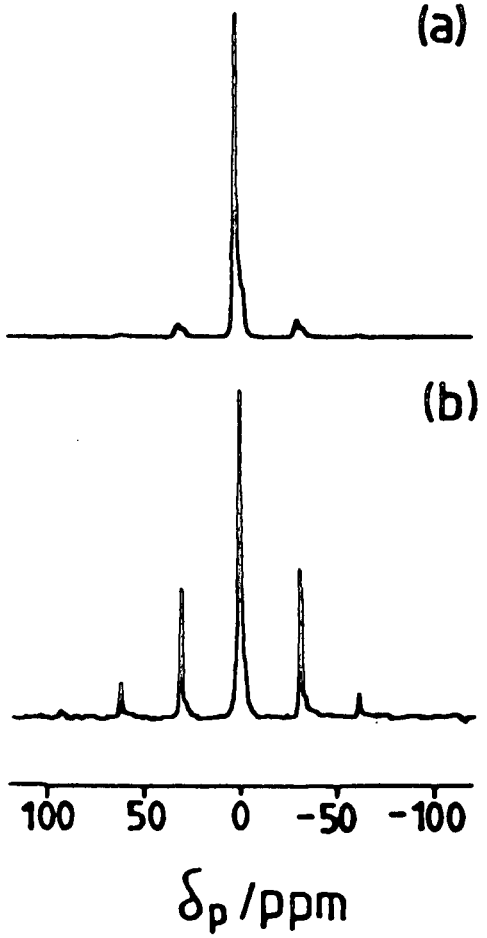

linewidths are relatively narrow it can be concluded that this sample consists of reasonably crystalline species and thus is not ACP. The CP spectrum shows an isotropic shift of 1.1 ppm., linewidth 150 Hz and a rich sideband pattern, which is expected from a phase containing protonated phosphate units (as is consistent with efficient cross-polarization). The SPE spectrum shows a resonance at 2.1 ppm, linewidth also 150 Hz, with a shoulder at -1.7 ppm. indicating the presence of two more species. The difference in shifts observed between CP and SPE spectra is significant, and thus it can be concluded that there must be at least three phosphate species present.

The CP and SPE spectra of sample 4 corresponded almost exactly with those for sample 2. Clearly halving the reactant concentrations had little effect on the product produced.

In conclusion, the phosphorus NMR spectra of these solid samples have been informative. The value of performing both CP and SPE experiments has become clear. In the case of samples of 1 and 3 the two types of experiment allow observation of completely different types of phosphate environment. These two samples appear to be a mixture of crystalline phases, none of which are ACP. Samples 2 and 4 appear to be much more like ACP, they have poor crystallinity and show a similar chemical shift to hydroxyapatite.

5.3.1.2 ^{1}H CRAMPS NMR Studies

The ^{1}H CRAMPS data presented in this section were obtained before improvements in probe design and tune-up procedure were devised. Thus the resolution achieved was somewhat inferior to the results presented in chapter 4, but the information contained within such spectra is still informative. ^{1}H CRAMPS spectra of monetite and brushite obtained at the same time as the spectra of samples 1 to 4 are illustrated in Figure 5.4 so that comparisons can be made directly with the results presented here. It is also interesting to compare the spectra with those in chapter 4 in order to appreciate the level of improvement in the implementation of the CRAMPS technique since this project was started.

Figure 5.5 shows ^{1}H CRAMPS spectra for samples 1 to 4. It is clear that samples 2 and 4 are very similar, but different to either sample 1 or sample 3. For clarity samples 2 and 4 will be discussed first, followed by sample 1 and finally sample 3.

Samples 2 and 4 gave very similar CRAMPS spectra showing a reasonably sharp resonance at 7.0 ppm. with evidence of a broad underlying resonance. Bearing in mind that ammonia was used to control the pH of the solutions during the preparation and that $(NH_4)^+$ resonates in the region between 7.0 and 8.0

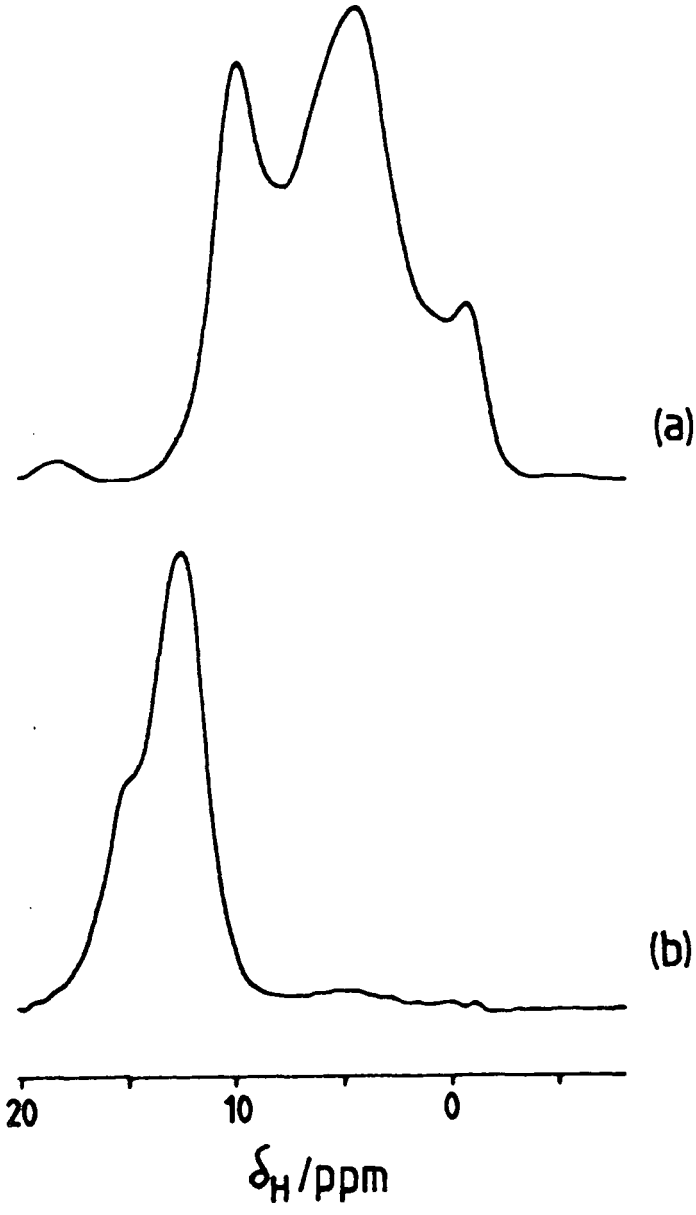

Figure 5.4 : ^1H CRAMPS Spectra of Brushite and Monetite
(Before improvements in probe design and tune-up procedure)

Recycle delay = 10 s, 90^0 pulse duration = 3 μs
spinning rate = 2.5 kHz, number of transients = 32
frequency offset = 5000 Hz

(a) $CaHPO_4.2H_2O$ (b) $CaHPO_4$

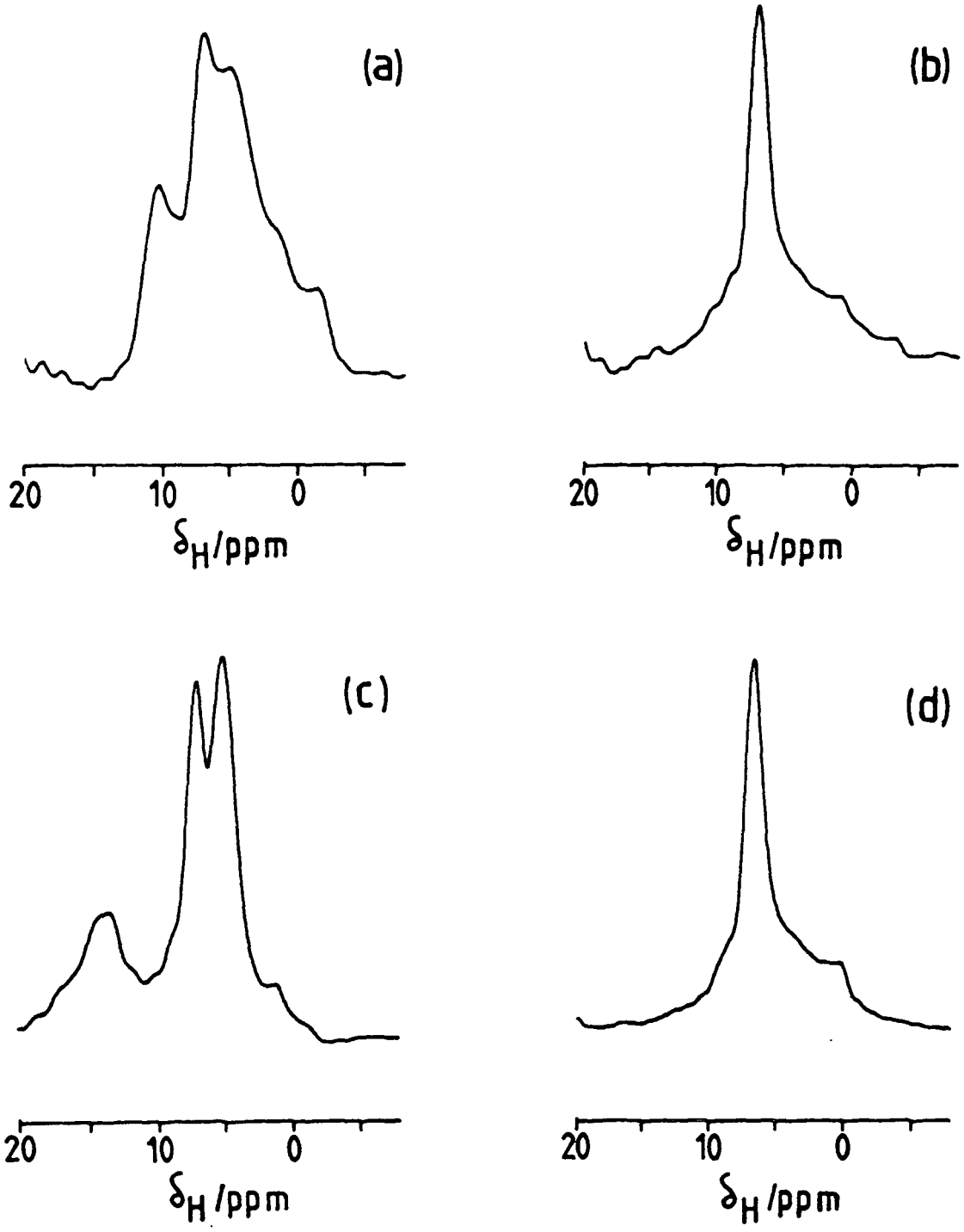

Figure 5.5 : ^1H CRAMPS Spectra of Samples 1 to 4

Recycle delay = 10 s, 90^0 pulse duration = 3 μs
spinning rate = 2.5 kHz, number of transients = 64
frequency offset = 5000 Hz

(a) Sample 1 (b) Sample 2
(c) Sample 3 (d) Sample 4

ppm (see Chapter 4) it would seem reasonable to assign this resonance to the ammonium ion. The underlying signal may be due to water or even an artifact.

Sample 1 gave a complicated CRAMPS spectrum, with resonances at 10.5, 7.0, 5.0, 2.0 and -1.5 ppm. Comparison with Figure 5.4 reveals that part of the spectrum can be assigned to brushite, namely the resonances at 10.5, 5.0, and -1.5 ppm. The resonance at 7.0 ppm almost certainly being due to $(NH_4)^+$, the resonance at 2.0 ppm as yet being unassigned.

Sample 3 showed three main resonances at 13.5, 7.0, and 5.0 ppm. Comparison with Figure 5.5 reveals that the signal at 13.5 ppm is due to monetite. Once again the signal at 7.0 ppm is assignable to $(NH_4)^+$. The resonance at 5.0 ppm has not been conclusively identified. However, it occurs in the same spectral region as water. If the species is water, it must be highly mobile since the linewidth observed is significantly narrower than for bound water found in brushite (for example).

In conclusion, it is clear that ^1H CRAMPS has been extremely useful in the study of this particular series of samples. The presence of brushite and monetite in samples 1 and 3 respectively has been proven beyond reasonable doubt. When compared with the phosphorus data, the CRAMPS results tie in well. The CP spectrum of sample 1 indicates a species

consisting of protonated phosphate units with a chemical shift (1.2 ppm) identical to that of pure brushite. Likewise sample 3 shows phosphorus NMR evidence for the presence of monetite in the form of the shoulder at -1.7 ppm. in the SPE spectrum. The ^{1}H CRAMPS spectra suggest the presence of $(NH_4)^+$ in samples 2 and 4, but from the ^{31}P spectra it would appear that it is not present in the form of an ammonium phosphate species in significant amounts.

5.3.1.3 Proton Relaxation Time Data

Proton spin-lattice relaxation times were made using a homebuilt spectrometer operating at a field strength of 1.41 T. The T_1 data successfully picked out the different proton characteristics for samples 1 and 3 (T_1 = 0.14 and 0.10 s respectively) compared to samples 2 and 4 (T_1 = 0.33 and 0.32 respectively). Thus the proton environments in the two types of sample are different, consistent with the phosphorus NMR data, indicating the presence of protonated phosphate units in samples 1 and 3 and only non-protonated phosphate in samples 2 and 4.

5.3.1.4 Electron Microscope Photographs

Use was made of the scanning electron microscope (SEM) facility at the Food Research Institute, Norwich. The four samples were studied at a number of magnifications and a selection of photographs are shown in Figure 5.6.

Samples 2 and 4 were very similar in appearance, consisting of approximately spherical particles of diameter ca. 175 Å.

Sample 1 was rather different. At low magnification (x640), particles of size ca. 3.5 microns were observed. They appeared to be of a polycrystalline nature. At higher magnification (x20,000), a second phase could be observed consisting of randomly shaped particles of approximate size 200 Å.

Sample 3 showed very interesting SEM photographs. At low magnification (x640) particles several microns across were observed. Within these aggregates needle and plate like crystals were apparent. At higher magnification (x20,000), no isolated small particles were observed. It would appear that any small particles have been incorporated into the bulk structure of the aggregates.

In conclusion, the SEM photographs have indicated that samples 2 and 4 are very similar, but different to either samples 1 or 3. Samples 1 and 3 are clearly different to each

Figure 5.6 : SEM Photographs of samples 1 to 4
(Magnification indicated in brackets next to sample name)

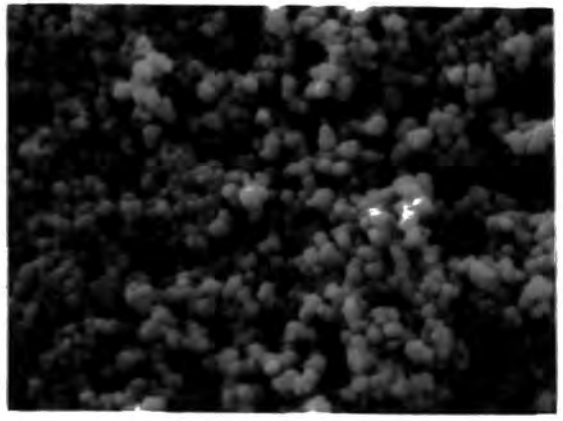

Sample 2 (x20,000)

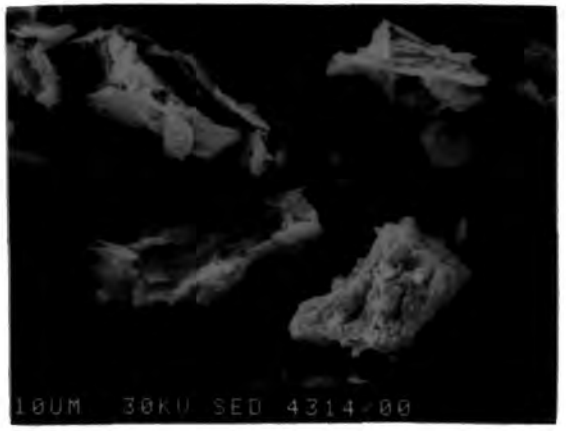

Sample 1 (x640)

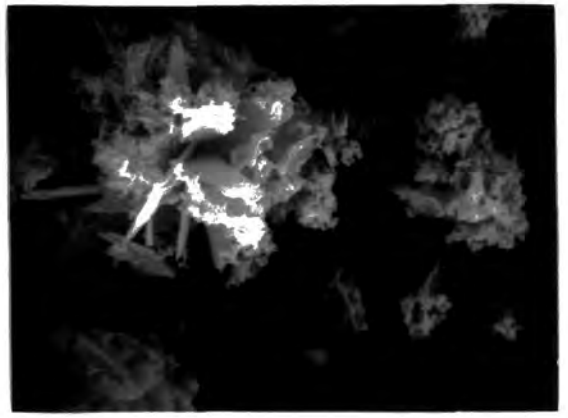

Sample 3 (x640)

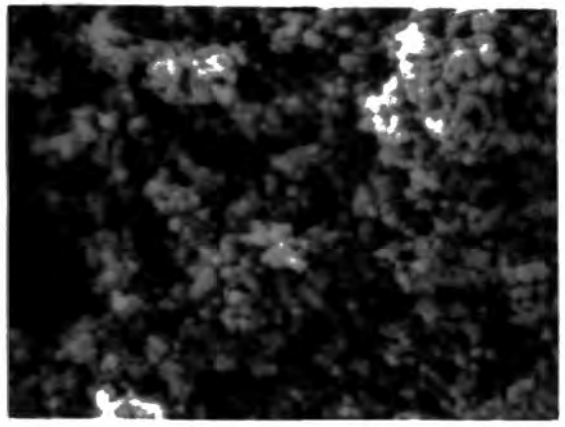

Sample 4 (x20,000)

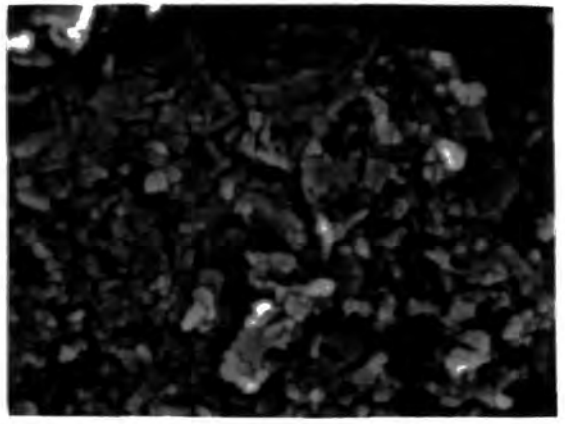

Sample 1 (x20,000)

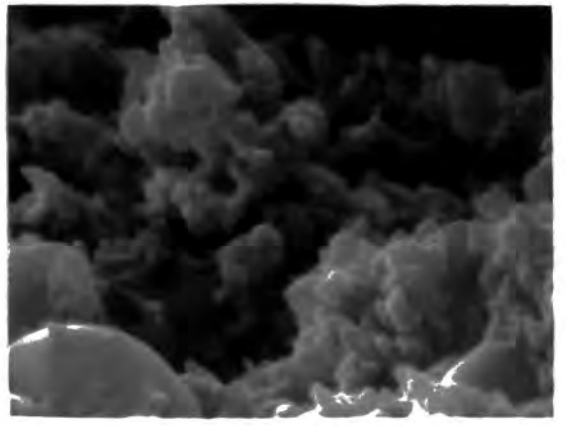

Sample 3 (x 20,000)

other, although the species present cannot be identified on the basis of the photographs. The information obtained from SEM photographs thus complements the NMR findings.

5.3.1.5 Summary of Infra-red, X-ray and EXAFS Data for Samples 1 to 4

Infra-red, X-ray and EXAFS data for this series of samples were acquired and interpreted by J. E. Harries and D. W. L. Hukins and are briefly summarised here in order to enable comparison with the NMR data.

Sample 1 gave an infra-red spectrum that closely resembled that of pure hydroxyapatite, although an additional maximum and two slight shoulders were also evident in the spectrum, suggesting that another phase may have been present. X-ray powder diffraction yielded a pattern that was not of apatite.

Infra-red data for sample 2 indicated that the sample was similar to hydroxyapatite and in fact was a poorly crystalline apatite. X-ray diffraction gave a pattern characteristic of HAP although the diffraction lines were generally broader than those associated with well crystalline HAP. EXAFS measurements showed that over a short distance (approx. 2.2 Å) which corresponds to the nearest-neighbour oxygen shell of the calcium atom, the sample was very like hydroxyapatite. However longer range order was somewhat reduced. There was

evidence for a slight difference in the radial distribution function compared to HAP, suggesting that some other structural feature may have been at work.

The infra-red spectrum of sample 3 indicated that more than one crystal phase was present. X-ray diffraction gave the same pattern as for sample 1.

Sample 4 was confirmed to be very similar to sample 2 using infra-red and X-ray methods, with evidence for marginally better crystallinity.

In conclusion it can be seen that the non-NMR data ties in very well with the conclusions drawn from solid state NMR. Clearly NMR is a viable and accurate means of characterising systems of this type.

5.3.2 A Detailed Study of Sample 3

On a later occasion samples 1 to 4 were reinvestigated using NMR. The spectra were accurately reproduced in all cases except for sample 3. Although sample 3 was of little interest from the point of view of ACP compounds it was interesting in its own right and was chosen for detailed study.

Figure 5.7 shows a comparison of CP and SPE spectra run 45 days after the spectra shown in Figure 5.3. The most significant changes have taken place in the CP spectrum, where the single sharp line has been replaced by a broad band consisting of several resonances. Additionally a resonance at -6.5 ppm. with a rich sideband manifold has appeared (indicated by arrows in Fig. 5.7) Resolution enhancement of the centrebands revealed six distinct resonances (Figure 5.8). Comparison of the observed shifts enabled assignment of resonances 4 and 5 to monetite. Dipolar dephasing spectra (Fig. 5.9) acquired on a later occasion provided supporting evidence for this assignment, with the high-frequency signal (resonance 4) being suppressed most easily, as was observed for monetite in chapter 4, Fig. 4.6(b). Further supporting evidence came from ^{1}H CRAMPS data discussed earlier in this chapter and some more recent CRAMPS spectra presented later in this section. Shielding tensor analysis for peak 5 gave tensor components of 46, 9, and -50 compared to 42, 4, and -44 for monetite (Chapter 4 Table 4.3), which is considered to be within experimental error in view of the complexity of the spectrum of sample 3. The four remaining phosphorus sites in the sample could not be conclusively identified. However, differences in the intensity of the sideband patterns imply that some species were protonated whereas others were unprotonated. The chemical shift data and intensity of sidebands for sample 3 are summarised in Table 5.4.

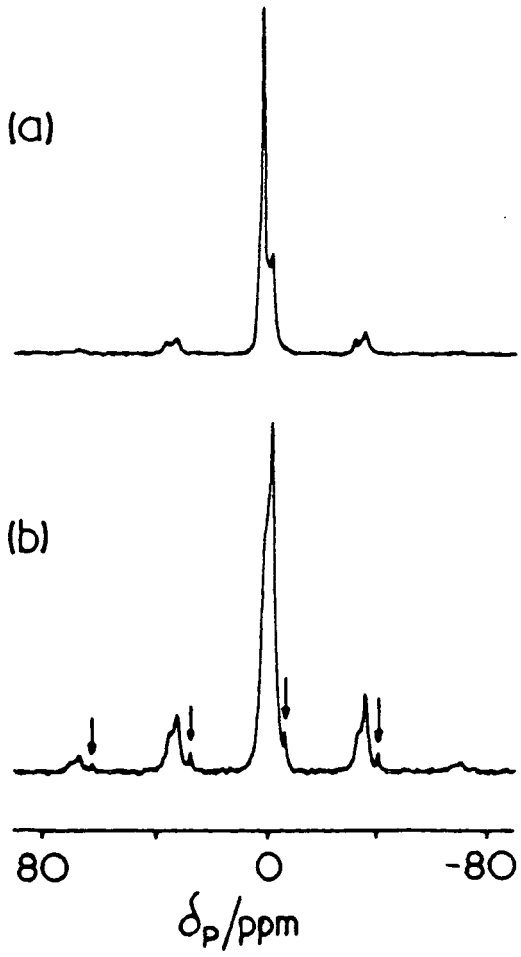

Figure 5.7 : Sample 3, comparison of ^{31}P CP and SPE spectra 45 days after acquisition of spectra shown in Figure 5.3. Spectrometer parameters as for Figure 5.3 except number of transients = 80

(a) SPE/HPPD/MAS
(b) CP/HPPD/MAS, Arrows indicate low intensity, highly anisotropic resonance at -6.5 ppm.

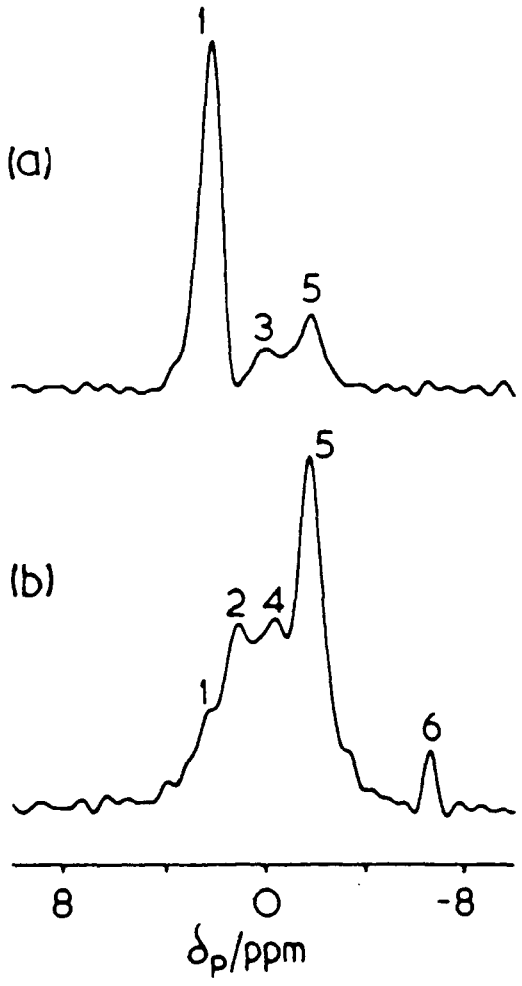

Figure 5.8 : Sample 3, centreband expansions for the ^{31}P spectra shown in Figure 5.7. 100 Hz resolution enhancement was carried out.

(a) SPE/HPPD/MAS
(b) CP/HPPD/MAS

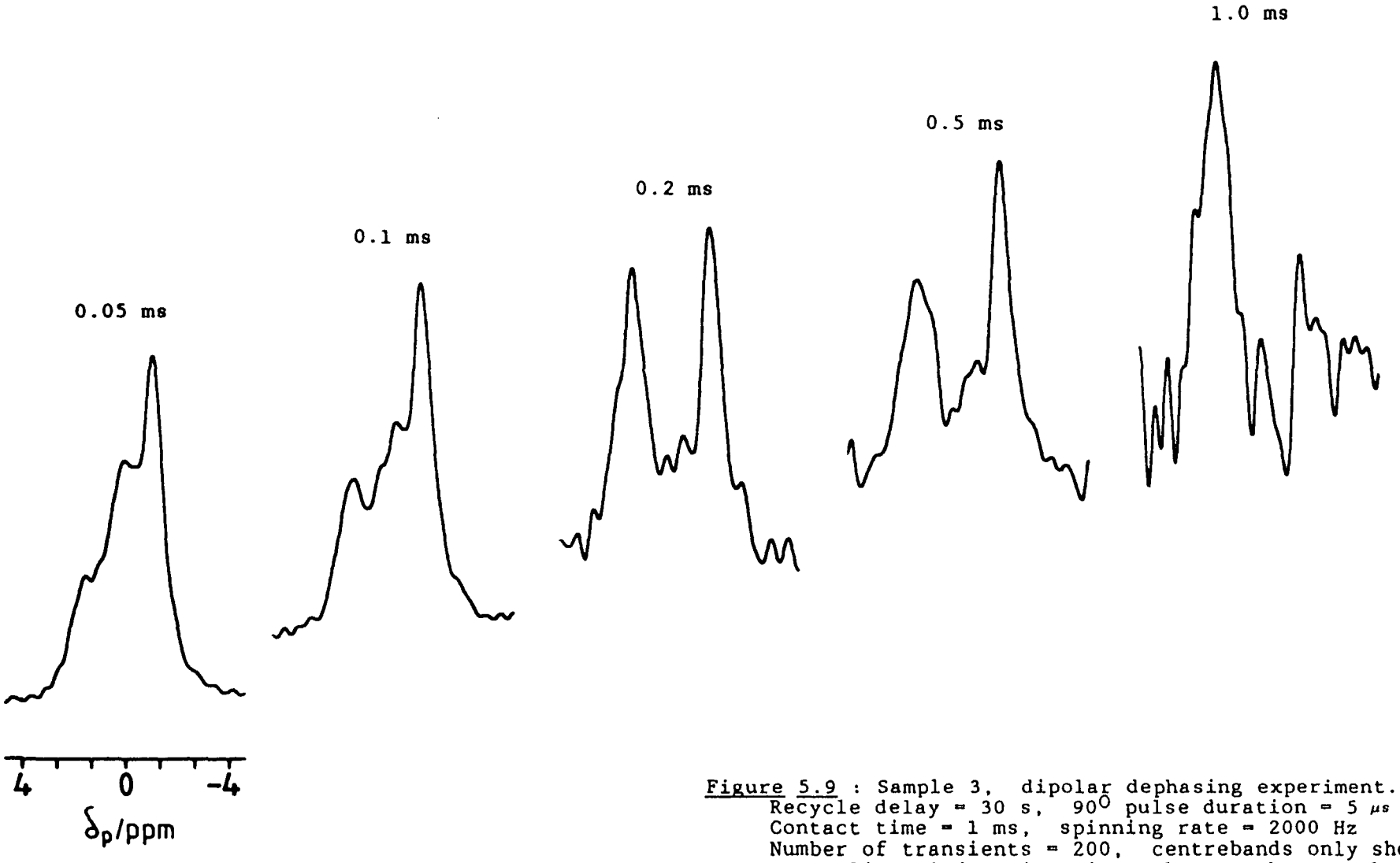

Figure 5.9 : Sample 3, dipolar dephasing experiment.
Recycle delay = 30 s, 90^{0} pulse duration = 5 μs
Contact time = 1 ms, spinning rate = 2000 Hz
Number of transients = 200, centrebands only shown.
Decoupling window time given above each centreband.
All spectra scaled to the same height

Table 5.4 : Summary of CP and SPE data for sample 3.

Resonance	^{31}P Chemical shift / ppm. CP	SPE	Sideband Intensity
1	+2.3	+2.3	weak
2	+1.3	----	intense
3	----	+0.2	weak
4	-0.2	----	intense
5	-1.7	-1.7	intense
6	-6.5	----	intense

Changes continued to be observed (especially in the peak intensities of the SPE spectra) each time the sample was studied. In Figure 5.10, a series of SPE spectra are shown illustrating the way in which the relative amount of monetite varies. The actual processes responsible for the changes are not clear. It may be that maturation and/or changes of moisture content within the sample are taking place despite constant storage conditions.

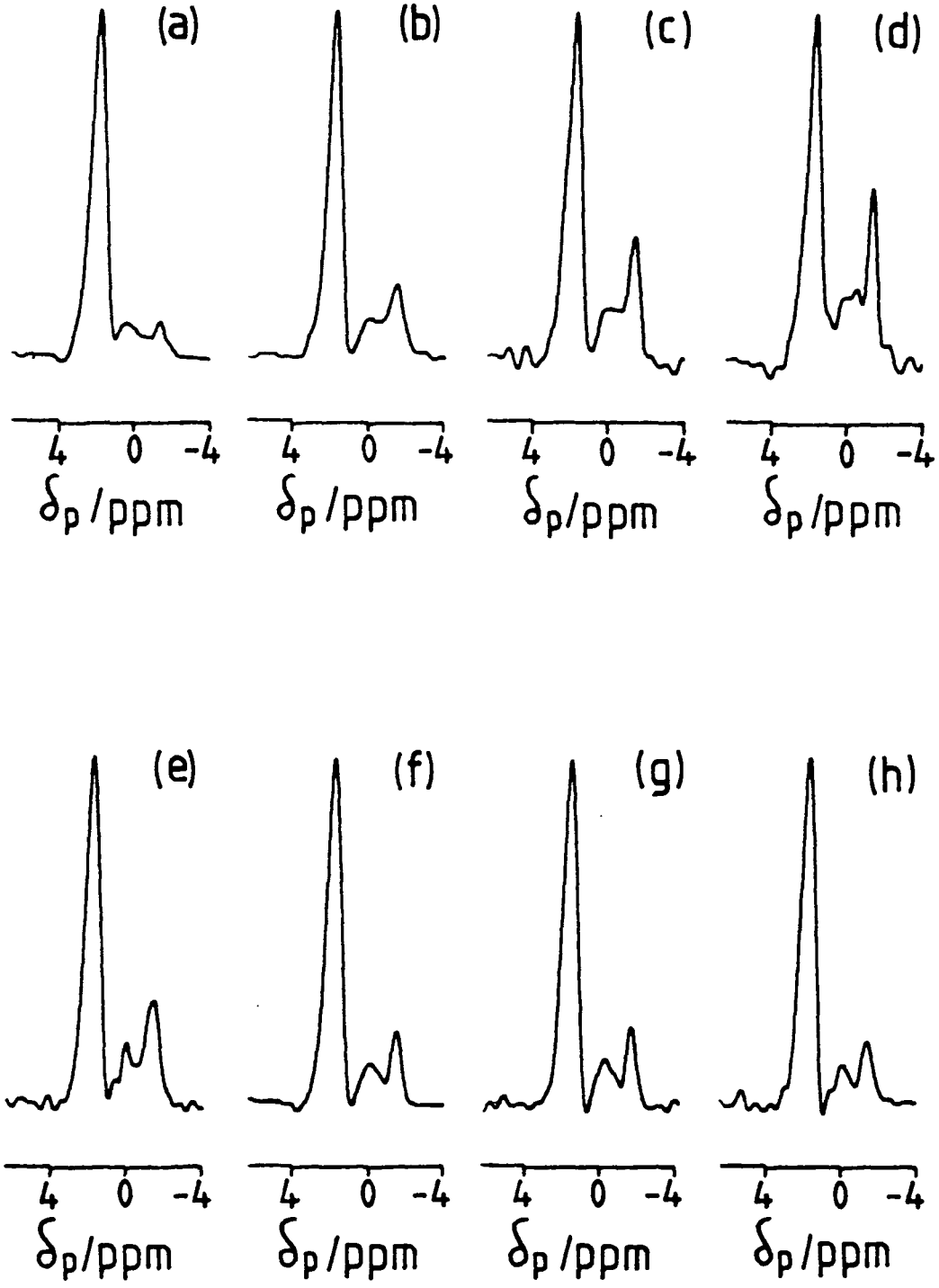

Figure 5.10 : Sample 3, SPE/HPPD ^{31}P spectra run on eight separate occasions. Parameters as for Fig 5.3 but with varying number of transients. (Scaling such that main peak heights remain constant)
(a) Original spectrum; (b) after 45 days; (c) after 85 days; (d) after 104 days; (e) after 238 days; (f) after 290 days; (g) after 340 days; (h) after 436 Days.

A further quantity of sample 3 was obtained from J. E. Harries and D. W. L. Hukins. The storage conditions for this and the original sample had inevitably been slightly different, so some differences in the spectra were expected. For simplicity the two samples will be referred to using the terms "old" and "new". Both samples were investigated using ^{31}P CP and SPE experiments and also using the ^{1}H CRAMPS technique.

The phosphorus SPE spectra (Figure 5.11) of "old" and "new" samples were very similar. The major difference between the samples was observed in the CP spectra, where the resonance at 2.2 ppm was absent for the "new" sample. The ^{1}H CRAMPS spectra (illustrated in Figure 5.12) proved very interesting since the two samples gave rather different spectra. The spectrum obtained for the "old" sample reproduced quite closely the spectrum obtained on an earlier occasion (recall Figure 5.5(c)). The band at 13.1 ppm was assigned to monetite, the resonance at 7.1 ppm to $(NH_4)^+$ protons, and the band at 5.1 ppm to water. The low-frequency resonance could not be assigned. The "new" sample gave a very different spectrum with a band at 7.0 ppm. due to $(NH_4)^+$ protons and a sharp resonance at 4.7 ppm assignable to mobile water. The presence of mobile water in this sample did not come entirely as a surprise since the sample had a very damp appearance. An initially worrying feature of the CRAMPS spectrum was the absence of a signal due to protons in

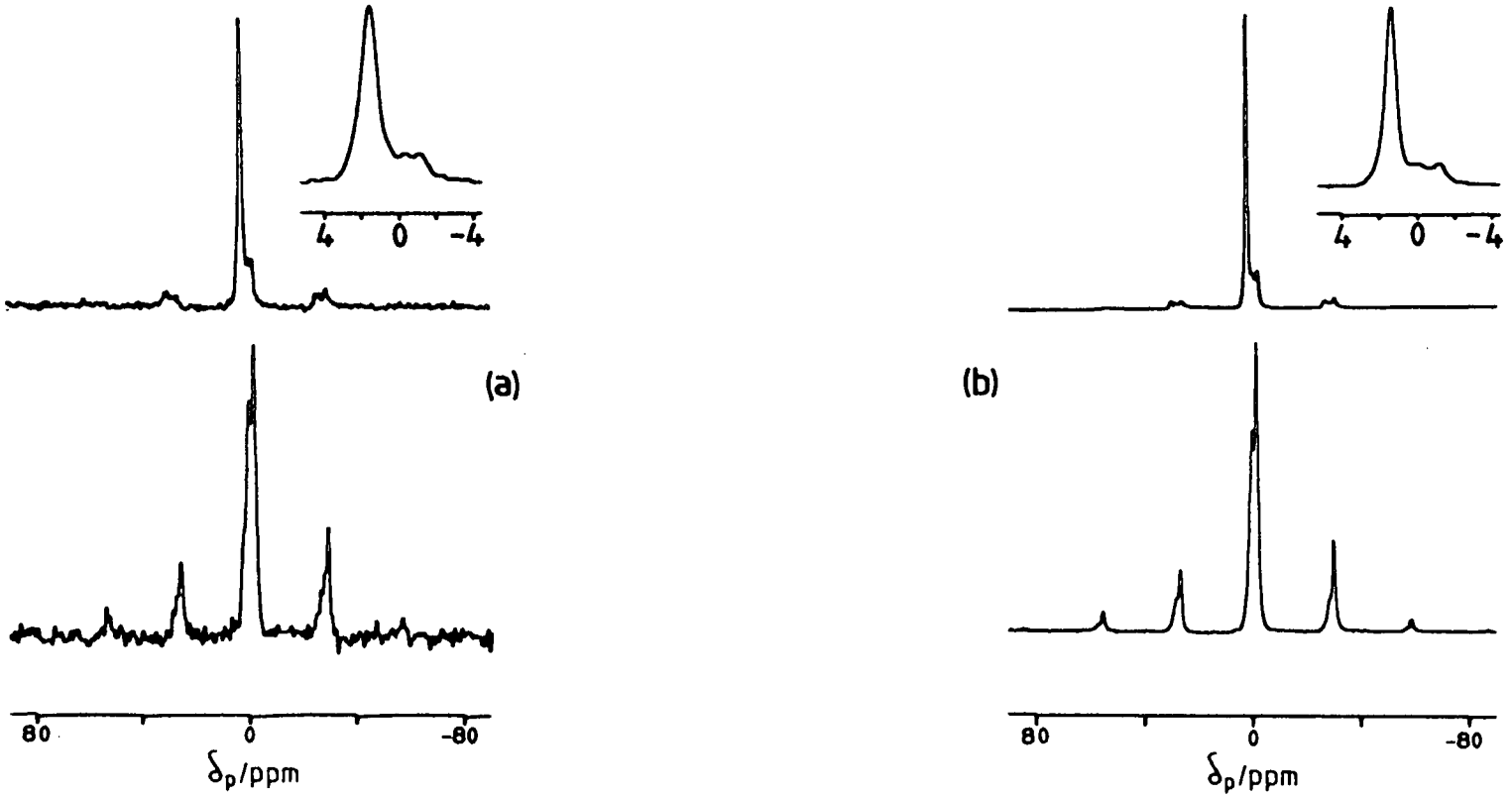

Figure 5.11 : Comparison of CP and SPE spectra for "old" and "new" sample 3.

Spectra acquired 646 days after spectra in Fig. 5.3
Recycle delay = 30 s, 90^0 Pulse length = 5 μs
Number of transients = 200, spinning rate = 2.4 kHz, CP contact time = 1 ms
(a) "Old" sample 3, Top: SPE/HPPD/MAS, Bottom: CP/HPPD/MAS.
(b) "New" sample 3, Top: SPE/HPPD/MAS, Bottom: CP/HPPD/MAS.

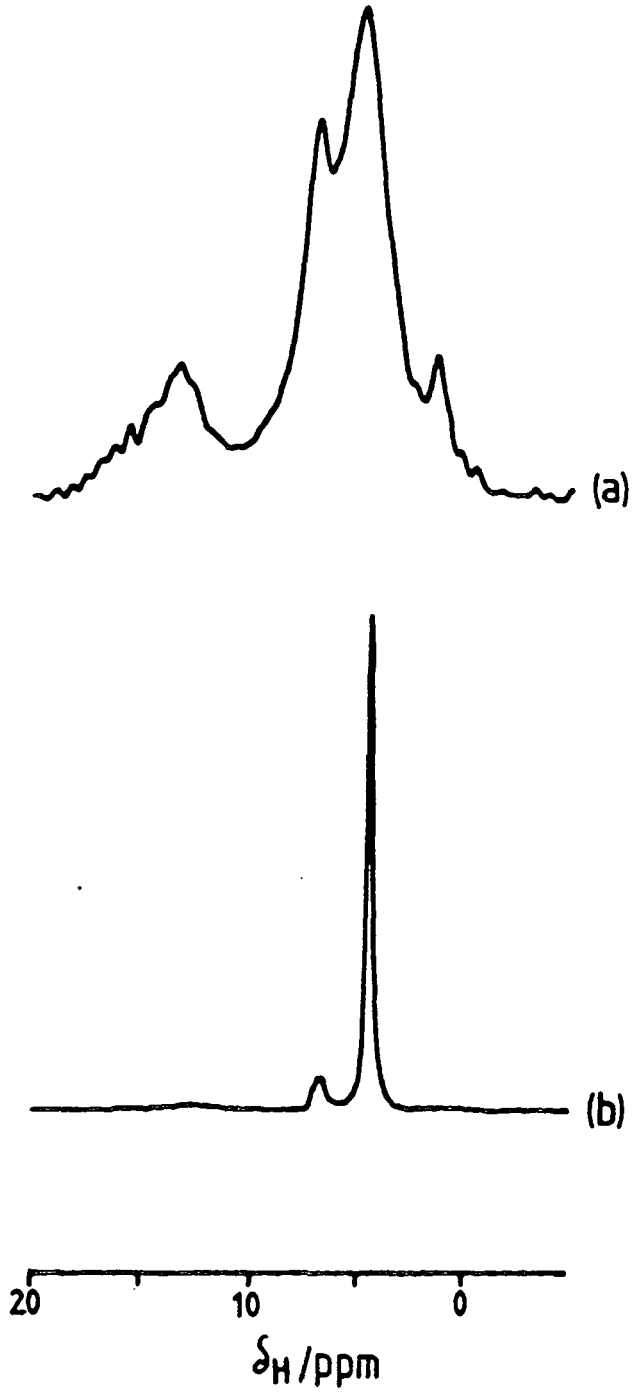

Figure 5.12 : Comparison of ^1H CRAMPS spectra for "old" and "new" sample 3

Recycle delay = 10 s, 90^0 Pulse length = 2 μs,
spinning rate = 2400 Hz, number of transients = 32,
frequency offset = -1000 Hz.

(a) "Old" sample 3 (b) "New" sample 3

monetite, especially when a monetite signal had been observed in both SPE and CP ^{31}P spectra. Closer inspection of the CRAMPS spectrum revealed that monetite protons were indeed present, but in low concentration compared to mobile water. Figure 5.13 shows a vertical expansion of the CRAMPS spectrum of the "new" sample, obtained after further refinement of the spectrometer tune-up. The triplet structure due to $\{^{14}N\text{-}^{1}H\}$ scalar coupling (J=50 Hz) in the $(NH_4)^+$ region is now resolved and the monetite signals are evident. This spectrum is an example of the resolution and dynamic range that can be achieved for a well set up CRAMPS experiment. Having resolved the $(NH_4)^+$ triplet structure for the "new" sample, effort was made to resolve similar structure for the "old" sample. A complicating factor in attempting to resolve this structure was the broad water resonance underlying the $(NH_4)^+$ signal. An inversion recovery experiment was performed in place of the preparation pulse for the CRAMPS sequence. The series of spectra obtained are illustrated in Figure 5.14. It is clear that the water signal recovers most rapidly, a null for this resonance was obtained when a recovery delay of 40 ms was used. In the spectrum corresponding to the water signal being at a null (Figure 5.14(e)), there was evidence of fine structure in the $(NH_4)^+$ region. Figure 5.15 shows the spectrum, resolution enhanced and inverted (for ease of viewing). The $\{^{14}N\text{-}^{1}H\}$ triplet structure is clearly evident, with J=47 Hz. From the spectra of both samples it would appear that the proportion of $(NH_4)^+$ compared to monetite is

Figure 5.13 : ^{1}H CRAMPS spectrum of "New" sample 3
(Acquired after further spectrometer adjustment)

Recycle delay = 10 s, 90^{0} Pulse length = 2 μs,
spinning rate = 2400 Hz, number of transients = 32,
frequency offset = -1000 Hz.
*Adamantane reference

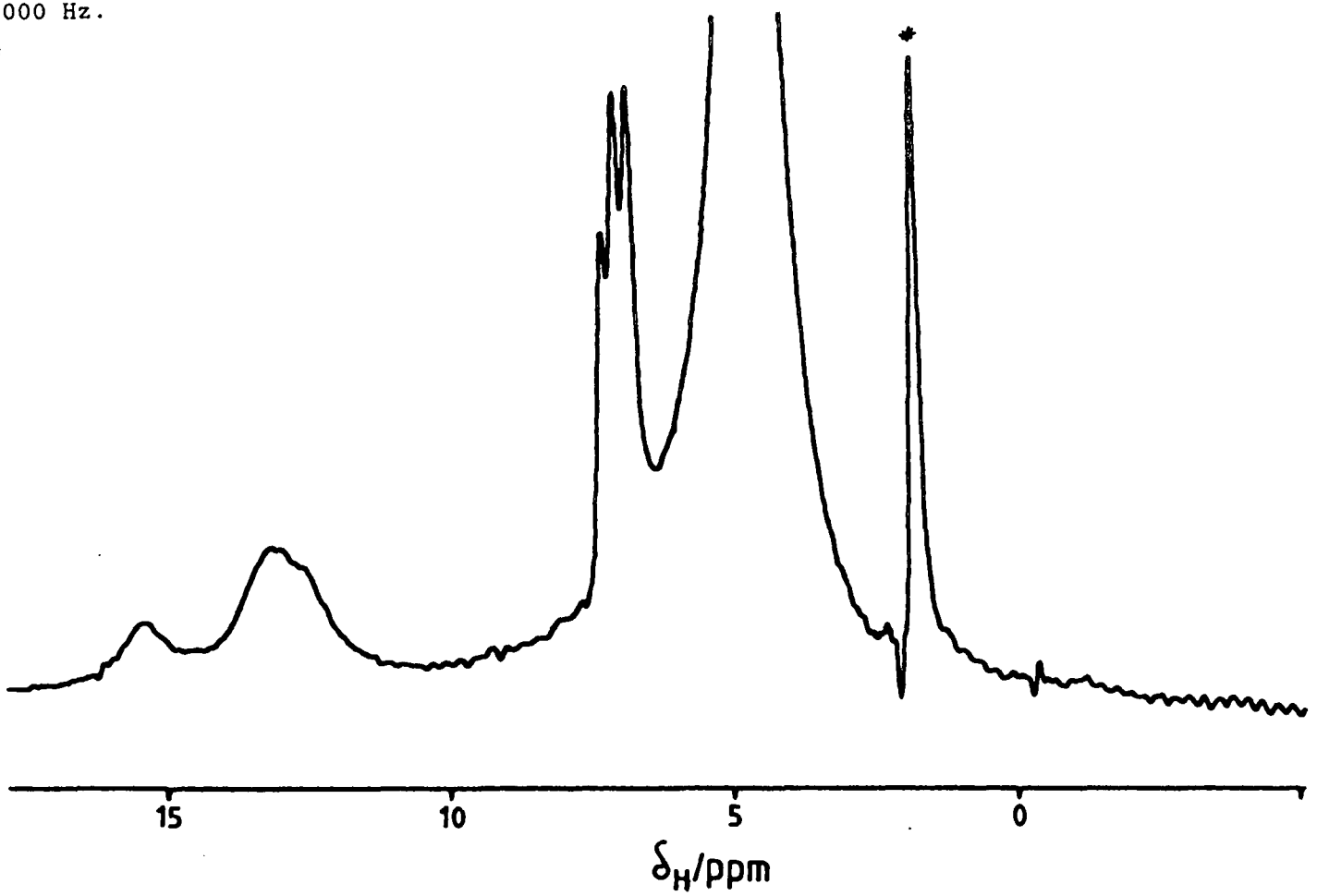

Figure 5.14 : "Old" Sample 3 ^{1}H Inversion recovery experiment with ^{1}H CRAMPS acquisition

Recycle delay = 60 s, 90^{o} Pulse length = 2 μs,
spinning rate = 2400 Hz, number of transients = 100,
frequency offset = -3000 Hz.
Recovery delays as follows: (a) 1 μs, (b) 1 ms, (c) 10 ms, (d) 30 ms
(e) 40 ms, (f) 50 ms, (g) 100 ms, (h) 500 ms

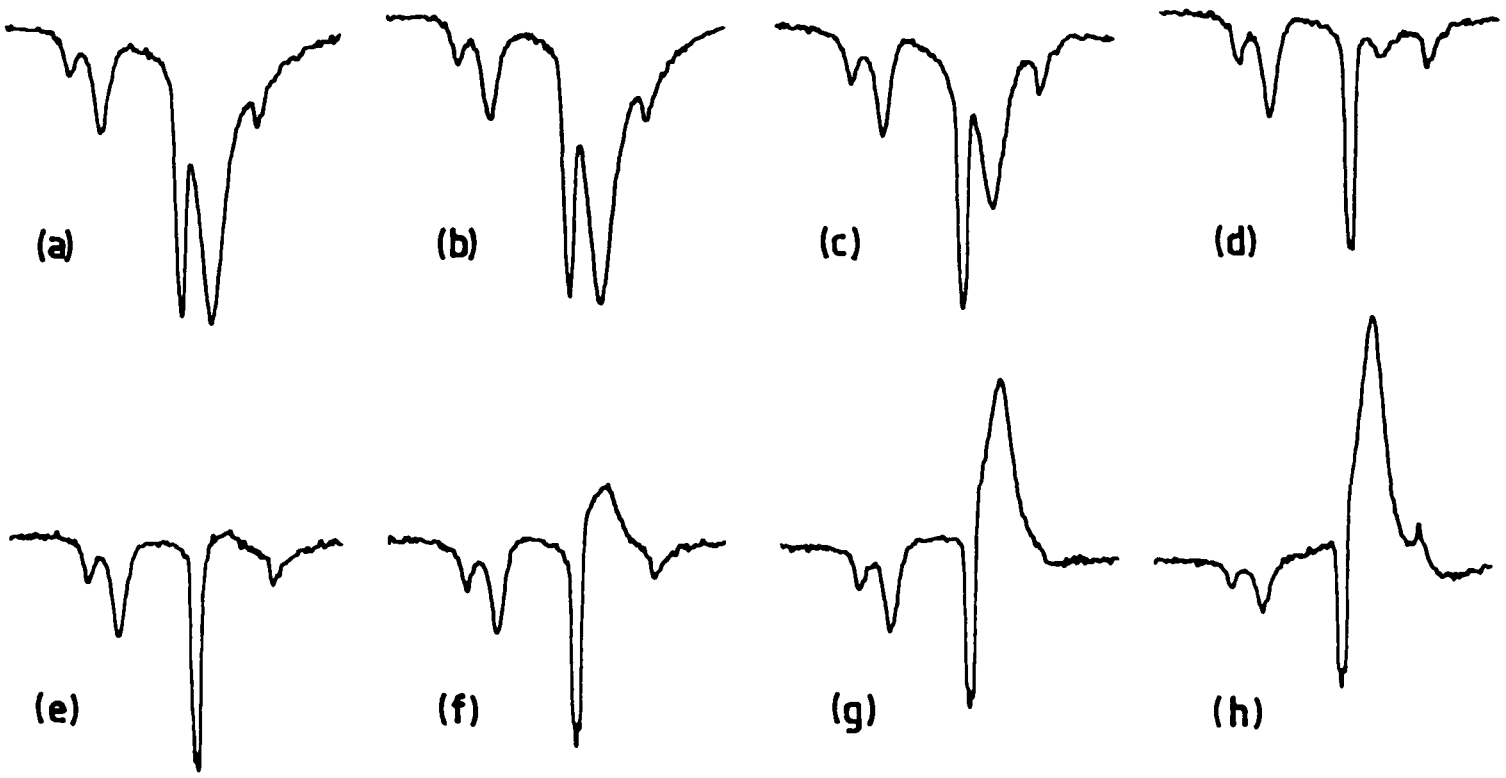

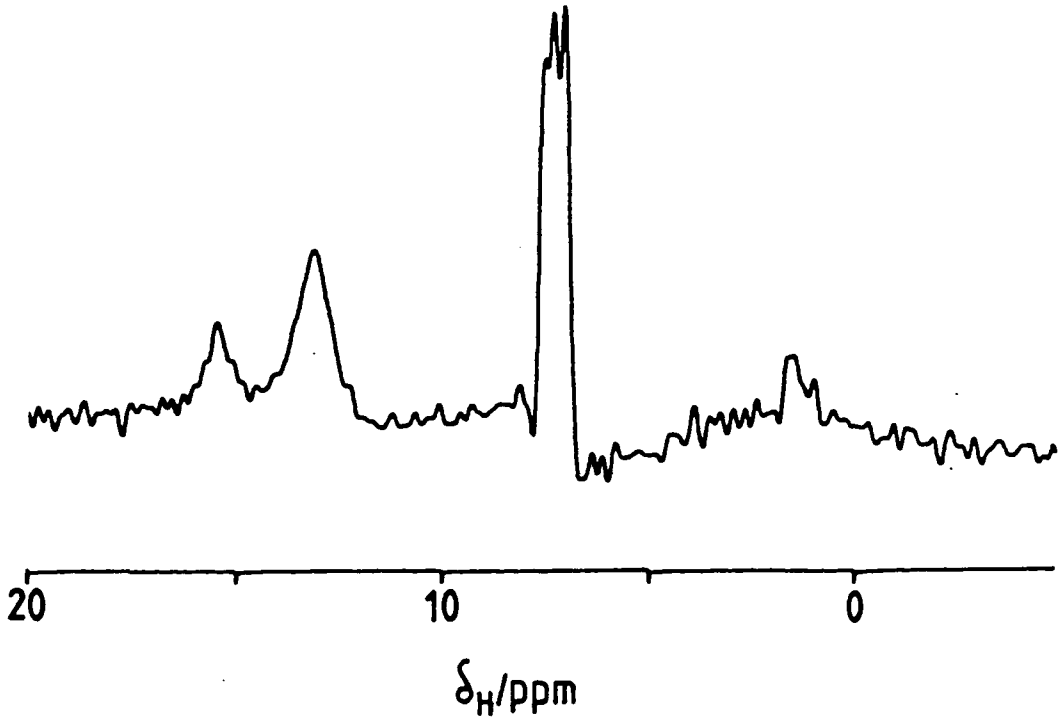

Figure 5.15 : "Old" sample 3 ; expansion of spectrum shown in Fig. 5.14(e)

Inverted for ease of viewing.
Resolution enhanced to highlight triplet structure.

quite large, although it would seem that it is not present in the form of an ammonium phosphate since the ^{31}P chemical shifts of mono, di- and tri-ammonium phosphate (0.8, 1.1 and 3.1ppm. respectively) do not coincide with those of any resonance of sample 3.

In conclusion, ^{31}P and ^{1}H NMR experiments have given a great deal of information regarding the nature of sample 3. It would appear that the storage conditions of the samples were of considerable importance, because "old" and "new" samples gave different spectra. The most significant differences were observed in the CRAMPS spectra, in particular the water region, thus giving evidence that water content within the sample is variable according to the conditions of sample storage. ^{1}H CRAMPS is a valuable technique for studies of systems of this type, giving a wealth of information to complement ^{31}P NMR studies.

5.3.3 ACP SAMPLES

5.3.3.1 ^{31}P NMR Studies

The ACP samples had ^{31}P linewidths of up to 500 Hz indicating that they were amorphous. A typical pair of CP and

SPE spectra are shown in Figure 5.16 and a summary of the chemical shift and linewidth data for the series ACP samples is given in Table 5.5.

Table 5.5 : Summary of ^{31}P chemical shift and linewidth data for the ACP series of compounds.

Sample	Cross-polarization		Single-Pulse-Excitation	
	Shift/ppm	Linewidth/Hz	Shift/ppm	Linewidth/Hz
ACP	3.3	550	3.2	520
ACP19H	3.0	430	2.9	330
ACP22H	2.9	290	2.9	175
ACP26H	3.1	280	2.9	160
ACP5D	2.9	175	2.8	120
ACPCO3-1	2.7	412	2.7	276
ACPCO3-2	3.0	452	3.0	434
ACPCO3-3	3.0	485	2.9	455

All of the spectra showed weak spinning sidebands, indicating that the phosphate units were not protonated. However, since some sidebands were observed, it is likely

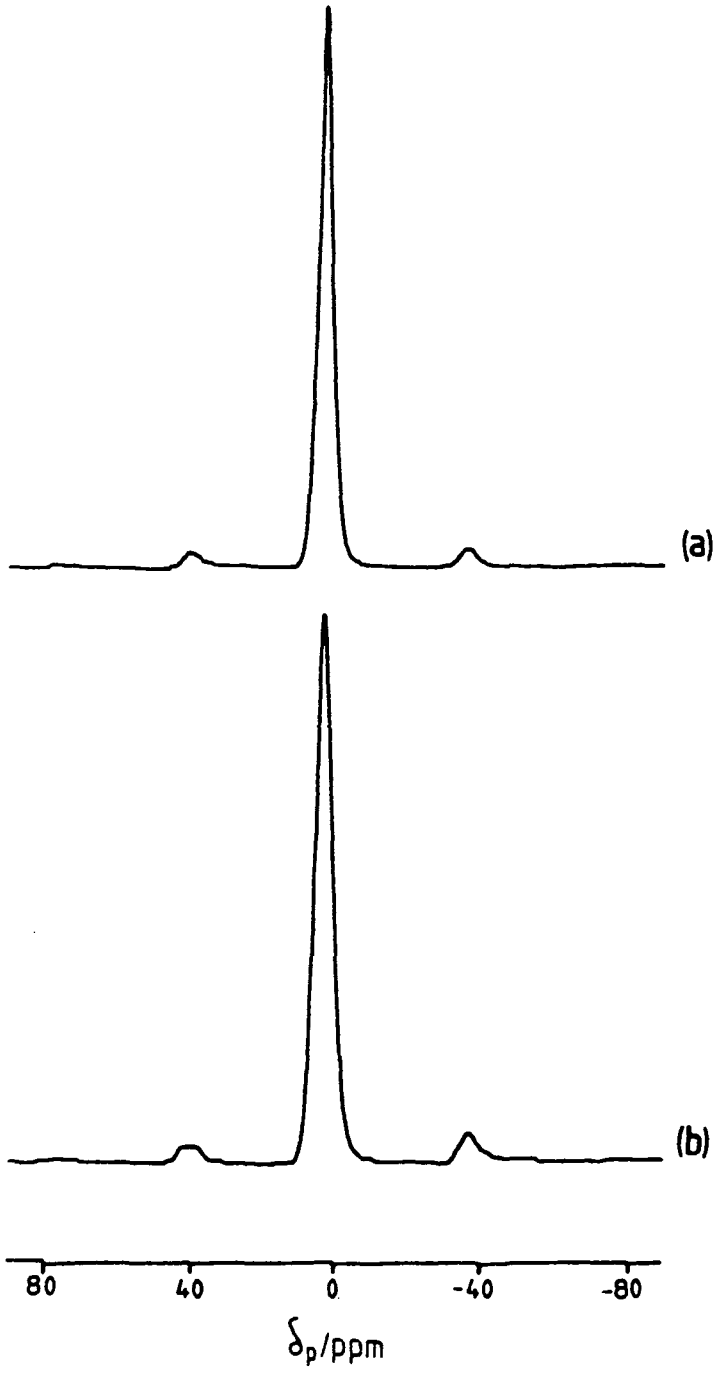

Figure 5.16 : ACP19H - ^{31}P SPE and CP spectra

Recycle delay = 20 s, 90^0 Pulse length = 5 μs,
spinning rate = 3130 Hz, number of transients= 200
(a) SPE/HPPD/MAS (b) CP/HPPD/MAS, contact time = 1 ms

that the phosphate units are either distorted or weakly bound to protons, perhaps from nearby water molecules. For all samples it was possible to get a reasonable CP spectrum. Thus protons (from which the phosphorus magnetisation is derived) are near to the phosphate units. All of the ACP spectra consisted of a single line with a chemical shift very similar to that of hydroxyapatite, which is not surprising when one recalls that ACP is a precursor phase to HAP. A decrease in linewidth in both CP and SPE spectra was observed with increasing maturation time, indicating a growth in crystallinity. An interesting feature seen in the spectra of all the samples studied was that CP linewidths were greater than for SPE experiments and also that the sideband intensity compared to the centreband was always greatest in the CP spectrum. This can be interpreted as there being at least two types of phosphate unit present, types A and B say. Both species appear to be poorly crystalline, but type A (CP experiment) must be closest to protons as it shows the more intense sidebands and it cross-polarizes more efficiently than the species B observed in the SPE spectrum. The broader linewidth observed in the CP spectrum may be due to the poor crystallinity of A or it may simply be that A and B have slightly different shifts and that both resonances contribute to the observed CP linewidth. ACP5D gave the sharpest lines and was thus the most crystalline sample, but even so the linewidth would have to fall below 100 Hz before it could be considered to be a well-crystallized hydroxyapatite.

The carbonated ACP samples also showed similar trends (Table 5.5) to those that have just been mentioned for the ACP samples. In addition it should be noted that for the ACPCO3 samples the linewidths observed were greater than for an ACP sample matured for the same length of time in the absence of carbonate. ACPCO3-1 clearly shows two phases. Both have a shift of 2.7 ppm but they have very different linewidths, as can be seen by comparing CP and SPE spectra. It can be concluded that the two phases have very different crystallinity, but, even so, the most ordered phase (B) is still less crystalline than ACP22H. Thus the introduced carbonate is impairing ordering of the phosphate units within HAP and it appears to do it most efficiently for the type A component of the ACP. Samples ACPCO3-2 and ACPCO3-3 showed even poorer crystallinity with increased carbonate content, although the distinction between components A and B has become much smaller.

5.3.3.2 ^{1}H NMR Studies

Proton CRAMPS, wideline and T_1 measurements were also made on the ACP series of compounds, but in the most part were rather disappointing.

The ^{1}H CRAMPS spectrum of ACP is illustrated in Figure 5.17. The spectrum is rather featureless, with a broad band

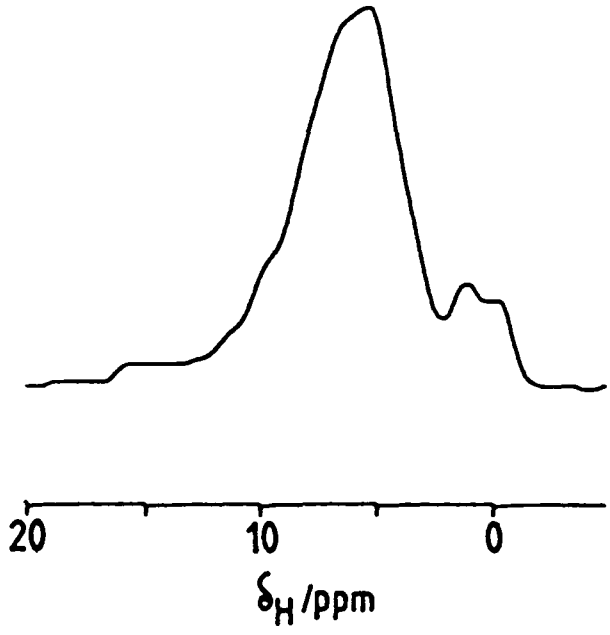

Figure 5.17 : ^1H CRAMPS spectrum of ACP

Recycle delay = 10 s, 90^0 Pulse length = 2 μs,
spinning rate = 2400 Hz, number of transients = 64,
frequency offset = -1000 Hz.

at ca. 6.0 ppm. probably due to a combination of bound water and weakly hydrogen-bonded protons. The presence of $(NH_4)^+$ protons could not be ruled out. The other features at 2.0 ppm and 0.0 ppm have not been conclusively assigned. It is possible that the signal at 2.0 ppm is due to adamantane contamination of the rotor. Adamantane, the ^1H CRAMPS reference sample, has been observed to be absorbed by the rotor material and has a chemical shift of 1.74 ppm. The signal at 0.0 ppm may be due to OH^-. The other ACP samples gave very similar CRAMPS spectra. Thus it would appear that the technique is insensitive to maturation of the ACP samples.

Wideline spectra were acquired for the ACP samples and were all very similar. Spectra of ACP and ACP5D are illustrated in Figure 5.18 in order to demonstrate the two extreme types of wideline spectra obtained. In both spectra a central resonance of linewidth 1.3 kHz was observed which can be attributed to mobile water. In the cases of ACP (Figure 5.18(a)) and ACP19H (not shown) there was evidence of a broad doublet with splitting ca. 50 kHz which could be assigned to tightly bound water. This structure was not present in the spectra of the more mature samples.

Proton T_1 data (measured at 4.7 T and 7.04 T) for the ACP samples are given in Table 5.6. All samples gave single exponential behaviour, with T_1 values becoming shorter with increasing sample maturation period. It is also interesting to note that ACP and ACP19H have significantly longer T_1

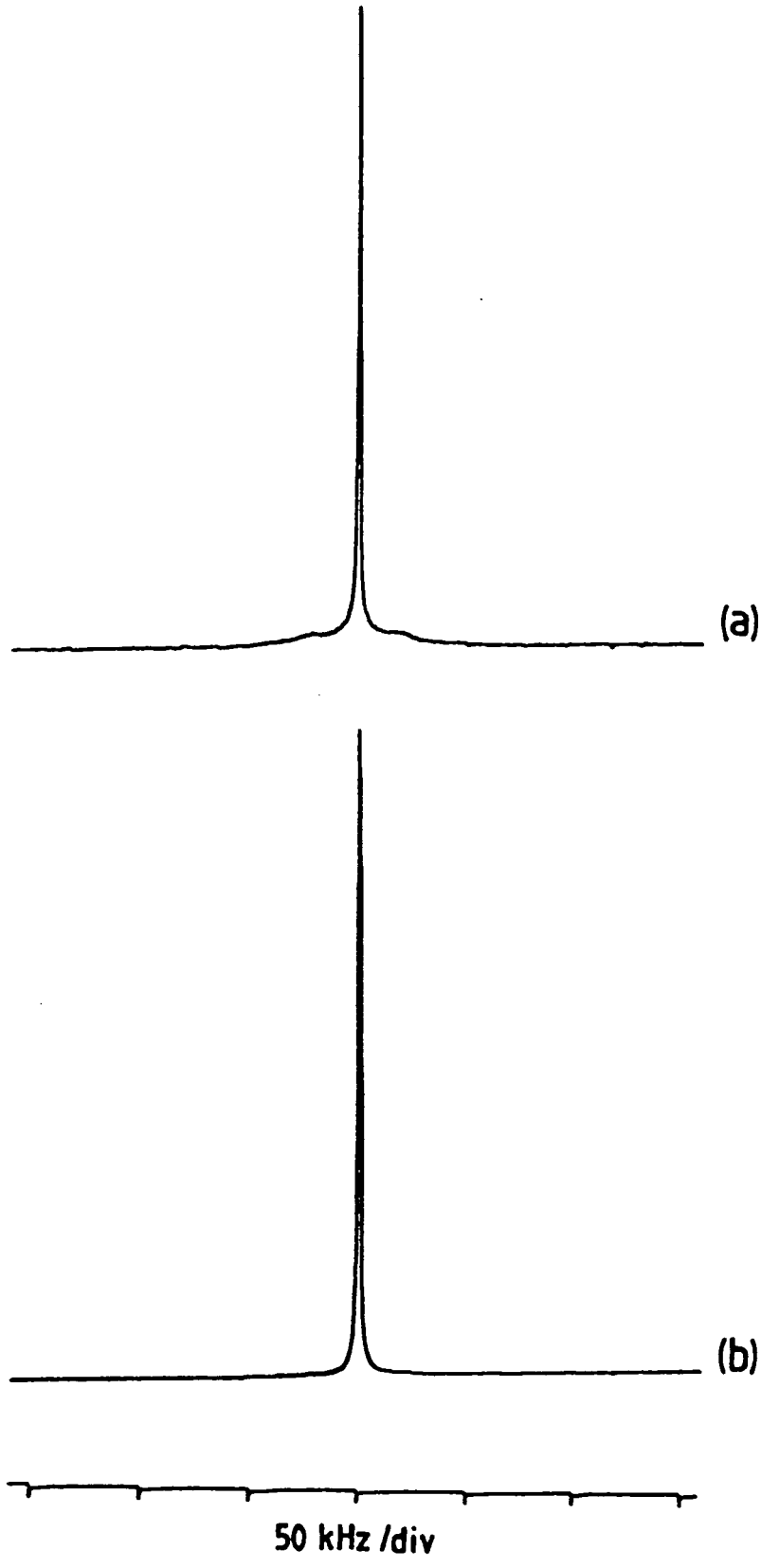

Figure 5.18 : ^{1}H static wide-line spectra of ACP and ACP5D
Recycle delay = 10 s, 90^{0} Pulse length = 1.5 μs, number of transients = 8
(a) ACP (b) ACP5D

values compared to the other samples. These were the only samples to show doublet structure due to tightly bound water in their wideline spectra. It is therefore probable that the T_1 data is distinguishing between systems containing tightly bound water and those that do not (a shorter relaxation time indicates a more mobile species).

Table 5.6 : Summary of ^1H T_1 data for selected ACP compounds at 4.7 T and 7.04 T

Sample	T_1 /s (4.7 T)	T_1 /s (7.04 T)
ACP	0.38	0.74
ACP19H	0.44	0.60
ACP22H	0.28	0.34
ACP26H	0.26	0.36
ACP5D	0.20	0.22

5.3.3.3 Summary of Infra-red Spectra of ACP, ACP19H, ACP22H and ACP5D.

Infra-red and X-ray data for this series of samples were acquired and interpreted by J. E. Harries and D. W. L. Hukins.

The X-ray data were seen to simply confirm the findings of the i.r. spectra. Consequently only the i.r. data will be mentioned.

The infra-red spectrum of ACP gave clear indication that the sample was of an amorphous nature by two broad maxima at 1000 cm^{-1} and 600 cm^{-1}. In crystalline hydroxyapatite these peaks, especially the latter, would be split into two or more maxima[9]. Indeed, for ACP19H the maximum at 600 cm^{-1} showed evidence of splitting, indicating that an amorphous-crystalline transformation was taking place. Further splitting of the maximum at 600 cm^{-1} for ACP22H indicated that the phase change was continuing. ACP5D gave an i.r. spectrum characteristic of crystalline hydroxyapatite.

In conclusion, the infra-red spectra show that maturation of the ACP is taking place and that the final product is similar to HAP. These results agree reasonably well with the NMR data presented, although there was no i.r. evidence for two phases being present, which was in contrast to the NMR.

5.4 CONCLUSION

This work has illustrated the application of solid-state phosphorus-31 NMR to the study of calcium phosphates. The usefulness of performing both CP and SPE experiments on each sample has become apparent since different phosphate species

are selected according to the pulse sequence used. NMR can be used in the study of multicomponent systems, and in favourable circumstances the species present can be identified from chemical shift data and sideband intensity analysis. Even if such assignments cannot be fully made the spectra contain information regarding protonation, proximity of protons and the degree of crystallinity. Changes in the composition of multicomponent systems can be effectively monitored by ^{31}P NMR. Proton NMR was seen to complement the phosphorus studies. ^{1}H CRAMPS was of particular use in the examination of sample 3 and offers great potential in studies of systems consisting of a mixture of crystalline species. Unfortunately the technique was rather less informative for the amorphous systems. ^{1}H relaxation time and wideline data provided a useful insight into the nature of water within the ACP systems.

A wealth of information regarding the phosphate environments within ACP has been obtained from our NMR measurements. We can conclude that ACP contains $(PO_4)^{3-}$ units which are slightly distorted and/or weakly bound to protons. Furthermore, there are two types of phosphate unit, of which type A is closer to protons and may be less ordered. The crystallinity of both species improves with maturation in solution before extraction. These results seem to fit quite well with the $Ca_9(PO_4)_6$ cluster structure proposed by Betts and Posner[3]. Perhaps the two different phosphate species

could be due to type A environments being on the surface of such clusters and hence close to interstitial water, with type B environments being phosphate units in the bulk of the cluster. On the introduction of carbonate the ordering within the ACP is clearly reduced. The fact that type A environments seem to be affected most by the introduction of carbonate would also be consistent with the cluster model, with introduced carbonate hindering surface ordering more than the bulk at low carbonate concentration. With increased carbonate concentration environments A and B seem to be affected more evenly, suggesting that there has been deeper penetration of carbonate into the clusters, thus affecting the ordering of the bulk also.

REFERENCES

[1] E. D. Eanes , I. H. Gillessen and A. S. Posner, *Nature* 208, (1965) 365.

[2] M. C. Francis, W. S Briner and J. A. Gray, "Hard tissue growth, repair and remineralisation" (Edited by R. F. Sognnaes and J. Vaughn) Elsevier, London, p 57 (1973).

[3] F. Betts and A. S. Posner, *Trans. Am. Cryst. Assoc.* 10, (1974) 73.

[4] N. C. Blumenthal, F. Betts and A. S. Posner, *Calcif. Tissue. Res.* 23, (1977), 245.

[5] A. S. Posner, *Physiol. Rev.* 49, (1969), 760.

[6] G. Montel, *Bull. Soc. Chim. Fr.* , 1693-1700 (1968).

[7] I. J. Cox, Ph.D. Thesis, University of East Anglia (1984).

[8] W. P. Rothwell, J. S. Waugh and J. P. Yesinowski, *J. Amer. Chem. Soc.* 102, (1980), 2637.

[9] A. S. Posner, F. Betts , N. S. Blumenthal, *Prog. Crystal Growth Charac.* Vol. 3 (1980) 49. Pergamon Press.

CHAPTER 6 - THE ORIGIN OF ^{31}P NMR LINEWIDTHS IN THE SOLID-STATE

6.1 INTRODUCTION

In this chapter the origins of linewidths in phosphorus-containing systems will be examined in some detail. Firstly, possible line-broadening mechanisms will be considered, followed by a discussion of practical results obtained for phosphate systems and their implications concerning the origins of line broadening. Multiple-pulse sequences have been applied to a number of phosphate samples with pleasing improvements in resolution being achieved for static and slow-spinning samples.

6.2 THE ORIGIN OF LINEWIDTHS

A great number of NMR phenomena can contribute to the linewidth observed in the solid state. Techniques such as magic-angle spinning and high-power proton decoupling suppress the dominant interactions in the solid state, enabling high resolution spectra to be obtained. However, linewidths obtained even when MAS and HPPD are used are significantly broader than those observed for solutions (tens of Hz compared to less than a Hz). The additional broadening arises from interactions not fully averaged in the solid state, combined with additional effects as a consequence of constraints on probe and spectrometer design resulting from the special techniques used in order to achieve the relatively narrow

lines.

Line-broadening mechanisms in the solid state have been considered by a number of workers[1-4] in some detail, although the majority of the work was specifically directed to the study of ^{13}C-containing systems. There are two distinct classes of interaction responsible for line-broadening effects, namely homogeneous and inhomogeneous. The former result in general from relaxation effects, whereas the latter cause a dispersion of chemical shifts. The two classes of line-broadening mechanism will now be considered in turn.

6.2.1 Homogeneous Interactions

6.2.1.1 Homonuclear Dipolar Effects

The homonuclear dipolar interaction for an isolated pair of spins is in the most general case homogeneous, although there is the exception of when the spins are related by a centre of symmetry[5] where the problem becomes inhomogeneous. The centreband behaves in the same manner regardless of whether or not the situation is homogeneous - any differences occur in sideband structure. Thus the dipolar case will be discussed under the heading of homogeneous interactions.

In terms of isotopic substitution ^{31}P is 100% abundant in contrast to the low natural abundance of ^{13}C (1.1%). However,

in most cases it is realistic to consider phosphorus to behave as if it were a dilute system since [P-P] internuclear distances are generally large, resulting in relatively small homonuclear dipolar interactions which are in principle suppressed by MAS. Homonuclear scalar coupling is mediated by electrons and therefore requires nuclei to be linked through bonding in order for this effect to be observed. Typically coupling constants are $^{1}J_{PP}$ = hundreds of Hz, whereas $^{2}J_{PP}$ = tens of Hz. Scalar coupling is not present in the majority of the systems considered in this thesis because the phosphorus nuclei are in different molecular units and are therefore not linked by bonding. The obvious exception to this case is for the P_4S_n series of compounds considered in Chapter 7, where one-bond couplings were observed and higher-order couplings were thought to contribute towards the residual linewidths observed.

In chapter 4 a series of results were presented showing the dependence on spinning rate of the observed linewidth. The question of the efficiency of MAS in the removal of homonuclear dipolar interactions therefore arises. It is generally accepted in the literature that provided spinning rates are of the order of magnitude of the dipolar interaction, its effects will be fully removed by MAS. Clearly in the experiments reported in this thesis some interaction, be it dipolar or otherwise, is being suppressed more efficiently when higher spinning rates are used. The nature of the dipolar interaction will now be considered in

the light of the results presented in chapter 4.

Consideration of the homonuclear dipolar interaction for the entire spin system in the solid state is prohibitively difficult to be considered here. However, the simple case of a pair of isolated spins will now be discussed as it will give a useful insight into the nature of the dipolar interaction.

The dipolar splitting ($\Delta\nu$) for a pair of isolated, like spins is given in equation 6.1[6];

$$\Delta\nu = \frac{3}{2}R\left(3\cos^2\theta - 1\right) \qquad (6.1)$$

where R is given by;

$$R = \left(\frac{h}{2\pi}\right)\frac{\mu_o\gamma^2}{8\pi^2 r^3} \qquad (6.2)$$

θ is the is the angle that the vector connecting the two spins makes with the applied magnetic field, h is Planck's constant, μ_o is the permeability of free space, γ is the magnetogyric ratio of the nucleus in question, and r is the distance separating the two nuclear spins. From expressions (6.1) and (6.2) it is immediately obvious that the dipolar splitting shows an inverse cube relationship with the distance separating the two spins. The splitting has its maximum value when θ =0°, 180°, 360° ...etc, and a minimum value of zero. The interaction drops off rapidly with increasing internuclear distance so it is reasonable to consider only relatively short-range contacts between ^{31}P nuclei.

A system that may act as a reasonable model for the isolated spin pair is the compound tetraethyl diphosphine disulphide;

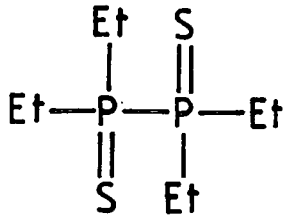

This compound is to a certain extent a special case since there are directly-bonded phosphorus atoms (intermolecular effects can be neglected as a consequence of the r^{-3} dependence of the interaction).

The crystal structure is known [7], indicating space group $P\bar{1}$, with one phosphorus atom in the asymmetric unit, with a [P-P] bond length of 2.2 Å. Using the [P-P] distance it is possible to estimate the magnitude of the dipolar interaction using equation (6.1), giving;

$$\Delta\nu = 2704\left(3\cos^2\theta - 1\right) \qquad (6.3)$$

The function $\cos^2\theta$ is periodic every 180^O. If we consider that θ can take any value between 0 and 180^O, in a powdered sample the most likely value of θ will be 90^O, which would lead to a dipolar breadth $\Delta\nu$, of 2704 Hz (The maximum value of $\Delta\nu$ would be twice this value). Variable spinning-speed data for tetraethyl diphosphine disulphide are shown in Figure 6.1.

Figure 6.1 : ^{31}P CP/HPPD/MAS linewidth as a function of spinning rate for tetraethyl diphosphine disulphide.

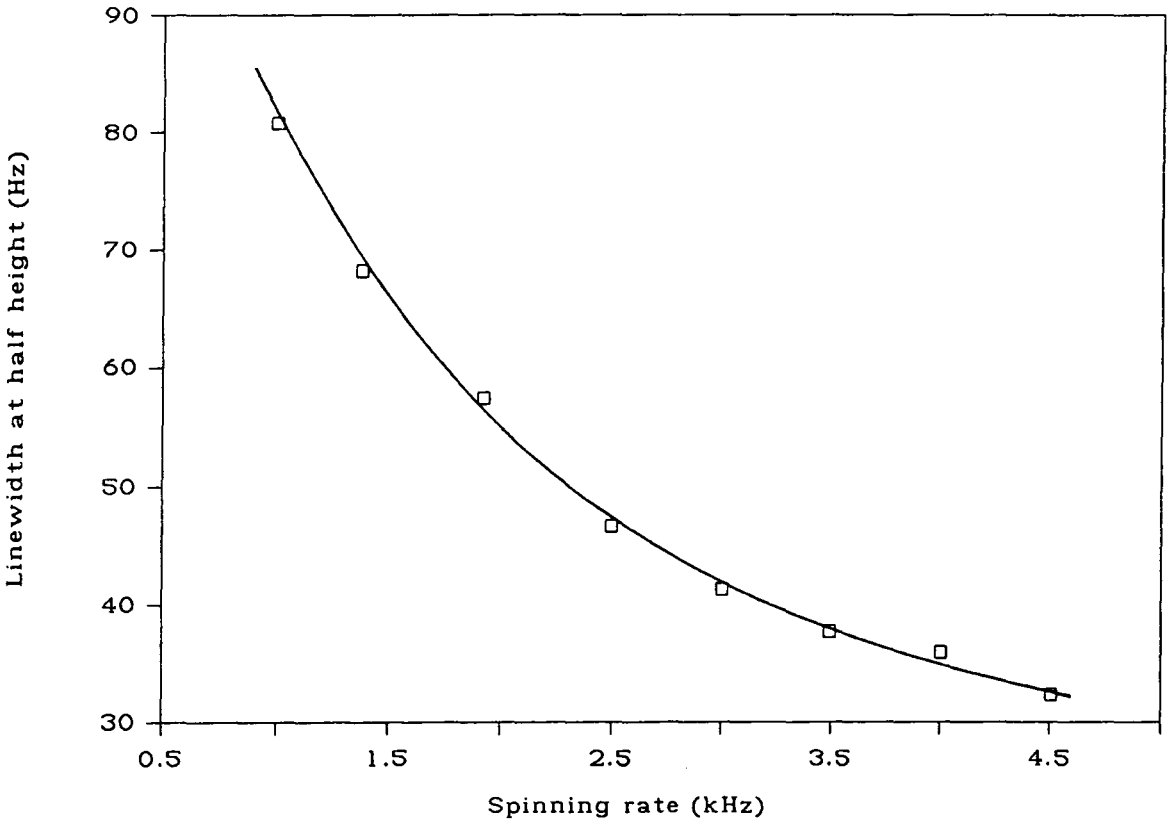

(The data were acquired by L. H. Merwin, University of Durham, who has an interest in diphosphine disulphide compounds). A marked dependence of linewidth upon spinning rate was noted, with narrowing occurring right up until the maximum spinning rate of 4500 Hz was achieved. From the general trend in the data indicated by the solid curve, it would appear that further narrowing of the resonance could be realised if spinning rates in excess of 4500 Hz were used. The spinning rates used for typical MAS experiments are of a similar magnitude to the dipolar broadening just calculated for tetraethyl diphosphine disulphide. The problem now arises as to the behaviour of the dipolar interaction under such conditions. A survey of the literature revealed that this problem is complex and has not been fully resolved. A number of workers[8,9,10] have addressed the problem of the behaviour of the dipolar interaction with spinning speed. However, several simplifying approximations had to be made in each case. Evans and Powles[9] considered a single crystal, with a cubic lattice undergoing magic-angle rotation along the [1,1,1] axis. The work proved useful for predicting the the initial shape of the free induction decay rather than an estimate of T_2 (which governs the lineshape itself). Clough and Gray[9] and Clough and McDonald[10] applied more general treatments, giving results applicable to actual linewidths observed. In the latter paper, the form of the relaxation function G(t) was considered. The calculations assumed a particular lineshape and that only dipole-dipole interactions

were present. Their treatment made it possible to separate out terms which contributed to the second moment of the absorption line by the generation of sidebands at intervals of the rotation frequency, from those which gave a finite contribution to the width of the narrowed central line. In the special case of the rotation axis being at an angle of 54^{o} 44'. (the magic angle) it was predicted that the linewidth would show ω^{-3} dependence on the spinning rate. The results obtained were in close agreement with the earlier theoretical work of Clough and Gray[9]. The inverse cube relationship predicts a very rapid drop off of dipolar linewidth with increasing spinning rate, which is certainly not the case in Figure 6.1. Direct comparison of the above mentioned theory with experimental data was not entirely justified since, firstly the sample itself had other contributions to the observed linewidth (motional effects for example) and secondly the theory is based upon assumptions and approximations. Although theory and experiment fail to agree well, the general form of behaviour in both cases is similar in as much that the linewidth is expected to show continuing improvements (however small) as the rotation rate increases. The experimental data give an indication as to the likely size of residual dipolar broadening over the range of spinning speeds available in the laboratory. The resonance observed for tetraethyl phosphine disulphide has a linewidth of 81 Hz at a rotation rate of 1.0 kHz, which is narrowed to 32 Hz at rapid spinning rates. The P-P distance is 2.2Å, which is small

compared to those for orthophosphates. It would therefore appear that dipolar effects can contribute in the region of 50 Hz to the linewidth of slow-spinning samples. Residual linewidths are probably due to non-dipolar interactions, which will be discussed later in this chapter. The experimental data presented for tetraethyl diphosphine disulphide should in principle reflect the maximum contribution of dipolar effects for the samples considered in this thesis. The phosphorus nuclei are directly bonded. Consequently the P-P distance is small (compared to phosphate-containing systems), giving a large (relatively speaking) contribution from the dipolar interaction to observed ^{31}P linewidths. Dipolar splittings for a number of phosphate species have been calculated using the shortest P-P distance (determined from the crystal structure) and are given in Table 6.1.

The magnitude of the calculated interaction for the phosphate systems is considerably smaller than for diphosphine disulphide. However the reader should note that in the case of the orthophosphate species the P-P bond distances of the nearest-neighbour phosphorus nuclei are quite similar and it is therefore conceivable that the interaction should more properly consist of a summation of interactions over a chosen coordination sphere. This modification to the calculation was

not pursued further since the intention of the calculations was merely to give the reader a feel for the magnitude of the dipolar interaction.

The dipolar interaction is independent of the applied magnetic field. Thus higher B_o would render dipolar contributions to observed linewidths relatively less important.

Table 6.1 ; Dipolar Splittings Calculated Using Equation 6.1 for Selected Phosphates.

Compound	Minimum P-P distance /Å	$\Delta\nu(\theta = 90^o)/Hz$
$Na_4P_2O_7$	2.936	1166
Brushite	3.675	595
ADP	4.198	399
DAHP	4.438	338
HAP	3.39	757

6.2.1.2 Heteronuclear Dipolar Effects

The heteronuclear dipolar interaction alone is inhomogeneous, but when influenced by one or more homogeneous interactions, the resultant interaction will itself behave in a homogeneous manner. The combination of homogeneous and inhomogeneous interactions to produce an overall homogeneous effect has been demonstrated for solid samples using two-dimensional techniques[11]. Multiple pulse decoupling was applied in order to selectively remove H-H dipolar interactions, leaving behind purely inhomogeneous P-H broadening, which could then be readily removed by MAS.

For the systems considered in this thesis, P-H dipolar broadening will generally behave homogeneously, as a result of additional influence from P-P and H-H dipolar effects. Thus, heteronuclear line-broadening effects have been included under the overall heading of homogeneous interactions.

Heteronuclear dipolar broadening of NMR linewidths in solids can manifest itself in a number of ways. Firstly, there is the straightforward case of direct dipolar coupling between the two types of spin, namely phosphorus and protons (for the case considered here). Secondly, there are additional potential sources of line broadening arising from modulation of the P-H coupling via molecular motion.

The magnitude of the direct interaction can be calculated for an isolated spin pair in the same manner as the homonuclear case. The dipolar splitting being given by[6];

$$\Delta\nu = R\left(3\cos^2\Theta - 1\right) \qquad (6.4)$$

where;

$$R = \frac{h}{2\pi}\frac{\mu_o\gamma_1\gamma_2}{8\pi^2 r^3} \qquad (6.5)$$

Equation (6.4) differs from equation (6.1) simply by a factor of 3/2 which is a consequence of flip-flop transitions being non-secular for the heteronuclear case, since energy would not be conserved.

Heteronuclear dipolar splittings were calculated for a number of phosphate species in the same manner as for the homonuclear case, and are summarised in Table 6.2.

The calculated P-H dipolar interactions for phosphates are therefore generally larger than typical spinning rates (in contrast to the homonuclear case). In the majority of the proton-containing phosphate systems studied in this thesis the application of HPPD rendered a significant improvement in spectral resolution.

Table 6.2 : Dipolar Splittings Calculated Using Equation 6.4 for Selected Phosphates

Compound	Minimum P-H distance /Å	$\Delta\nu$(max)/Hz
Brushite	2.189	4634
ADP	2.171	4750
DAHP	2.3814	3599
HAP	3.847	853

The efficiency of HPPD was investigated at an early stage in this work, with the effect of both decoupler power and frequency offset being considered. The results obtained for brushite are illustrated in Figure 6.2. Two features are evident from the graph. Firstly, the decoupler power used had a marked effect on the resolution obtained. Even the series of spectra acquired at the highest decoupler power that the probe electronics would allow, suggest that even higher power levels would be beneficial. Secondly, the frequency of proton irradiation is crucial. For maximum resolution irradiation must be on resonance, especially at intermediate

Figure 6.2 : Effect of ^{1}H decoupler power on ^{31}P signal intensity for brushite - decoupler powers (in kHz) as follows ;

(a) 3.0 (b) 11.5 (c) 26.0 (d) 40.4 (e) 55.9 (f) 67.6

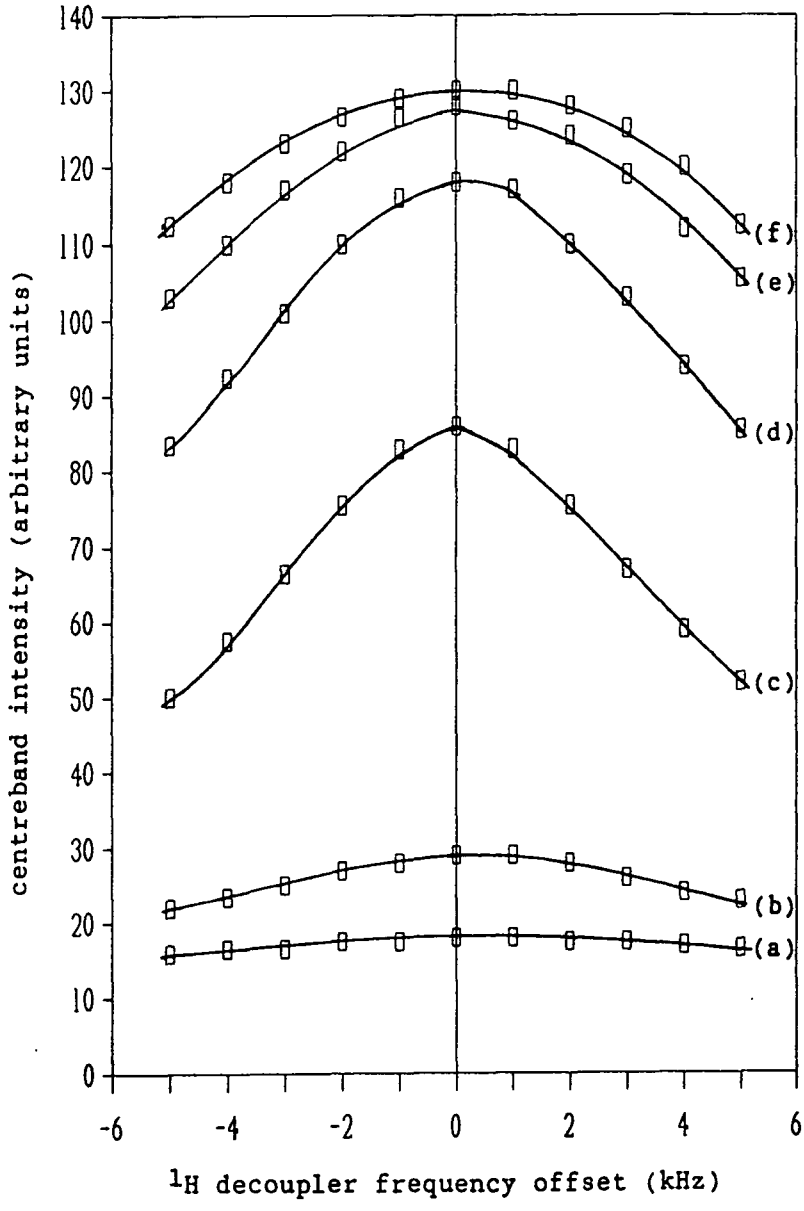

decoupler power levels. As a consequence of these observations experimental work was carried out with the irradiation frequency for the phosphate protons exactly on resonance, with the decoupler power level set as high as possible (typically 50 kHz for the Andrew-Beams type probe and 62.5 kHz for the double-bearing probes.)

The large difference between the decoupler power needed (typically 60 kHz) and the calculated dipolar interaction of 4.6 kHz for brushite indicate that a further heteronuclear broadening mechanism is at work. It is believed that the additional decoupler power needed results from the width of the ^{1}H spectrum as affected by (H-H) interactions.

An additional potential source of broadening when HPPD is being applied is lifetime broadening (as a consequence of molecular motion) at a frequency close to the decoupling field strength. This effect was largely ruled out however, since no modulation of the linewidths was observed in the variable decoupler power experiments. Low-temperature measurements in order to "freeze out" any molecular motion would help to confirm this.

Insufficient decoupler power is clearly a potential problem in the study of phosphate systems. However, brushite is a somewhat extreme case of strongly-coupled protons. This was indeed why it was selected for study. On the basis of the results presented in Figure 6.2 it is possible to estimate

that incomplete decoupling contributes approximately 4% (or 4 Hz) to the linewidth of brushite when a decoupling field strength of 50 kHz is used. Thus for other phosphates the contribution is likely to be small -a few Hz at most.

6.2.2 Inhomogeneous Interactions

6.2.2.1 Chemical Shift Dispersion

Chemical shift dispersion is an important line-broadening mechanism for amorphous and poorly crystalline solids. For phosphate systems the most significant sources of chemical shift dispersion arise from the nature of molecular packing. Bond angles and/or lengths may be modified, nearest-neighbour distances may vary. The resulting effect is that the electron clouds become disturbed via short-range variable interactions. Also, the applied magnetic field can become perturbed by variability in the orientations of sources of anisotropic molecular magnetic susceptibility. Later in this chapter magnetic susceptibility broadening will be discussed further.

6.2.2.2 Magic-Angle Missetting

If the angle between the sample rotation axis and B_o is not exactly $54^o\ 44'$ then the term $(3\cos^2\theta - 1)$ will not be fully averaged to zero. In cases where the magic angle is mis-set an approximation exists[12] indicating that the resultant linewidth is given by;

$$\Delta\nu(mis-set) \approx \frac{1}{2}\left(3\cos^2\phi - 1\right)\Delta\nu(static) \qquad (6.6)$$

where ϕ is the angle made between the rotor axis and B_o. It is therefore possible to estimate the contribution of this effect for the types of system considered in this thesis. From the form of Equation 6.6 it is evident that nuclei with highly anisotropic shielding are going to be most sensitive to magic-angle mis-set. Static powder lines typically have $\Delta\nu_i$ = 8 kHz for protonated phosphate units and $\Delta\nu_i$ = 2.5 kHz for unprotonated species. The magic angle could be reproducibly set to an accuracy of better than 0.05^o. The maximum likely contributions for magic angle mis-set are therefore 20 Hz and 7 Hz for protonated and non-protonated phosphate units respectively. Linewidth variations from one spectrometer session to another scarcely differed by more than 10 Hz so it is probable that the contributions from rotor angle mis-set are actually somewhat smaller than predicted here, i.e. we actually achieve better than +/- 0.05^o accuracy in setting of the magic angle.

The two types of spinning system available (Andrew-Beams and Double-bearing) behaved quite differently when setting the magic angle. The Andrew-Beams probe required the rotation angle to be reset for every sample by including a small quantity of KBr in the sample rotor, and observing the ^{79}Br signal. Details of the precise angle setting procedure can be found in the experimental chapter. Having set the angle it appeared to be stable provided the spinning rate was not altered. Changing the spinning rate had a marked effect on

the rotor angle. Variations in packing also affected the rotation angle. The same rotor angle could not be reproduced for a particular spinning rate if the rotor was emptied and re-packed, however this effect was less serious than changing the spinning rate. The double bearing probe was far superior in terms of angle setting. The angle remained stable virtually indefinitely, regular checks were made but the angle never required adjustment unless the probe was removed from the magnet. No perceptible variation of the rotor angle with spinning rate could be detected.

6.2.2.3 Rotor Instabilities

Instability in sample rotation can manifest itself in a number of forms which include vibration of the rotor/stator assembly, rotor precession/nutation, and variation in the spinning rate. The above-mentioned types of rotor instability apply strictly only to rotors of the Andrew-Beams type. Advances in sample spinning technology have seen the recent introduction of double-bearing spinning systems which have significantly reduced most of the sources of rotor instabilities. The double-bearing design removes the freedom which allowed Andrew-Beams rotors to precess. Moreover the spinning rate appears to be significantly more stable: +/- 5 Hz compared to +/- 30 Hz. For probes of the Andrew-Beams design the rotor angle is seen to vary as a function of

spinning speed. Thus minor variations in the rotor angle will result from the instabilities in rotor speed. (Variation in rotor speed alone would not affect centreband resolution, but would manifest itself by broadening the sideband signals.) Clearly it is therefore preferable to perform experiments using double-bearing technology wherever possible. Conceptually, rotor instabilities are similar to magic angle mis-setting. If the shielding anisotropy is large, the corresponding effect due to rotor instabilities may be significant. The contribution that this line-broadening mechanism makes for the samples considered in this thesis is difficult to quantify. However it was noted that for identical conditions brushite gave a spectrum with centreband linewidth 10 Hz narrower using the double-bearing probe rather than the Andrew-Beams probe, suggesting that as much as 10% of the observed phosphorus linewidth may be due to rotor instabilities. This difference in observed linewidths should, however, be interpreted with caution, since the two types of probe are rather different in design, especially with respect to the manner in which the sample occupies the coil.

6.2.2.4 Inhomogeneities in Applied Zeeman Field

Inhomogeneity in B_o is is a potential source of line broadening. Careful shimming of the magnet results in linewidths of less than 4 Hz being routinely obtained for the

^{13}C signals of adamantane. Thus, any contribution to linewidths from field inhomogeneity is small, certainly less than 4 Hz. Attempts have been made to improve the linewidths obtainable even further by using a smaller sample volume. These experiments resulted in better lineshapes being obtained, but no measurable improvement in linewidth was observed.

6.2.2.5 Magnetic Susceptibility Broadening

The local magnetic field in a powdered sample is affected by the diamagnetic susceptibility of the nearby, randomly-orientated particles. This effect causes inhomogeneities in the magnetic field, which may in turn result in inhomogeneous broadening of the resonance line. For the case when the bulk magnetic susceptibility is isotropic, magic-angle rotation will average susceptibility effects to zero.[2] However, the bulk magnetic susceptibility may be anisotropic, in which case its effects will not be fully averaged to zero by MAS. Anisotropic bulk magnetic susceptibility (ABMS) has an effect which depends on the orientation of the susceptibility tensor with respect to B_o. Line broadening effects due to ABMS can in principle be reduced via dilution of the sample in a medium having isotropic BMS. However, this can not be realised in practice, since, even under conditions of infinite dilution

in an isotropic medium, there would still be ABMS broadening attributable to the particle shape. The converse effect, i.e. line broadening of a species with isotropic BMS when diluted in a medium with ABMS, has been demonstrated[2].

6.2.3 Linewidths as a function of field strength

Further insight into the dominant broadening mechanisms can be obtained by consideration of linewidths as a function of field strength, B_o. VanderHart et al[1] have demonstrated that broadening due to magic-angle mis-set, rotor instabilities, chemical shift dispersion and ABMS is linearly dependent on the magnetic field strength. The variable spinning speed data discussed in chapter 4 were performed at two field strengths for $NH_4H_2PO_4$ and hydroxyapatite. Indeed, the observed minimum linewidths were field dependent in the ratio approx 3:2 (the ratio of the applied field strengths). It would appear that for these samples the dominant interactions are close to linearly dependent on the field strength at high spinning rates. Since the measurements were carried out using the double-bearing probe magic-angle mis-set and rotor instabilities are likely to be minor sources of broadening. Thus chemical shift dispersion and ABMS are the probable causes of the residual linewidth at high spinning speeds.

6.3 Application of ^{31}P multiple pulse sequences to phosphates.

In this section two multiple pulse sequences will presented and the results discussed. Both are modifications of already known pulse sequences. The two types of experiment were devised in order to further investigate the origins of linewidths in the solid state.

The pulse sequences used for these MAR NMR experiments are illustrated in Figure 6.3. The rotation-synchronised CPMG sequence, Fig. 6.3(a), is based on the Carr-Purcell-Meiboom-Gill sequence[13], with the addition of HPPD. For experiments carried out on rotating solid samples the 180^{O} pulses must be synchronous with the rotor period. The CP/CRAMPS, Fig. 6.3(b), originates from the MREV-8 pulse sequence[14,15] which when combined with magic-angle rotation is known as CRAMPS (combined rotation and multiple pulse spectroscopy)[16-19]. The CP/CRAMPS technique develops the concept even further by introducing CP to generate the magnetization, followed by HPPD whilst performing CRAMPS on the phosphorus channel. The CP/CRAMPS work presented in this chapter was carried out in a collaborative study with Peter Jackson, a contemporary research student in the same research group as the author of this thesis, at University of Durham.

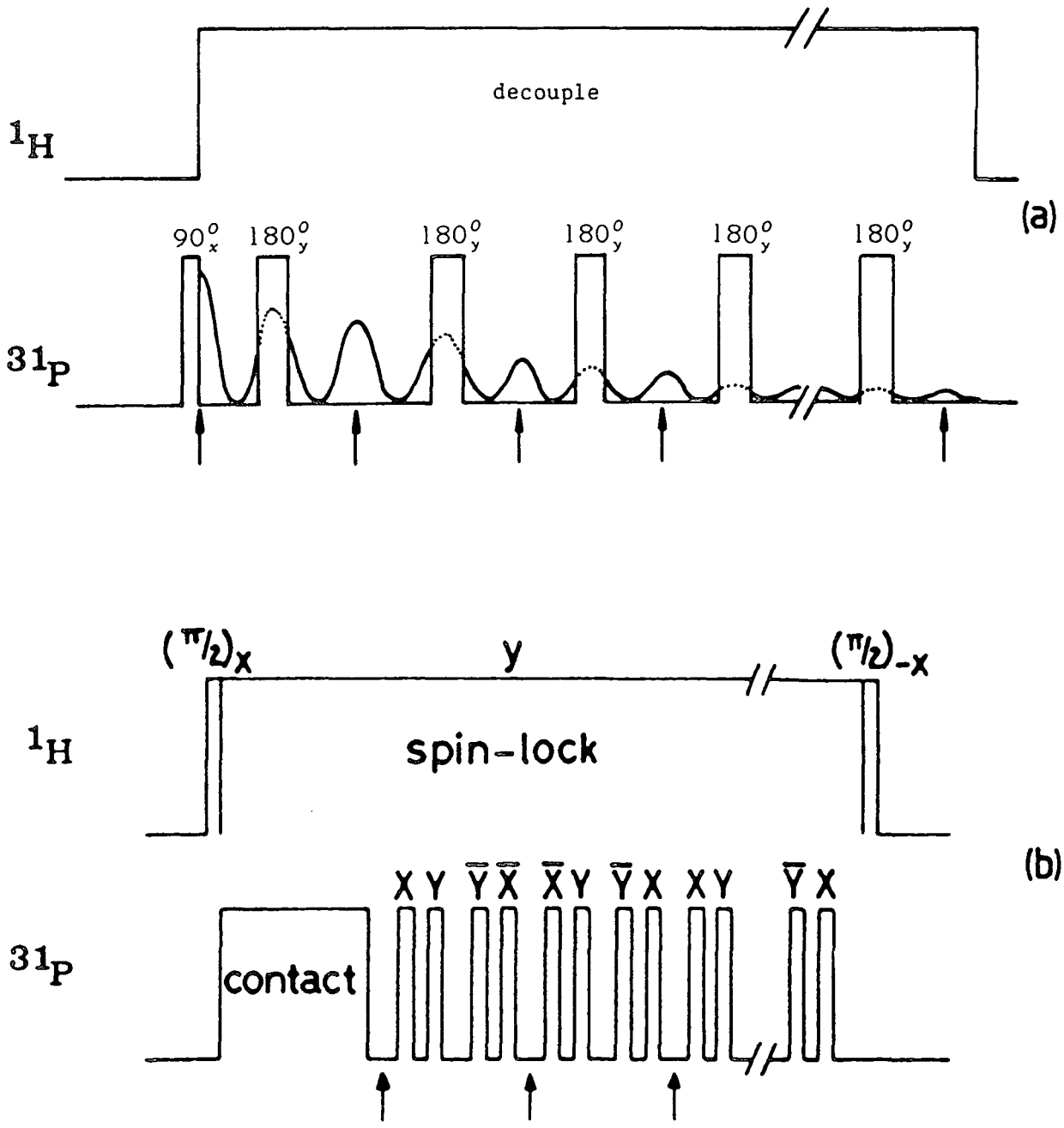

Figure 6.3 : Rotation synchronised CPMG sequence with HPPD and CP/CRAMPS/HPPD sequences.

(a) Rotation synchronised CPMG sequence. Arrows indicate the sampling points. The decay shown represents a signal on resonance with rotational echoes (as a consequence of MAS). HPPD is applied throughout the acquisition.

(b) CP/CRAMPS/HPPD. ^{31}P data points are sampled twice per cycle at the points indicated by arrows. The four rf phases of the ^{31}P 90^o pulses are indicated by X, -X, Y, -Y.

6.3.1 Rotation-Synchronised CPMG Experiments

Rotation-synchronised CPMG experiments were performed with the aim of determining a true value for T_2. The sequence described here was expected to remove virtually all line broadening mechanisms. The MAS was carried out to eliminate direct dipolar interactions, HPPD was applied in order to assist in the removal of heteronuclear dipolar effects, and the CPMG sequence was required to remove sources of inhomogeneous line broadening. Contributions from homonuclear J-coupling were not expected for the samples used in this study since there was only one phosphorus atom per molecule in each case.

The pulse sequence used was as in Figure 6.3(a) with the spacing of the 180^{o} pulses being exactly one rotor revolution period. This constraint made it essential to measure the spinning speed very accurately, which was done by averaging the spacings between as many spinning sidebands as possible. Individual data points were acquired every other rotor period at the points indicated by arrows. The data were essentially non-quadrature in form, but for ease of phasing of the final spectrum the data were acquired using quadrature detection, Fourier transformed and the measured linewidth used as an indication of T_2. A typical free induction decay obtained using the rotation synchronised CPMG sequence is illustrated in Fig. 6.4. The number of data points acquired was typically 256. In the case of the very narrow signals (ca. 10 Hz)

Figure 6.4 : Brushite; Free induction decay obtained when using the rotation sychronised CPMG sequence. Spinning rate = 2509 Hz. Separation between sampling points = 797 μs

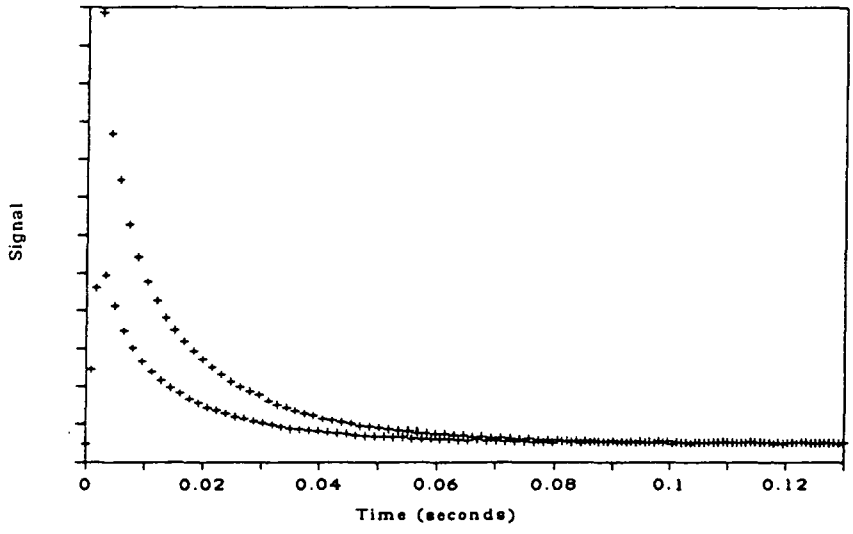

being obtained, it was necessary to acquire the maximum number of data points that the spectrometer system would allow without arcing taking place, (ca. 500 points). Indeed some of the linewidth values appeared to be rather similar (bearing in mind the accuracy to which the linewidths could be measured), and were perhaps upper limits resulting from such experimental limitations. The method of data acquisition limited the accessible spectral width since the dwell time was equal to twice the rotor period. Typical spinning rates used were = 2.5 kHz giving a spectral width of = 625 Hz. The narrow accessible spectral width made it necessary to perform the experiment with the signal of interest exactly on resonance. Several experiments were performed on each sample;

(i) Conventional SPE/HPPD

To establish the precise rotation rate and to locate the exact resonance frequency of the signal of interest.

(ii) $(90^{o})_{x}$ pulses on, $(180^{o})_{y}$ pulses on

To acquire the rotation-synchronised CPMG decay data.

(iii) $(90^{o})_{x}$ pulses on, $(180^{o})_{y}$ pulses off

To determine the linewidth of the resonance of interest without the use of CPMG (The linewidth measured should be identical to that measured in experiment (i))

(iv) $(90^{O})_{x}$ pulses off, $(180^{O})_{y}$ pulses on

To verify that any contributions to the signal due to inaccurate pulse angles and pulse imperfections are insignificant.

A typical set of spectra for experiments of types (ii)-(iv) are illustrated in Figure 6.5. A significantly narrowed signal was observed when the rotation-synchronised CPMG sequence was used. Signals from pulse errors obtained with sequence (iv) above were generally unobservable compared to the intensity of the true signal. Linewidths and T_2 data obtained using the rotation-synchronised CPMG technique are summarised in Table 6.3 for a selection of phosphate species. The results obtained were not exactly as expected since the values of T_2/residual linewidths were still not as good as for solution-state studies. It is possible that inefficient removal of P-P dipolar interactions by MAS may result in some contribution to the residual linewidth.

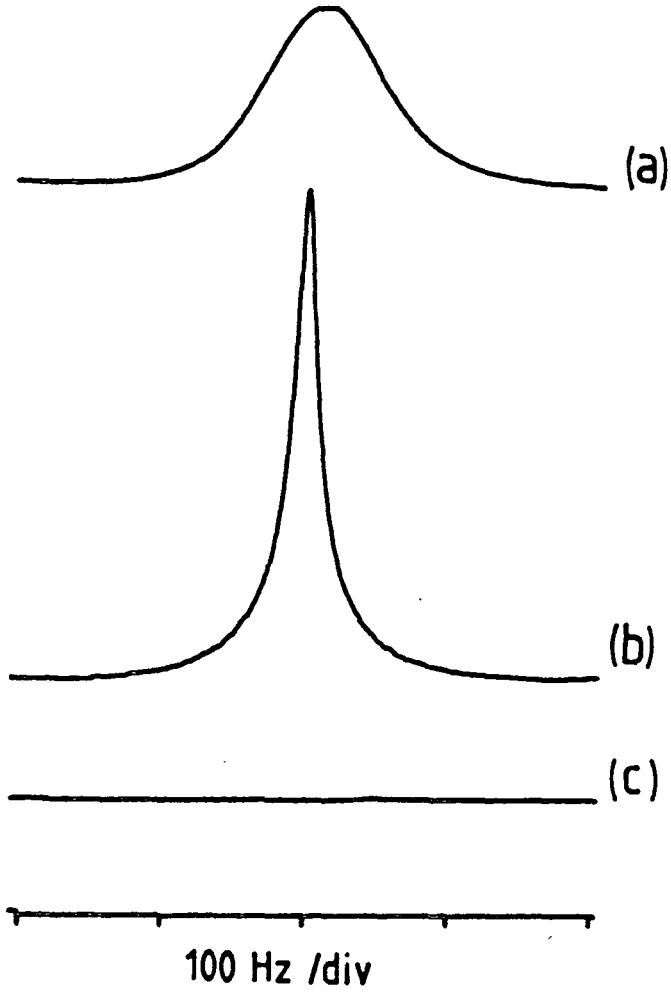

Figure 6.5 : Typical series of rotation synchronised CPMG spectra using brushite as an example.
Recycle delay = 30 s, 90^0 pulse length = 5 μs,
spinning rate = 2509 Hz, number of transients = 16
dwell = 797 μs, spectral width = 627 Hz.

(a) Rotation sychronised CPMG sequence with ^{31}P 180^0 pulses off.
(analogous to conventional SPE spectrum)
(b) Rotation synchronised CPMG sequence
(c) Rotation synchronised CPMG sequence with 90^0 pulses off, 180^0 pulses on.
(to verify that contributions from pulse errors etc. are insignificant.)

Table 6.3: Linewidth[a] and T_2 Data for Selected Phosphate species determined using the rotation-synchronised CPMG sequence;

Sample	$\Delta\nu_{\frac{1}{2}}$ (SPE/HPPD) /Hz	$\Delta\nu_{\frac{1}{2}}$ (Rot-Sync CPMG) /Hz	T_2/s
Brushite	100	20	0.016
Monetite	217[b]	32	0.010
ACP	510	11	0.029
ACP22H	200	8	0.039
ACP5D	142	9	0.035
$Ph_2Me_2P^+I^-$	28	12	0.027

[a]Linewidths measured at half peak height, estimated error +/- 1 Hz.

[b]Combined linewidth of two overlapping peaks.

It is especially interesting to note that brushite (which showed a quite significant calculated P-P dipolar interaction) should give CPMG lines significantly broader than for species such as ACP (which is believed to have HAP like structure).

HAP showed a significantly smaller value for the P-P interaction (recall Table 6.1). Heteronuclear dipolar effects should have been efficiently suppressed by the application of HPPD. Indeed, in the absence of HPPD significantly broadened signals were observed. The ACP series of samples gave particularly substantial narrowing when subjected to the CPMG sequence. In the case of ACP the magnitude of the broadening effects removed is 500 Hz. On application of the CPMG sequence the values obtained for all three ACP samples were very close, supporting the proposal made in chapter 5 that these samples had rather similar fundamental structure. The samples were thought to have different levels of crystallinity according to the length of time they were allowed to age. It is possible that a great deal of the broadening removed could have been due to variations in the extent of chemical shift dispersion. This would result from the less crystalline samples possessing a greater variation in molecular packing.

The rotation-synchronised CPMG technique described here has been applied by another member of the Durham NMR group in the determination of ^{119}Sn homonuclear coupling constants from $\{^{119}Sn,^{119}Sn\}$ satellites in the spectrum of $[Me_2SnS]_3$.[20] In the solid state, $[Me_2SnS]_3$ has two inequivalent tin environments.

A further potential use of the sequence is in the tune-up procedure for nuclei with broad, relatively weak signals, showing a large shielding anisotropy. The potential gain in signal to noise obtained in the transformed rotation synchronised CPMG spectrum (as a consequence of substantial line narrowing) compared to conventional CP/MAS could be quite large, resulting in significant time savings during the tune-up procedure. The drawback with this practice is that the exact frequency of the signal being optimised must be known before this technique can be applied.

6.3.2 ^{31}P CP/CRAMPS Experiments

Multiple-pulse experiments have been successfully used to suppress homonuclear dipole-dipole interactions between protons (^{1}H,^{1}H) and fluorines (^{19}F,^{19}F), enabling shielding tensor components to be determined[14,15,20,21]. When combined with magic-angle-spinning (^{19}F or ^{1}H CRAMPS)[16-19], high-resolution solid-state spectra can be obtained. In the experiments reported here HPPD, CP and ^{31}P CRAMPS have been combined to improve resolution for relatively slow-spinning and static samples. The CRAMPS approach was prompted by the observation of variations of linewidth with spinning speed (as discussed earlier in this chapter). It is generally accepted that MAS suffices to fully remove broadening arising from heteronuclear dipolar coupling and shielding anisotropy provided that the spinning rate is greater than the static

bandwidth. Our experience shows that substantially greater speeds often offer improved linewidths for some phosphates although the relevant (P,P) dipolar coupling constants (which are, of course homonuclear) are < 1 kHz. Further narrowing continues to be observed for several compounds (Table 6.4) at speeds exceeding 2 kHz. For brushite spinning rates up to 5 kHz prove to be beneficial.

The spectra were acquired using a Bruker dual-channel CP/MAS probe, with the simple modifications listed below:

(a) replacement of the standard Andrew-Beams stator and rotor by a double bearing, extended-rotor spinning system,

(b) use of a narrow-diameter, high-homogeneity coil, combined with a small-volume spherical sample cavity (3mm diameter) in a kel-F rotor,

(c) introduction of a bundle of low-inductance, non-magnetic resistors to facilitate a short recovery time for the tuned circuit.

The pulse sequence used is illustrated in Figure 6.3(b). Homonuclear multiple-pulse decoupling was achieved using the MREV-8 sequence. The tune-up procedure used was as described

Table 6.4 : Linewidth data (in Hz) for three phosphate species at different spinning rates under CP/MAS/HPPD and CP/CRAMPS/HPPD experiments. Linewidths are measured as full width at half height. They are corrected for the necessary scaling factor in the CRAMPS case.

	CP/MAS/HPPD					CP/CRAMPS/HPPD	
Spinning rate /Hz	500	1000	2400	3000	5000	1000	2400
Ammonium dihydrogen phosphate	130	83	37	34	30	28	28
Diammonium hydrogen phosphate	80	68	55	40	--	--	37
Brushite	90	87	87	83	68	66	65

for ^{1}H CRAMPS but with the ^{31}P signal of 85% phosphoric acid being observed rather than a ^{1}H signal. Decoupling was not necessary whilst observing signals from liquid phosphoric acid. A pulse duration, t_d, of 3 microseconds and a four-pulse cycle time, t_c, of 36 microseconds were used. The best resolution is obtained from MREV-8 operation when the carrier frequency is near the NMR signals. The multiple-pulse scaling factor (ca. 0.5) was determined by the co-addition of signals obtained from a liquid sample of 85% phosphoric acid, H_3PO_4, separated by 1 kHz offsets. The spectra obtained were also referenced with respect to the signal from H_3PO_4.

Figure 6.6 shows the results obtained for ammonium dihydrogen phosphate spinning at 1.0 kHz. The CP/CRAMPS spectrum is scaled to give a direct comparison of linewidths. The apparent increase in spinning speed arises from the fact that the spinning is not scaled by the multiple-pulse sequence. (It should be noted that this fact opens up possibilities of obtaining very fast apparent spinning rates.) At present, spinning sidebands may be folded back into the spectrum, since the spectral width is limited by the probe ring-down time, and quadrature detection is not used. Further probe modifications, leading to shorter multiple-pulse cycle times should lead to an increase in the accessible spectral width.

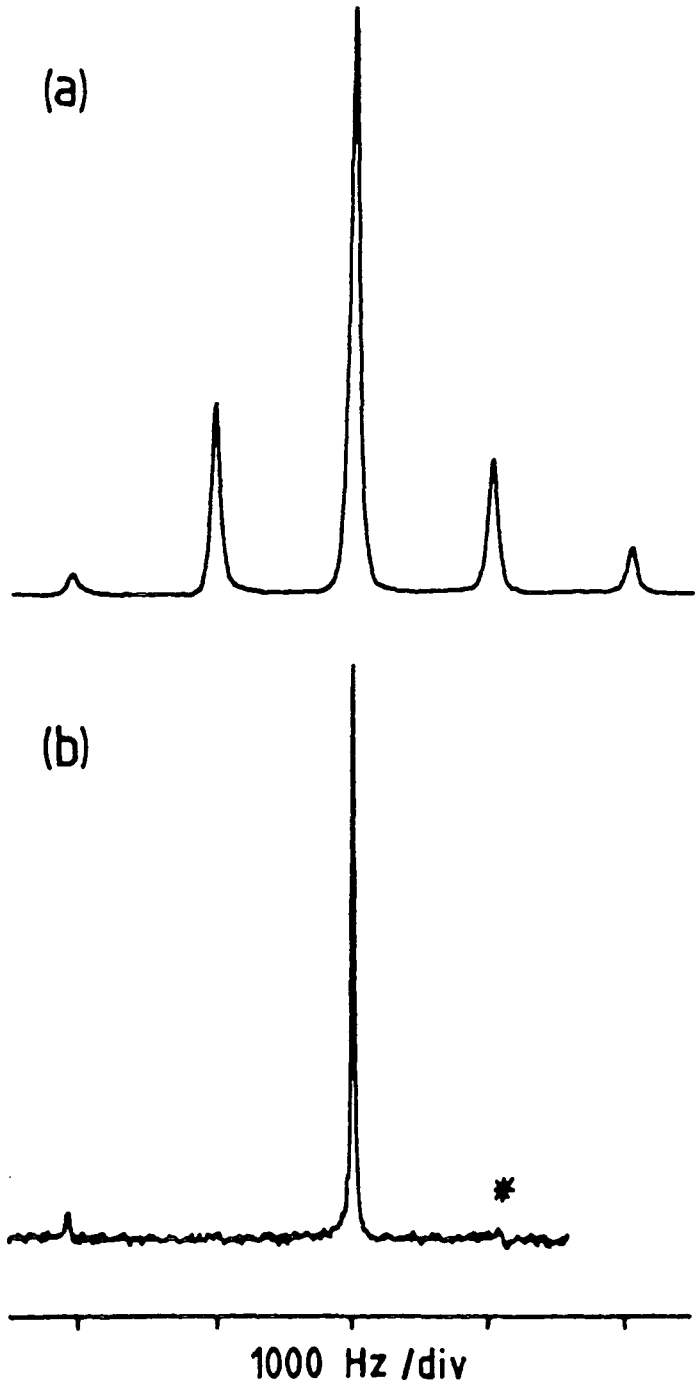

Figure 6.6 : Comparison of CP and CP/CRAMPS for ammonium dihydrogen phosphate

(a) Standard CP/MAS/HPPD spectrum of $NH_4H_2PO_4$ spinning at 1.0 kHz. The linewidth at half peak height is 83 Hz.
(b) CP/CRAMPS/HPPD spectrum at the same spinning rate after scaling. The centreband is narrowed to 28 Hz. The sideband marked with an asterisk is folded back into the spectrum, since quadrature detection was not used.

The relatively high noise level in (b) arises from the requirement to open the filter bandwidth to avoid ring-down problems. Spectrometer conditions; contact time 1 ms, recycle delay 5 s, number of transients = 24.

Table 6.4 lists the linewidths obtained for three phosphate species using CP/MAS/HPPD and CP/CRAMPS/HPPD at various spinning rates. It may be seen that modest spinning speeds with CP/CRAMPS give linewidths comparable or better than those obtained at the highest spinning speed (5 kHz) in the absence of the multiple-pulse sequence. No change in linewidth was observed for the multiple pulse experiment on changing the spinning rate.

Figure 6.7 illustrates the improved resolution made possible by the use of ^{31}P CRAMPS when the carrier can be placed near the signals. The sample consisted of an approx. 1:1 mixture of ADP and hydroxyapatite. Figure 6.7(a) shows the CP/MAS spectrum obtained, with the ADP signal to lower frequency. The two components clearly have rather different linewidths. The relative intensities are apparently distorted, since the two components have different anisotropies, leading to a different number of spinning sidebands. Application of the CRAMPS technique leads to increased resolution (Figure 6.7(b)). The relative intensities are changed even though there is no difference in spinning rate between the two experiments, since the multiple pulse sequence makes the apparent spinning speed greater for CRAMPS operation after scaling. Identical contact times and recycle delays were used, and an equal number of transients

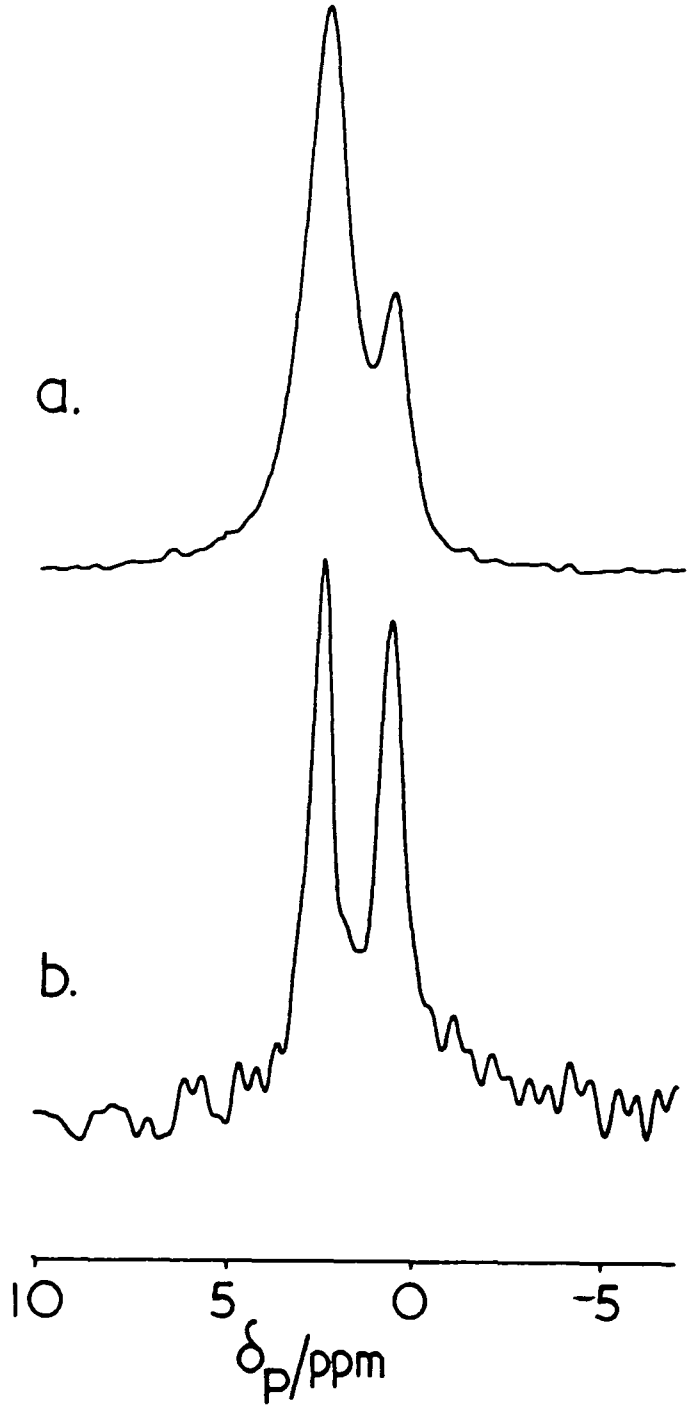

Figure 6.7 : ^{31}P HPPD/CP NMR spectra of a mixture of hydroxyapatite (higher frequency resonance) and ammonium dihydrogen phosphate (lower frequency resonance)

(a) with MAS (b) with CRAMPS

Spectrometer conditions: contact time 1 ms, recycle delay 5 s, number of transients = 200, 90^0 Pulse length = 3 μs.

were accumulated for each experiment. The decrease in signal to noise with CRAMPS operation reflects the increased filter bandwidth required.

The reasons for the improvement in resolution obtained when MREV-8 operation is added to the HPPD/CP/MAS suite of techniques are not entirely obvious. It is probable that (P,P) homonuclear dipolar interactions play a dominant role. Although the spinning speeds used are in excess of the relevant dipolar interaction constants it is likely that the MREV-8 sequence averages the coupling term more efficiently. It may be that mobility at a molecular level is of importance. It should be noted that combining HPPD and MAS for adamantane produces[22] better resolution than either technique alone.

Figure 6.8 shows how the use of ^{31}P MREV-8 pulse sequence can simplify the ^{31}P-{^{1}H} bandshape from a static sample of ammonium dihydrogen phosphate so as to define the powder pattern arising from the shielding anisotropy more closely. In the presence of [^{31}P-^{31}P] dipolar coupling, a broadened , slightly asymmetric pattern is produced, while the multiple pulse experiment reveals a powder pattern characteristic of an axially symmetric tensor. Both static powder patterns were fitted using the "ASFITD" program which is described in detail elsewhere.[23] The tensor values and line broadening factor determined are summarised in Table 6.5.

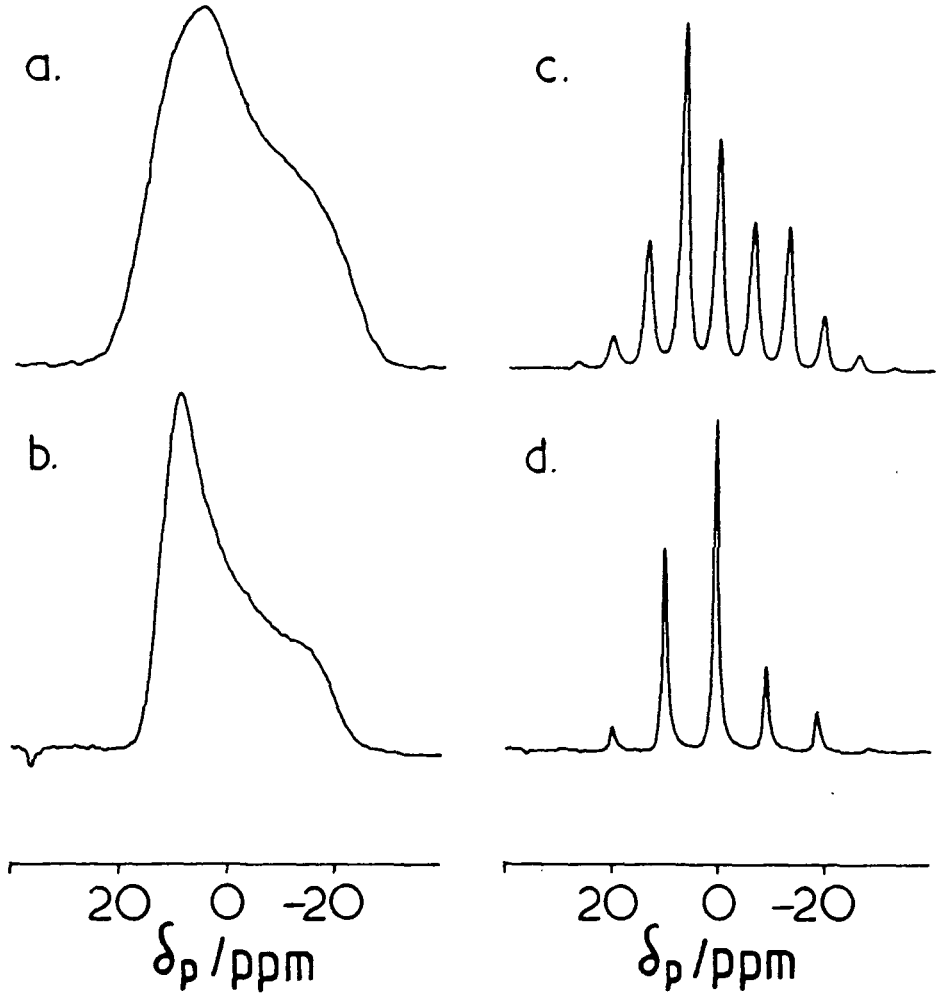

Figure 6.8 : ^{31}P CP/HPPD and CP/MREV-8/HPPD spectra of $NH_4H_2PO_4$
Recycle delay = 5 s, contact time = 1 ms,
90^0 pulse length = 3 μs

(a) Static, CP/HPPD only. Number of transients = 80
(b) Static, CP/HPPD with ^{31}P MREV-8 acquisition. Number of transients = 80
(c) CP/MAS/HPPD, spinning rate = 500 Hz. Number of transients = 32
(d) CP/CRAMPS/HPPD, spinning rate = 455Hz. Number of transients =12

Table 6.5 : Tensor components and gaussian broadening factors for Ammonium Dihydrogen Phosphate :Comparison of CP/HPPD and MREV-8 results

	σ_{11}	σ_{22}	σ_{33}	broadening factor /Hz
CP/HPPD	-18	-8	+19	809
MREV-8/HPPD	-14	-9	+22	378

Clearly the tensor components are very similar for the two types of experiment, indeed they are within experimental error bearing in mind the relatively small shielding anisotropy. However the important factor to note is the broadening factor, which has been significantly reduced using the MREV-8 sequence. Clearly a significant broadening mechanism has been suppressed. The residual broadening that exists even when the MREV-8 sequence is used indicates that some sources of line broadening remain. One possible broadening mechanism, which is not removed by the MREV-8 sequence, is that of bulk magnetic susceptibilty.

The spinning sideband manifold from the low-speed CRAMPS spectrum of Figure 6.8(d) can also be used to obtain the shielding anisotropy, but the linewidths are not optimum

because the carrier frequency must be placed well away from the sideband pattern in our non-quadrature mode of operation. The shielding tensor components must be scaled accordingly since the apparent spinning rate will be much higher than actually used, as a consequence of the multiple pulse scaling factor affecting the chemical shift only.

6.4 Conclusion

The purpose of this chapter has been to examine in detail the nature of line broadening in phosphate systems, and to quantify the potential contribution of each mechanism to experimentally observed linewidths. It has become clear that the 100 % natural abundance of ^{31}P must not be overlooked. Also HPPD powers must be as high as current probe technology will allow. Rapid sample spinning rates or the application of multiple pulse sequences can in a number of cases yield improved resolution. Thus for conventional CP/MAS experiments optimum resolution will be obtained when spinning rates and decoupler powers used are as high as possible. Clearly, pushing a spectrometer system to its absolute limits is not desirable. Thus, the application of MREV-8 sequences to reduce the required spinning rates whilst still obtaining optimum resolution is a useful option. Often probe design or sample limitations require low spinning rates, or necessitate the use of static samples.

REFERENCES

[1] D. L. VanderHart, W. L. Earl and A. N. Garroway.
J. Magn. Reson. 44, (1981), 361.

[2] M. Alla and E. Lippmaa.
Chem. Phys. Lett. 87, (1982), 30.

[3] M. A. Hemminga, P. A. de Jager, J Kruse and
R. M. J. N. Lamerichs.
J. Magn. Reson. 71, (1987), 446.

[4] A. N. Garroway, D. l. VanderHart and W. L. Earl.
Phil. Trans. R. Soc. Lond. A299, (1981), 609.

[5] M. M. Maricq and J. S. Waugh.
J. Chem. Phys. 70, (1979), 3300.

[6] R. K. Harris.
"Nuclear Magnetic Resonance Spectroscopy"
Pitman (1983).

[7] S. N. Dutta and W. M. Woolfson.
Acta. Cryst. 14, (1961), 178.

[8] W. A. B. Evans and J. G. Powles.
Proc. Phys. Soc. (Lond.) 92, (1967), 1046.

[9] S. Clough and K. W. Gray.
Proc. Phys. Soc. (Lond.) 79, (1962), 457.

[10] S. Clough and I. R. McDonald.
Proc. Phys. Soc. (Lond.) 86, (1965), 833.

[11] M. G. Monowitz, R. G. Griffin, G. Bodenhausen and T. H. Huang,
J. Am. Chem. Soc. 103, (1981), 2529.

[12] E. R. Andrew.
Phil. Trans. R. Soc. Lond. A299, (1981), 505.

[13] (a) H. Y. Carr and E. M. Purcell.
Phys. Rev. 94, (1954), 630.
(b) S. Meiboom and D. Gill.
Rev. Sci. Instr. 29, (1958), 688.

[14] P. Mansfield.
J. Phys. C4, (1971), 1444.

[15] W. -K. Rhim, D. D. Elleman and R. W. Vaughn.
J. Chem. Phys. 58, (1973), 1772 : 59, (1973), 3740.

[16] L. M. Ryan, R. E. Taylor, A. J. Paff and B. C. Gerstein.
J. Chem. Phys. 72, (1980), 508.

[17] L. M. Ryan, R. C. Wilson and B. C. Gerstein.
Chem. Phys. Lett. 52, (1977), 341.

[18] G. Scheler, U. Haubenreisser and H. Rosenburger.
J. Magn. Reson. 44, (1985), 134.

[19] R. K. Harris, P. Jackson, G. J. Nesbitt and B. J. Say.
Poster presented to BRSG, Oxford, April (1986).

[20] R. K. Harris and A. Sebald.
Poster presented at Eighth International Meeting on NMR Spectroscopy, University of Kent, 1987.

[21] J. S. Waugh, L. M. Huber and U. Haeberlen.
Phys. Rev. Lett. 20, (1968), 180.

[22] D. P. Burum and W. -K. Rhim.
J. Chem. Phys. 71, (1979), 444.

[23] L. H. Merwin
Ph. D. Thesis, University of Durham, 1987.

CHAPTER 7 - ^{31}P NMR STUDY OF SOME BINARY PHOSPHORUS SULPHIDES

7.1 INTRODUCTION

The phosphorus sulphides P_4S_n (n=3,5,7,9,10) form an interesting series of compounds which have previously been studied in the solid state using NMR[1-7] and the results compared with X-ray crystal data[8-15]. In this study high resolution solid-state spectra have been obtained by the use of magic angle spinning on a modern high field spectrometer, thus providing potential for more detailed information to be obtained than in the earlier studies[1-7]. The structure of each phosphorus sulphide is derived from a P_4 tetrahedron with replacement of appropriate P-P units by P-S-P units and addition of the relevant number of terminal S atoms. The molecular structures of the P_4S_n molecules are illustrated in Figure 7.1.

The samples were prepared by D. Woollins and Paul Wood (Department of Chemistry, Imperial College of Science and Technology, London). Most of the samples were hydroscopic and/or readily oxidised, which presented us with two problems. Firstly there was the possibility of the sample decomposing before a solid-state NMR spectrum could be acquired. This problem was largely overcome by packing of the sample rotor in a dry nitrogen atmosphere and ensuring that rotors were as airtight as possible by using tight-fitting end caps together with PTFE sealing tape. Secondly, the samples tended to attack the rotor material (Delrin), causing a rotor explosion after only a few minutes. Delrin was discovered to be very susceptible to attack by small amounts of phosphoric acid (a very likely decomposition product

Figure 7.1 : Molecular structures of P_4S_n compounds (where n = 3,5,7,9,10)

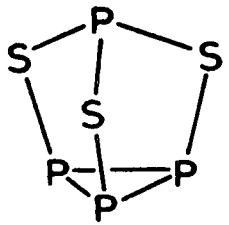

(a) P_4S_3

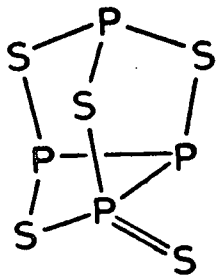

(b) α-P_4S_5

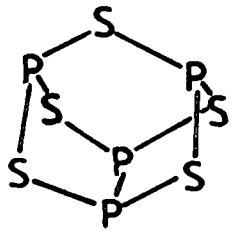

(c) β-P_4S_5

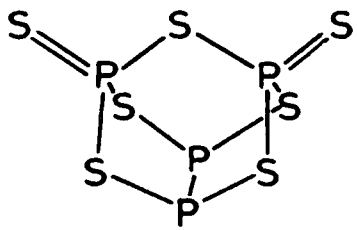

(d) P_4S_7

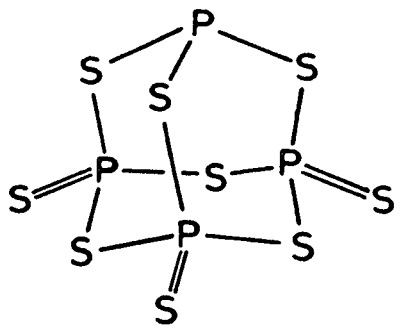

(e) P_4S_9

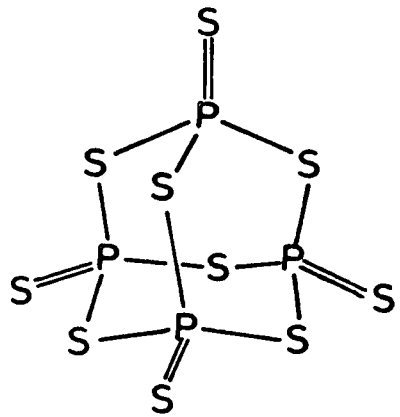

(f) P_4S_{10}

of the phosphorus sulphides coming into contact with moisture and oxygen). A sharp resonance at 0.0 ppm relative to 85% H_3PO_4 was often seen in the spectra of these samples which supports this theory. The problem was largely overcome by using a different spinning system which used rotors made from KEL-F. The samples do not appear to attack this material.

7.2 Discussion

7.2.1 Phosphorus sesquisulphide

Phosphorus sesquisulphide (P_4S_3) is probably the most well-known phosphorus sulphide. It is commonly used in the manufacture of "strike anywhere" matches. Early low field work[2] yielded approximate shifts for solid P_4S_3 of -72 (+/- 10 ppm) and 103 (+/- 10 ppm) with an intensity ratio of 1:3 for apical and basal phosphorus sites respectively. Relaxation studies[4] had shown that there was little dependence of T_1 on the field, B_o, at which measurements were made. Relaxation times were typically in excess of 100 seconds. P_4S_3 undergos a first order solid-state phase transition at 313.9 K with the high temperature phase (phase I) undergoing rapid molecular reorientation and diffusion whereas the low temperature phase (phase II) is a rigid solid for which the crystal structure is known[8]. An AB_3 pattern has been obtained for phase I[5] without the assistance of artificial line narrowing techniques giving shifts of -72 ppm and 113 ppm with coupling constant J= 70

+/- 3 Hz. Single crystal data[6] have been obtained for phase II giving shielding tensor components for both apical and basal sites.

The samples of P_4S_3 studied here belong to phase II and we have not at any time seen any evidence for the presence of phase I.

Figure 7.2(a) shows the first SPE spectrum obtained for P_4S_3 at the start of this study, at which time optimum spectrometer parameters were not known. A recycle delay of just 10 seconds was used whereas, consistent with the relaxation measurements of Andrew et al[4], a far more suitable delay was later found to be 300 seconds, which was used in all subsequent acquisitions. The spectrum shows a pair of resonances (1 and 2) at 91.0 and 84.4 ppm respectively, with very similar shielding anisotropies. Resonances 3 to 9 were assigned to impurities since firstly, these resonances appeared in the wrong spectral region for P_4S_3 and secondly they had no spinning sideband pattern associated with them (and are therefore likely to arise from fluid components resulting from contact with moisture). Unfortunately there did not appear to be a resonance from the basal site in the region of +100 ppm. The missing resonance, combined with the unwanted impurities prompted the preparation of a second sample of P_4S_3, which gave the spectra shown in Figure 7.2(b). Again, resonances 1 and 2 appeared in the same place but with the addition of a resonance at -87.5 ppm showing a very large shielding anisotropy. This resonance was probably present for

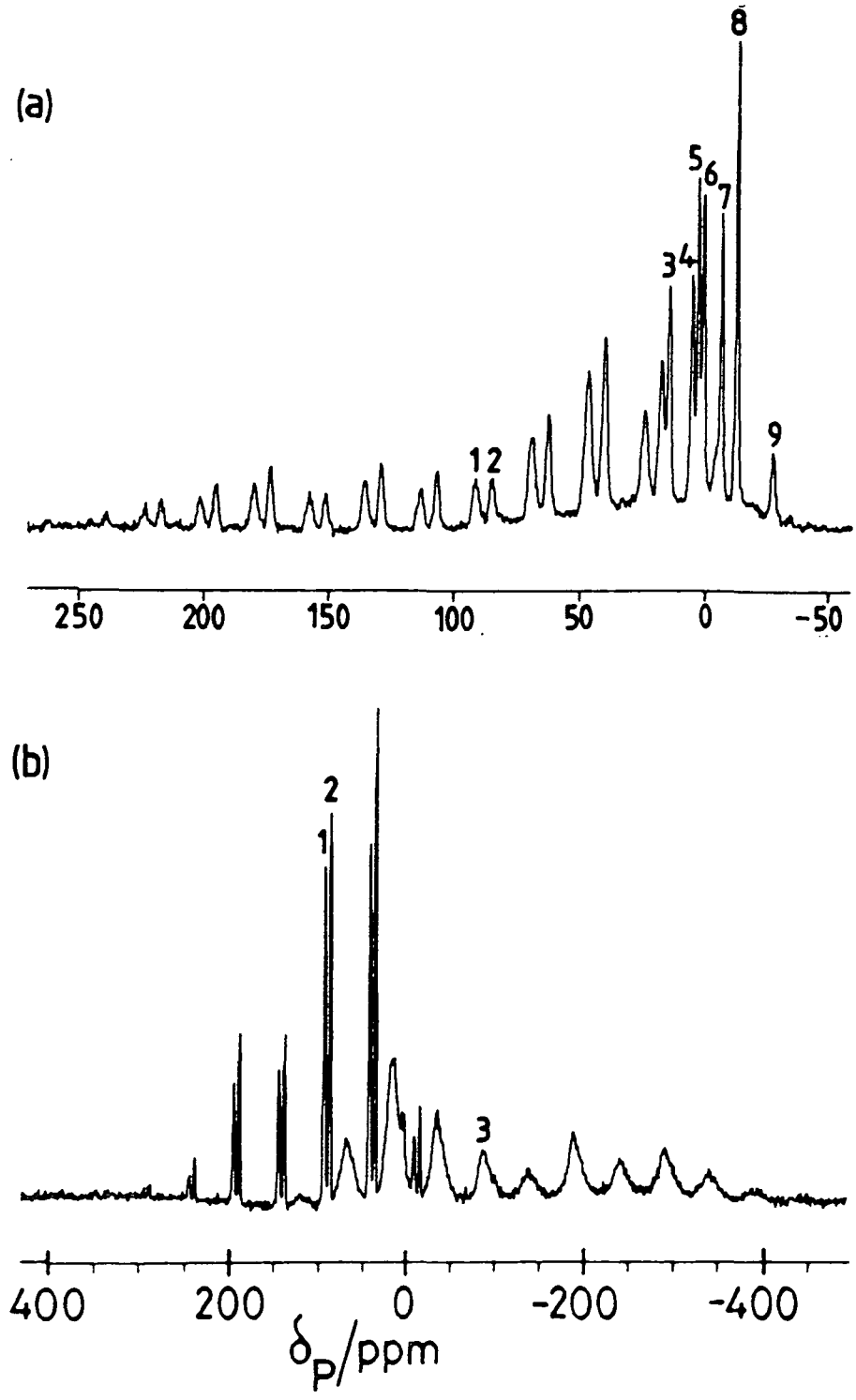

Figure 7.2 : ^{31}P SPE/MAS spectra of P_4S_3 (Centrebands indicated by numbers)

(a) Early sample of P_4S_3 : Recycle delay = 10 s, spinning rate = 1780 Hz, Number of transients = 460, 90^0 pulse length = 5 μs.

(b) Later sample of P_4S_3 : Recycle delay = 300 s, spinning rate = 4100 Hz, Number of transients = 196, 90^0 pulse length = 4 μs.

the original sample, but not apparent since firstly, it is rather weak and could have been lost in the noise level of the baseline, and secondly, a much higher spinning rate was used for 7.2(b), thus resulting in the signal intensity being distributed amongst fewer spinning sidebands. The observed spectrum 7.2(b) can be rationalised by considering the X-ray structure of P_4S_3 phase II[8]. The asymmetric unit consists of halves of two different molecules. Each of the two molecules going to make up the asymmetric unit has a mirror plane along the molecular C_3 axis thus rendering two of the basal nuclei equivalent in each case. One would therefore expect to observe two apical resonances each J-coupled to the basal nuclei, and a complex pattern of basal resonances consisting of an AB_2 second order pattern from each of the independent half molecules, with the situation being further complicated by the likely overlapping of resonances and additional J-coupling to the apical nuclei. Essentially this is what we have observed with resonances 1 and 2 being the two types of apical nuclei and resonance 3 being due to the complicated system of resonances from the basal nuclei merging together. A summary of chemical shift, linewidth and tensor data is given in Table 7.1. It would appear that all J-coupling has been obscured due to the linewidth of the resonances (apical nuclei) and/or overlapping signals plus second-order effects (basal nuclei). Typical P-P couplings are ca. 200 Hz and P-S-P couplings ca. 70 Hz. The ratio of apical:basal NMR signal intensity is 1:2.6 (by integration) which is reasonably close to the expected ratio of 1:3 bearing in mind

Table 7.1 : Chemical shift, linewidth and shielding tensor data[a] for P_4S_3 phase II.

Resonance Number	δ_P / ppm[b]	Linewidth /Hz	Tensor components /ppm σ_{11}	σ_{22}	σ_{33}
1	91.0	250	-6	-39	-228
2	84.5	200	-2	-18	-233
			(-3)	(-25)	(-238)
3	-87.5	1200	-109	7	365
			(-101)	(-44)	(406)

[a]Tensor data from ref [6] shown in brackets

[b]Chemical shift data verified using ^{31}P NMR at 7.04 T. Spectra acquired using Varian VXR 300, situated at Industrial Research Laboratories, University of Durham.

the signal to noise level, overlapping of resonances and the huge shielding anisotropy for the basal phosphorus signal. The calculated shielding tensor components (Table 7.1) agree well with the single crystal data of Gibby et. al.[6], supporting our assignments to apical and basal nuclei. It is interesting to note that although resonances 1 and 2 have slightly different peak heights the overall intensity ratio is still 1:1 due to resonance 1 having a broader linewidth. Despite the difference in environments the shielding tensor components for the two resonances are very similar (indeed they are probably equal within experimental error, with the possible exception of σ_{22}).

7.2.2 Tetraphosphorus pentasulphide

Tetraphosphorus pentasulphide, P_4S_5, can exist in α and β forms (recall Figure 7.1). Both forms have known crystal structures[10,11,12]. Andrew and Wynn[2] obtained data for a static sample, yielding very approximate chemical shift values of +200, +20 and -120 ppm, although it was not clear whether the phase studied was α , β or a mixture of the two.

The sample of P_4S_5 studied here yielded the spectra shown in Figure 7.3. The spectra illustrate the value of using different spinning speeds. The choice of spinning rate is rather critical if one is to be able to observe all the resonances without them being obscured by spinning sidebands from another signal. As can be seen from Figure 7.3(b) four bands can be

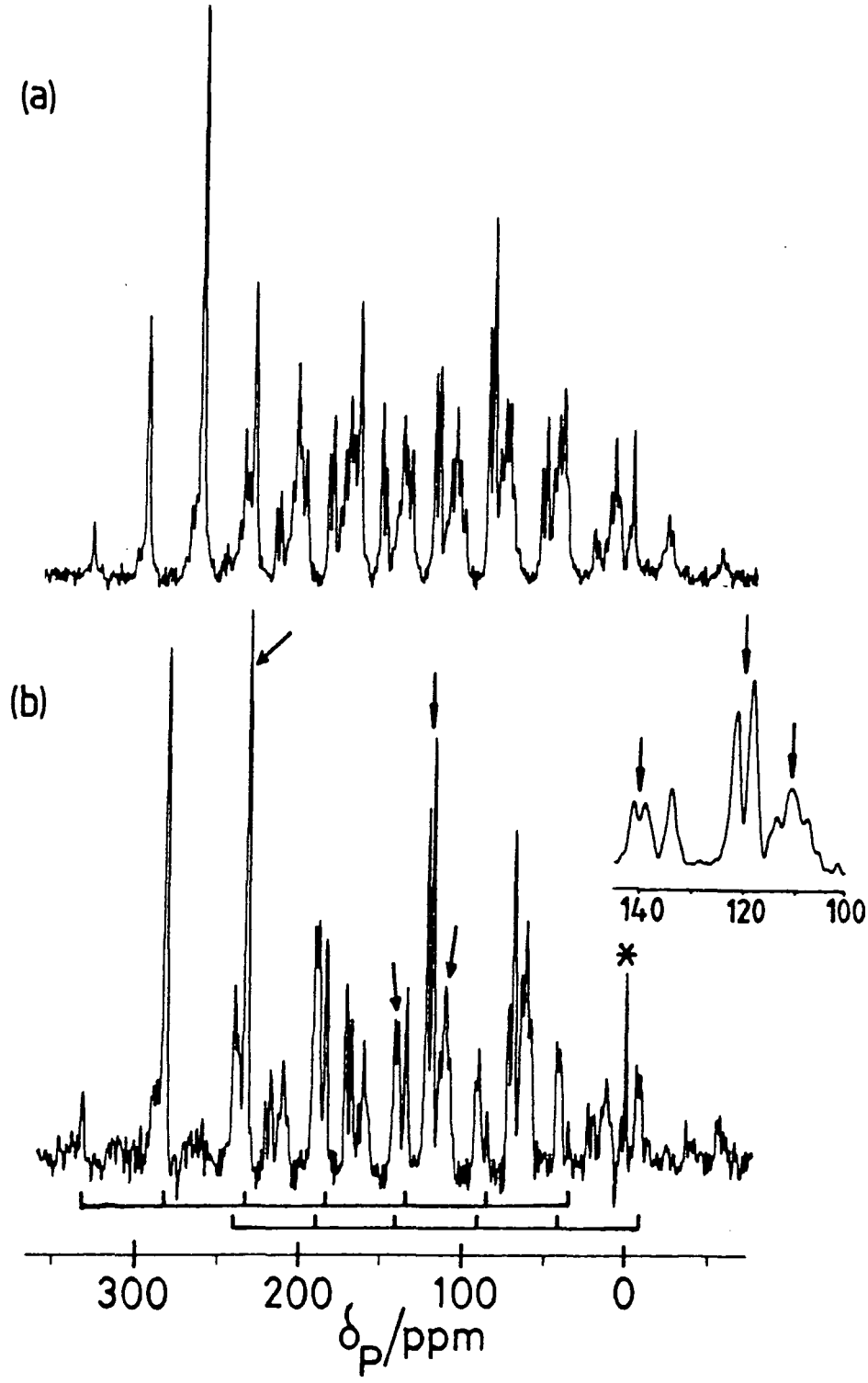

Figure 7.3 : ^{31}P SPE/MAS spectra of α-P_4S_5
Recycle delay = 300 s, 90^0 pulse length = 4 μs
number of transients = 24.

(a) Spinning rate = 2650 Hz

(b) Spinning rate = 4016 Hz. Centreband expansion inset, with centrebands indicated by arrows. The linkages show the spinning sideband manifolds for P_I and P_{III}. The asterisk indicates an impurity peak (possibly H_3PO_4).

identified: a singlet two doublets and a triplet. By making the assumption that any two-bond J-coupling would be obscured within the linewidths of the resonances we were able to assign the spectra obtained to α-P_4S_5 (illustrated in Figure 7.4).

The X-ray crystal structure[11,12] indicates that the asymmetric unit consists of a single molecule of P_4S_5. The singlet (resonance 1) arises from $P_{(I)}$, one doublet (resonances 2 and 3) due to $P_{(II)}$ coupling to $P_{(IV)}$, a second doublet (resonances 4 and 5) due to $P_{(III)}$ coupling to $P_{(IV)}$, and a triplet (resonances 6,7 and 8) due to $P_{(IV)}$ coupling to both $P_{(II)}$ and $P_{(III)}$. Chemical shift data for P_4S_5 are summarised in Table 7.2(a), with solution state data[7] shown in Table 7.2(b) for comparison. Comparison of the solution and solid-state data for α-P_4S_5 shows a dramatic shifting of the resonances due to $P_{(II)}$, $P_{(III)}$ and $P_{(IV)}$. It would seem that the environment of these phosphorus atoms is significantly different depending on whether the sample is crystalline or in solution. Large solution-to-solid changes have also been observed for P_4S_3. These effects cannot currently be fully explained, although the magnitude of the changes indicate substantial changes in geometry rather than mere inter-molecular packing considerations. Regardless of these discrepancies we can conclude that our sample of P_4S_5 is in the α-form and that there is no evidence for the β-form being present. The spectra shown in Figure 7.3 illustrate the ability of solid-state NMR to distinguish different isomers in these systems. The β-form of P_4S_5 has a structure with no

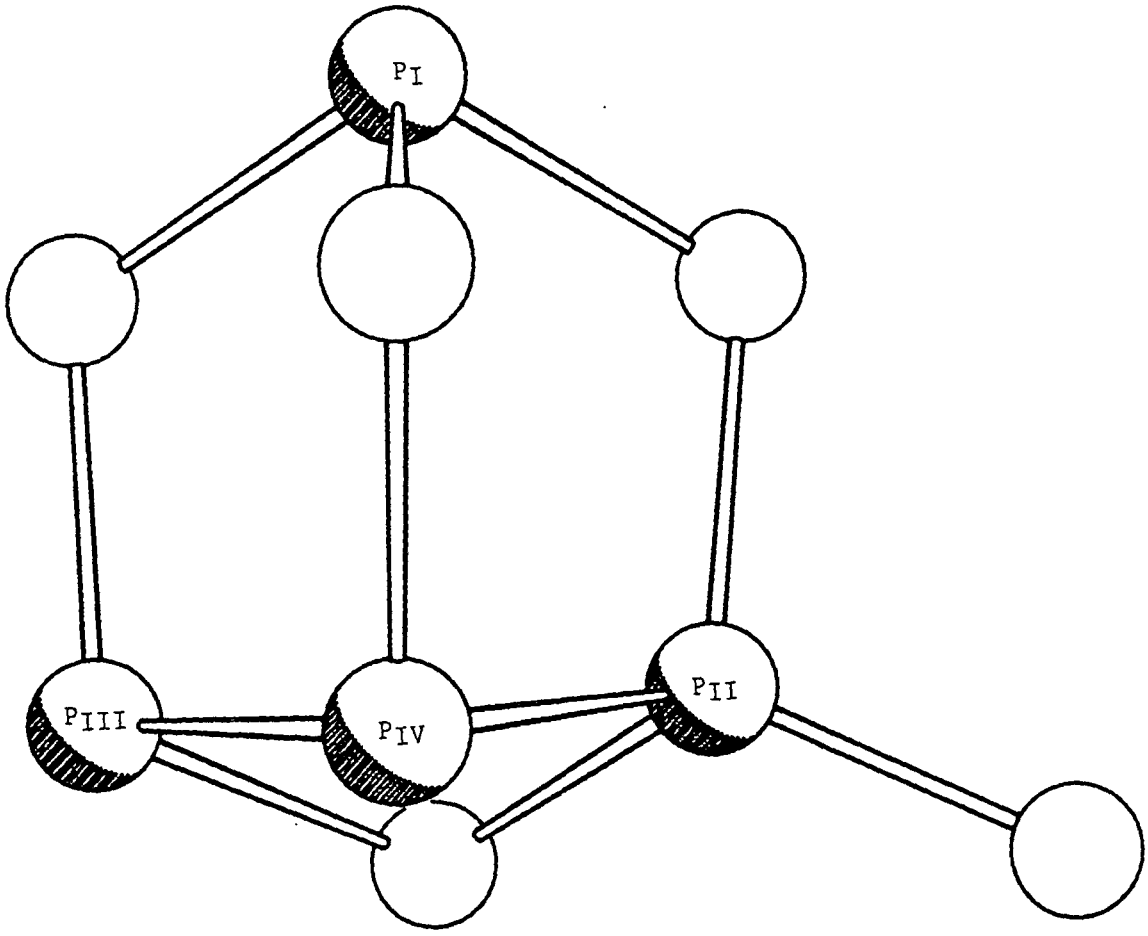

Figure 7.4 : α-P_4S_5 -Molecular structure

Table 7.2(a) : Solid-state chemical shift, linewidth and coupling constant data for α-P_4S_5

Phosphorus Site	δ_P / ppm	Linewidth /Hz	Jpp / Hz
P_I	232.7	190	-------
P_{II}[a]	120.2	140	210
P_{III}[a]	139.8	210(b)	194
P_{IV}	111.4	210(b)	203(c)

Table 7.2(b) : Solution-state chemical shift and coupling constant data for α-P_4S_5 in CS_2 solvent[d].

Phosphorus Site	δ_P / ppm	J-couplings /Hz
P_I	231.7	$J_{III,IV}$ =120 $J_{II,IV}$ = -284
P_{II}[a]	89.6	
P_{III}[a]	122.7	$^2J_{I,IV}$ = 28 $^2J_{II,III}$ = -84
P_{IV}	125.9	$^2J_{I,III}$ = 19 $^2J_{I,II}$ = 54

(a)P_{II} and P_{III} assignments may possibly be the opposite way round. A conclusive assignment could not be made.

(b)Estimated linewidth (due to overlapping resonaces).

(c)Doublet of doublets, hence this is an approximate coupling constant measured from the central peak, to the peaks either side of it.

(d)Data taken from Ref. [7].

phosphorus-sulphur double bonds, and the molecular site symmetry indicates that two of the phosphorus atoms are equivalent which is inconsistent with the spectra presented here.

7.2.3 Tetraphosphorus heptasulphide

Tetraphosphorus heptasulphide, P_4S_7, can exist in two crystalline forms, α and β. The α-form is composed entirely of molecules of the type indicated in Figure 7.1(d). The crystal structure[12] for this phase indicates one molecule in the asymmetric unit, with all four phosphorus nuclei being inequivalent. The β-form has an approximate composition $P_4S_{6.5}$ and is believed to contain a small proportion of P_4S_6 and P_4S_5 corresponding to either one or two of the terminal sulphurs being removed. X-ray crystallography[15] has shown that β-P_4S_7 has half a molecule in the asymmetric unit owing to the retention of the C_2 axis when crystalline.

The sample of P_4S_7 studied here gave a solution-state ^{31}P spectrum consisting of two lines at 110.3 and 89.3 ppm with intensity ratio 1:1. Two triplets would have been expected, since all other phosphorus sulphides show $\{^{31}P\text{-}^{31}P\}$ couplings in solution. It may be that on going from P_4S_9 to P_4S_3 the sign of the coupling constant changes and thus for P_4S_7 it is accidentally zero. Figure 7.5 shows the solid-state ^{31}P spectrum for P_4S_7 (centreband inset). The chemical shift, linewidth and tensor data are summarised in Table 7.3. If we once again assume

Figure 7.5 : ^{31}P MAS NMR spectrum of α-P_4S_7.

Recycle delay = 800 s, spinning rate = 3550 Hz, 90^0 pulse length = 4 μs , number of transients = 16.

The inset is an expansion of the centrebands, which are indicated in the main spectrum by arrows. The linkages show the spinning sideband manifolds for P_I and P_{II}.

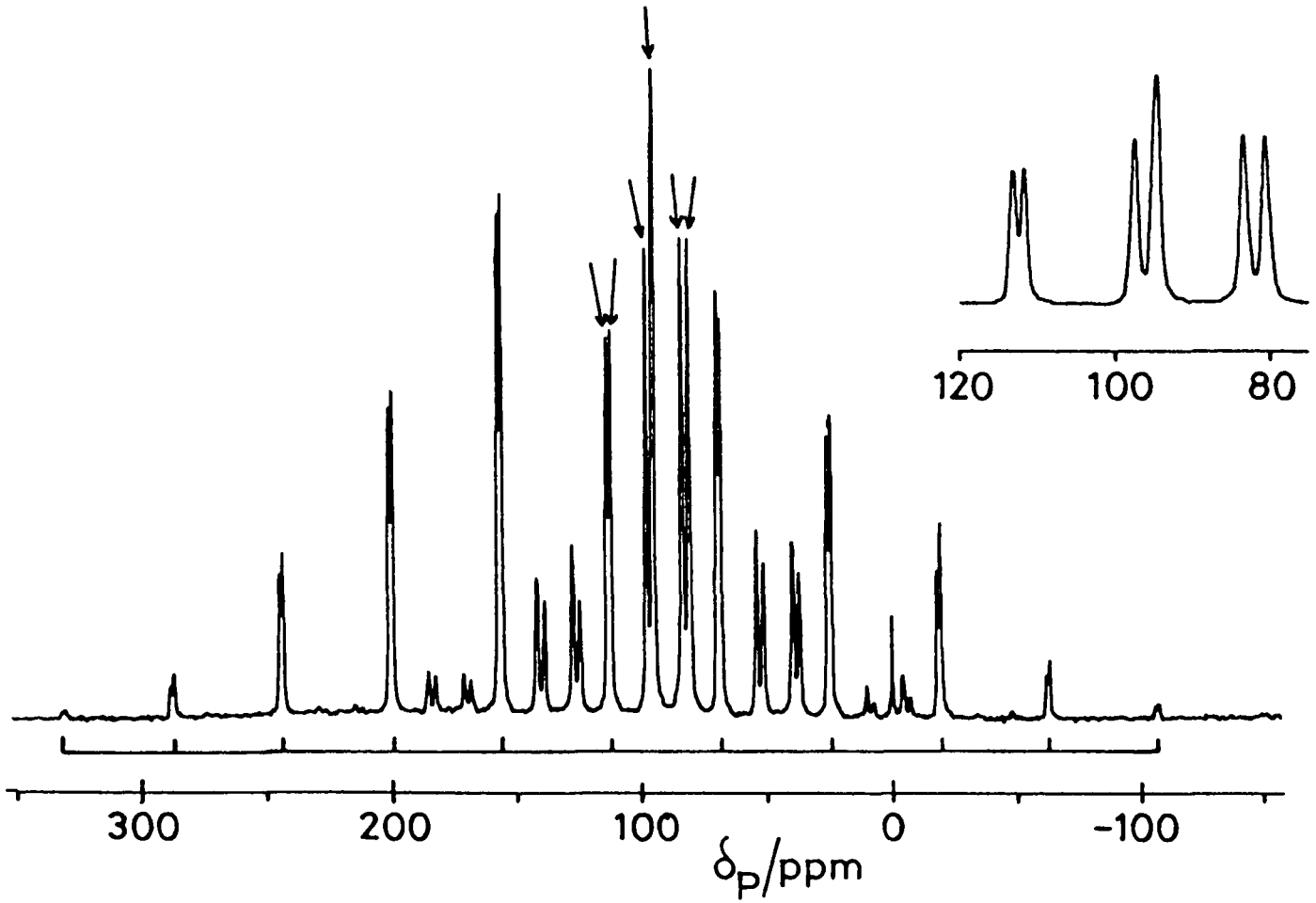

Table 7.3 : Chemical shift, linewidth and shielding tensor data for α-P_4S_7.

Phosphorus Site	Peak	δ_P / ppm[b]	Linewidth /Hz	Jpp /Hz	Tensor components /ppm σ_{11}	σ_{22}	σ_{33}
P_I	1	113.0	90	-----	-259[a]	-100	+20[a]
P_{II}	2	111.6	81	-----	-263	-113	+42
P_{III}	3,4	96.0	105	231	-186[a]	-81	-23[a]
					-152	-103	-28
P_{IV}	5,6	82.0	97	231	-146	-110	+7
					-159[a]	-69	-12[a]

[a] The labels σ_{11} and σ_{33} are retained here as for the remaining peaks of this spectrum though convention would reverse the subscripts. This is done to maintain the consistency and because experimental error may account for the apparent change in sign for the anisotropy

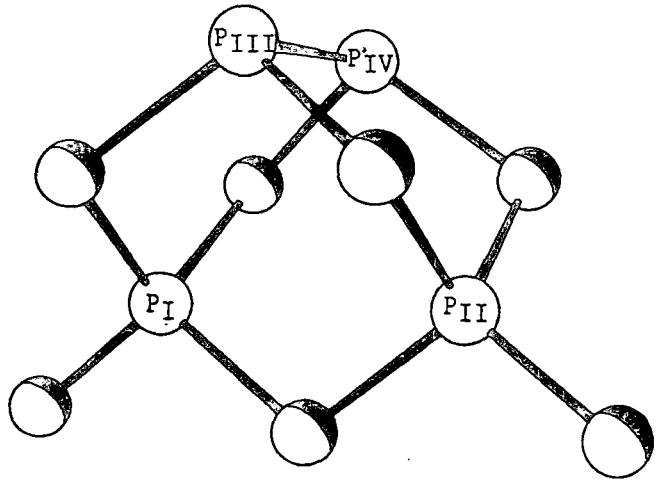

that two bond J-couplings are obscured it is possible to explain the spectrum observed. Since the resonances $P_{(I)}$ and $P_{(II)}$ have an average shift close to one of the solution-state shifts, and the resonances due to $P_{(III)}$ and $P_{(IV)}$ averaged, fall close to the other solution-state shift, it would seem likely that we have the same molecular unit in the solid but with a lowering of molecular symmetry within the crystal structure. This is consistent with sample being α-P_4S_7. Resonances 1 and 2 are due to $P_{(I)}$ and $P_{(II)}$ respectively, which have become inequivalent owing to the drop in molecular symmetry. Resonances 3,4,5 and 6 result from a large splitting (14.0 ppm) due to the lowering of symmetry, combined with a J-coupling of 220 Hz due to the phosphorus atoms $P_{(III)}$ and $P_{(IV)}$ being directly bonded. The splittings for resonances assigned to $P_{(III)}$ and $P_{(IV)}$ have been confirmed to be J-couplings by acquiring spectra at a higher field strength (7.04 T). The signal intensities for $P_{(I)}$, P(II), $P_{(III)}$ and $P_{(IV)}$, when integrated over the spinning sideband manifolds are equal within experimental error. It is interesting to note that rather different shielding anisotropies for types $P_{(I,II)}$ and $P_{(III,IV)}$. The results presented allow us to conclude that we have P_4S_7 in the α-form since firstly, the β-form would give a simpler NMR spectrum, and secondly because there are no additional resonances observed, which could have been attributed to P_4S_5 and P_4S_6 content within the sample.

7.2.4 Higher phosphorus sulphides

Tetraphosphorus nonasulphide, P_4S_9, and tetraphosphorus decasulphide, P_4S_{10} have very similar molecular structures, differing only according to whether or not one terminal sulphur is missing. In practice it is relatively easy to obtain P_4S_{10} but much more difficult to produce P_4S_9 free from P_4S_{10}. P_4S_{10} will therefore be discussed first so that the consideration of P_4S_9 can be done whilst allowing for the possibility of P_4S_{10} being present.

P_4S_{10} was studied by Andrew et. al.[2] in the solid state using ^{31}P MAS NMR, reporting a chemical shift of 45 ppm. Figure 7.6(a) shows the solid-state ^{31}P NMR spectrum for our sample of P_4S_{10}. There are apparently three poorly resolved signals with approximate shifts of 60.1, 56.0, and 50.2 ppm respectively. The X-ray crystal structure[12,14] indicates that there is one molecule in the asymmetric unit. Although only three signals have been resolved, the presence of a fourth signal cannot be ruled out. Should a fourth signal be present, the spectrum would be consistent with the crystal structure, with each of the signals being due to one of the four different phosphorus atoms in the asymmetric unit.

P_4S_9 can exist in two phases[13]. Phase I is a disordered crystalline solid and phase II is an ordered crystalline form. The ordered phase has a known crystal structure[13] with one third of a molecule in the asymmetric unit since the molecular C_3

axis is retained in the crystal. Two samples A and B of P_4S_9 have been studied and their spectra are shown in Figures 7.6(b) and 7.6(c) respectively. Raman analysis [16] of sample A indicated that a large proportion of P_4S_{10} was present whereas sample B was believed to be reasonably pure. Sample A has major ^{31}P NMR resonances at 67.6 , 57.8 and 49.5 ppm, and sample B shows major resonances at 67.5 and 57.8 ppm. Centreband expansions for P_4S_{10}, and samples A and B are shown in Figure 7.7. As can be seen, within reasonable error, both samples have resonances in the region of 67.5 ppm and 57.8 ppm in common, with the additional resonance in sample A probably being due to P_4S_{10} contamination (the extra resonance for sample A occurs in the spectrum of P_4S_{10}). It would therefore appear that P_4S_9 is showing at least two resonances with approximate intensity ratio 1:3 (others may be obscured within the rather broad lines). The spectra therefore suggest that P_4S_9 phase II material is present in samples A and B. The rather broad lines make it difficult to conclude whether or not phase I is present also. Likewise, the presence of impurities other than P_4S_{10} in samples A and B cannot be ruled out.

Other studies suggest that Raman spectroscopy is a rather better tool for identification of these species.

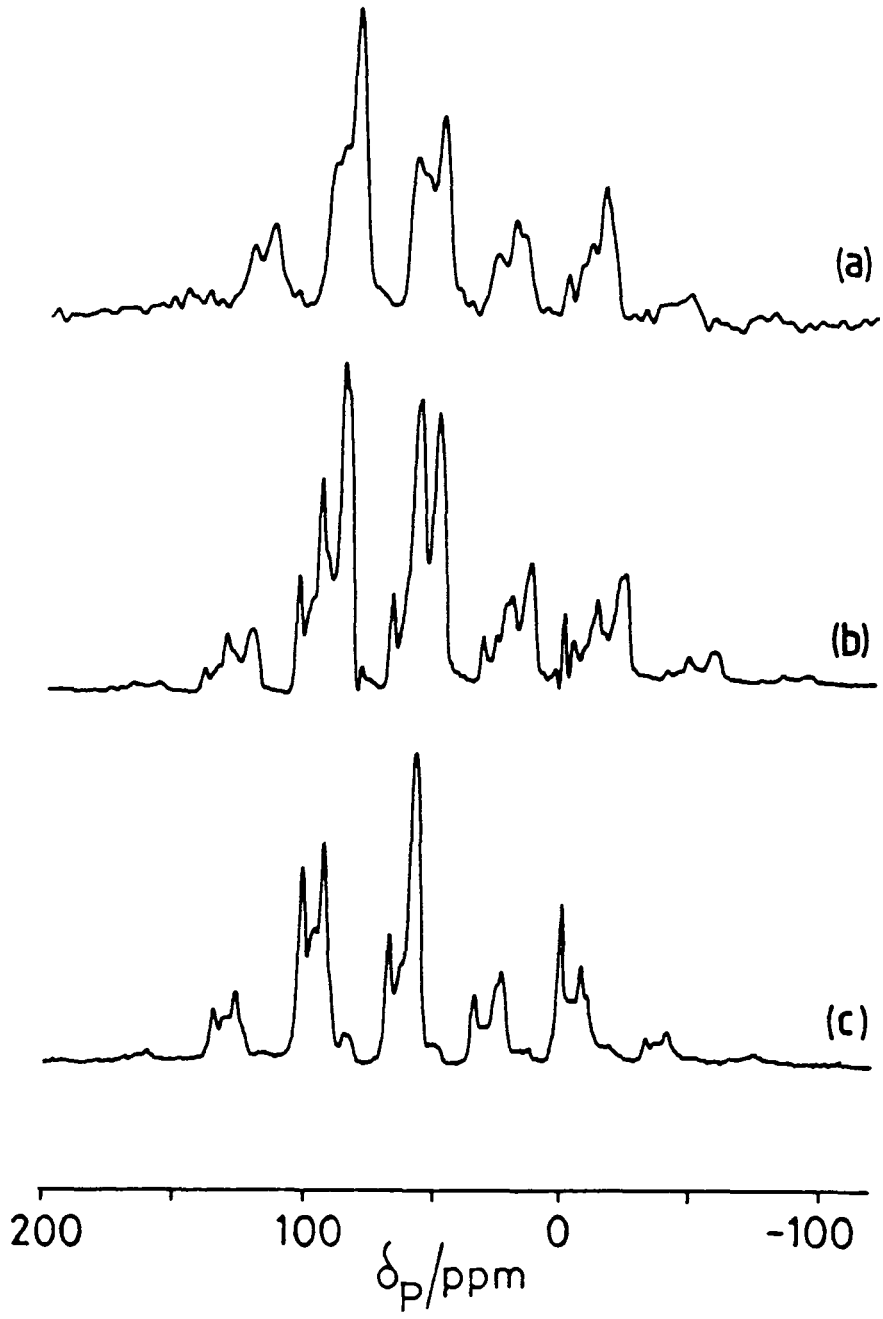

Figure 7.6 : ^{31}P MAS NMR spectra of P_4S_{10} and P_4S_9 samples A and B

(a) P_4S_{10} ; Recycle delay = 300 s, spinning rate = 2.7 kHz
90^0 pulse length = 4 μs, number of transients = 32.

(b) P_4S_9 -sample A ; Recycle delay = 800 s, spinning rate = 2.93 kHz
90^0 pulse length = 4 μs, number of transients = 56.

(c) P_4S_9 -sample B ; Recycle delay = 800 s, spinning rate = 2.73 kHz
90^0 pulse length = 5 μs, number of transients = 48.

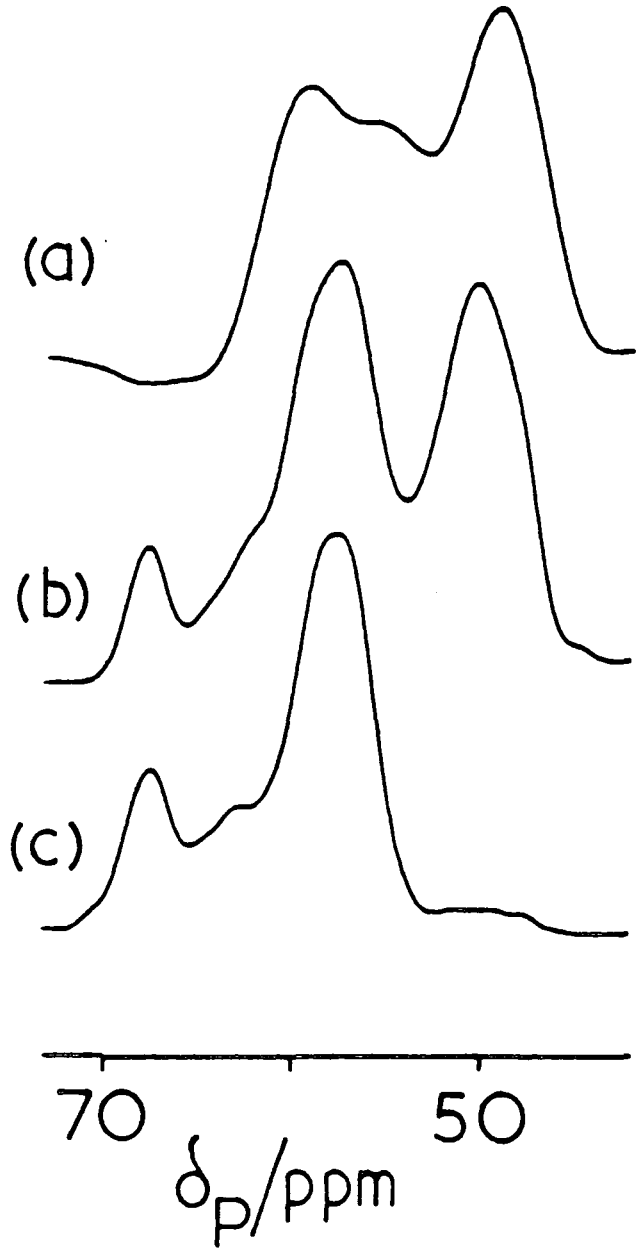

Figure 7.7 : Centreband expansions of the spectra shown in Figure 7.6.

(a) P_4S_{10} (b) P_4S_9 sample A (c) P_4S_9 sample B

7.3 Conclusion

This work has illustrated the application of solid-state phosphorus-31 NMR to the study of the P_4S_n series of compounds. Our data has certainly been more extensive and informative than the previous studies reported in the literature. In favourable circumstances information can be obtained regarding the molecular form present and/or the crystalline phase, yielding information of the kind which is normally only available from X-ray studies. Despite the practical difficulties discussed at the start of this chapter, solid-state ^{31}P NMR is generally more accessible and straightforward than a full scale X-ray crystal analysis.

While this thesis was in the final stages of being typed, a paper was published reporting[17] both solid (MAS) and solution-state NMR data for P_4S_7. The MAS results are in good agreement with those presented in this thesis (section 7.2.3).

REFERENCES

[1] C. F. Callis, J. R. Van Wazer, J.N. Shoorley and W. A. Anderson
J. Am. Chem. Soc. 79, (1957), 2719.

[2] E. R. Andrew and V. T. Wynn
Proc. Roy. Soc. A291, (1966), 257.

[3] G. Heckmann and E. Fluck
Z. Naturforsch 26B, (1971), 982.

[4] E. R. Andrew, W. S. Hinshaw, M. G. Hutchins and A. Jasinski
Chem. Phys. Lett. (1974), 96.

[5] E. R. Andrew, W. S. Hinshaw and A. Jasinski
Chem. Phys. Lett. (1974), 399.

[6] M. G. Gibby, A. Pines, W. K. Rhim and J. S. Waugh
J. Chem. Phys. 56, (1972), 991.

[7] R. Tann, S. Heckmann and E. Fluck
Phosphorus and Sulphur 11, (1981) 273.

[8] Yuen Chu Leung, Jur Waser, S. an Houten, Aafje Vos, G. A. Wiegers and E. H. Wiebenga
Acta. Cryst. 10, (1957), 574.

[9] A. M. Griffin, P. C. Minshall and G. M. Sheldrick
J. Chem. Soc. Chem. Comm. (1976), 809.

[10] A. M. Griffin and G Sheldrick
Acta. Cryst. B31, (1975), 2738.

[11] S. Van Houten and E. H. Wiebenga
Acta. Cryst. 10, (1955), 156.

[12] Aafje Vos, Roeli Olthof, F. Van Bolhun and Riemhe Botterweg
Acta. Cryst. 19, (1965), 864.

[13] Waltrund Hilmer
Acta. Cryst. B25, (1969), 1229.

[14] Aafje Vos and E. H. Wiebenga
Acta. Cryst. 8, (1955), 217.

[15] D. T. Dixon, F. W. B. Einstein and B. R. Penfold.
Acta. Cryst. 18, (1965), 221.

[16] D. Woollins and P. Wood.
Personal communication.

[17] T. Bjorholm,
Chem. Phys. Lett., 143, (1988), 259.

APPENDIX

The Board of Studies in Chemistry requires that each post graduate research thesis contains an appendix which lists;

(a) all research colloquia, research seminars and lectures arranged by the Department of Chemistry and the Durham University Chemical Society during the period of the author's residence as a postgraduate student;

(b) all research conferences attended and papers presented by the author during the same period;

(c) details of the postgraduate induction course.

UNIVERSITY OF DURHAM

Board of Studies in Chemistry

COLLOQUIA, LECTURES AND SEMINARS GIVEN BY INVITED SPEAKERS:
1st AUGUST 1984 to 31st JULY 1985

ATKINS, Dr. P.W. (University of Oxford) — 7th March 1985
'Magnetic Reactions'

AYLETT, Prof. B.J. (Queen Mary College, University of London) — 1st November 1984
'Silicon - Dead Common or Refined'

BELTON, Dr. P.S. (Food Research Institute, Norwich) — 4th June 1985
'Analytical Photoacoustic Spectroscopy'

BROWN, Dr. C. (IBM San Jose) — 19th September 1984
'New Superbase Reactions - Organic Compounds'

BROWN, Prof. I.D. (Institute for Materials Research, McMaster University, Canada) — 17th May 1985
'Bond Valence as a Model for Inorganic Chemistry'

CHAMBERS, Prof. R.D. (University of Durham) — 6th December 1984
'The Unusual World of Fluorine'

CLARK, Prof. D.T. (ICI New Science Group) — 22nd November 1984
'Structure, Bonding, Reactivity and Synthesis as Revealed by ESCA'

COATES, Prof. G.E. (formerly of University of Wyoming, U.S.A.) — 7th May 1985
'Chemical Education in Britain and America: Successes and Deficiencies'

COVINGTON, Dr. A.K. (University of Newcastle-upon-Tyne) — 24th January 1985
'Chemistry with Chips'

DILLON, Dr. K.B. (University of Durham) — 12th December 1984
'^{31}P NMR Studies of Some Anionic Phosphorus Complexes'

EVERALL, Mr. N. (University of Durham) — 21st November 1984
'Picosecond Pulsed Laser Raman Spectroscopy'

FEAST, Dr. W.J. (University of Durham) — 25th October 1984
'Syntheses of Conjugated Polymers. Why and How?'

FEAST, Dr. W.J. (University of Durham) — 27th November 1984
'A Plain Man's Guide to Polymeric Organic Metals'

FLEET, Dr. G.W.J. (University of Oxford) — 13th February 1985
'Syntheses of some Alkaloids from Carbohydrates'

GERMAIN, Dr. A. (Université du Languedoc, Montpellier) — 19th October 1984
'Anodic Oxidation of Perfluoro Organic Compounds in Perfluoroalkane Sulphonic Acids'

GIBSON, Dr. H.W. (Signal UOP Research Centre, Des Plaines, Illinois) — 21st September 1984
'Isomerization of Polyacetylene'

GOLDING, Prof. B.T. (University of Newcastle-upon-Tyne) — 15th November 1984
'The Vitamin B_{12} Mystery'

GREEN, Dr. M.L.H. (University of Oxford) — 31st January 1985
'Naked Atoms and Negligée Ligands'

GRIMMETT, Dr. R. (University of Otago, Dunedin, New Zealand) — 22nd May 1985
'Some Aspects of Nucleophilic Substitution in Imidazoles'

GROSSEL, Dr. M.C. (Bedford College, University of London) — 24th April 1985
'Hydroxypyridone Dyes - Bleachable One-Dimensional Metals?'

HARRIS, Prof. R.K. (University of Durham) — 24th October 1984
'NMR of Solid Polymers'

HARRIS, Prof. R.K. (University of Durham) — 9th May 1985
'Chemistry in a Spin: Nuclear Magnetic Resonance'

HUDLICKY, Dr. M. (Virginia State University, Blacksburg) — 22nd May 1985
'Preferential Elimination of Hydrogen Fluoride from Vicinal Bromofluorocompounds'

KATRITZKY, Prof. A.R., FRS (University of Florida) — 14th March 1985
'Some Adventures in Heterocyclic Chemistry'

LAALI, Dr. K. (Hydrocarbon Research Institute, University of Southern California) — 12th July 1985
'Recent Developments in Superacid Chemistry and Mechanistic Considerations in Electrophilic Aromatic Substitutions; a Progress Report'

LEDWITH, Prof. A. (Pilkington Bros.) — 7th February 1985
'Glass as a High Technology Material'

LOGAN, Dr. N. (University of Nottingham) — 18th October 1984
'N_2O_4 and Rocket Fuels'

LUX, Mr. P.J. (University of Durham) — 5th December 1984
'IR and GC Studies of the Interaction of CH_3OH with High Silica Zeolites'

MAITLIS, Prof. P.M., FRS (University of Sheffield) — 21st February 1985
'What Use is Rhodium?'

MINCHER, Dr. D.J. (University of Durham) — 19th February 1985
'Stereoselective Syntheses of Some Novel Anthracyclinones Related to the Anti-Cancer Drug Adriamycin and to the Steffimycin Antibiotics'

MITCHELL, Dr. T.N. (University of Dortmund) — 19th June 1985
'Some Synthetic and NMR-Spectroscopic Studies of Organotin Compounds'

MULVEY, Dr. R.E. (University of Durham) — 27th February 1985
'Some Unusual Lithium Complexes'

MUNRO, Dr. H.S. (University of Durham) — 7th November 1984
'New Information from ESCA Data'

PACKER, Dr. J.E. (University of Auckland, New Zealand) — 15th May 1985
'Studies of Free Radical Reactions in Aqueous Solution Using Ionising Radiation'

PACKER, Prof. K.J. (B.P. Research Centre) — 12th March 1985
'NMR Investigations of the Structure of Solid Polymers'

PARKER, Dr. D. (ICI plc, Petrochemical & Plastics Division, Wilton) — 1st May 1985
'Applications of Radioisotopes in Industrial Research'

PASSMORE, Prof. J. (University of New Brunswick) — 14th May 1985
'The Synthesis and Characterisation of some Novel Selenium-Iodine Cations, Aided by ^{77}Se NMR Spectroscopy'

POLIAKOFF, Dr. M. (University of Nottingham) — 21st March 1985
'New Methods for Detecting Organometallic Intermediates in Solution'

PORTERFIELD, Prof. W.W. (Hampden-Sydney College, U.S.A.) — 7th November 1984
'There is No Borane Chemistry (Only Geometry)'

RAPPOPORT, Prof. Z. (The Hebrew University, Jerusalem) — 14th June 1985
'The Rich Mechanistic World of Nucleophilic Vinylic Substitution'

RINGSDORF, Prof. H. (Organic Chemistry Institute, University of Mainz) — 28th March 1985
'Polymeric Liposomes as Models for Biomembranes and Cells?'

RODGERS, Dr. P.J. (ICI plc, Agricultural Division, Billingham) — 7th March 1985
'Industrial Polymers from Bacteria'

SALTHOUSE, Dr. J.A. (University of Manchester) — 14th February 1985
'Son et Lumiere' (A Chemical Energy Show)

SHAW, Prof. G. (University of Bradford) — 26th June 1985
'Synthetic Studies on Imidazole Nucleosides and the Antibiotic Coformycin'

STEPHENSON, Dr. T.A. (University of Edinburgh) — 28th November 1984
'Some Recent Studies in Platinum Metals Chemistry'

STIRLING, Prof. C.J.M. (University College of North Wales) — 29th November 1984
'Molecules Taking the Strain'

SUSCHITZKY, Emeritus Prof. H. (University of Salford) — 11th January 1985
'Fruitful Fissions of Benzofuroxanes and Isobenzimadazoles (umpolung of o-phenylenediamine)'

TUCK, Prof. D. (University of Windsor, Ontario) — 8th May 1985
'Lower Oxidation State Chemistry of Indium'

WILLIAMS, Dr. D.L.H. (University of Durham) — 21st May 1985
'Chemistry in Colour'

WILLIAMS, Prof. G. (University College of Wales, Aberystwyth) — 8th May 1985
'Liquid Crystalline Polymers'

WOOLLINS, Dr. D. (Imperial College, University of London) — 13th June 1985
'Metal-Sulphur-Nitrogen Complexes'

UNIVERSITY OF DURHAM

Board of Studies in Chemistry

COLLOQUIA, LECTURES AND SEMINARS GIVEN BY INVITED SPEAKERS:
1st AUGUST 1985 to 31st JULY 1986

BARNARD, Dr. C.J.F. (Johnson Matthey Group) 'Platinum Anti-Cancer Drug Development'	20th February 1986
BROWN, Dr. J.M. (University of Oxford) 'Chelate Control in Homogeneous Catalysis'	12th March 1986
CLARK, Dr. B.A.J. (Kodak Ltd.) 'Chemistry and Principles of Colour Photography'	28th November 1985
CLARK, Dr. J.H. (University of York) 'Novel Fluoride Ion Reagents'	29th January 1986
DAVIES, Dr. S.G. (University of Oxford) 'Chirality Control and Molecular Recognition'	14th November 1985
DEWING, Dr. J. (U.M.I.S.T.) 'Zeolites - Small Holes, Big Opportunities'	24th October 1985
ERTL, Prof. G. (University of Munich) 'Heterogeneous Catalysis'	7th November 1985
GRIGG, Prof. R. (Queen's University, Belfast) 'Thermal Generation of 1,3-Dipoles"	13th February 1986
HARRIS, Prof. R.K. (University of Durham) 'The Magic of Solid State NMR'	27th February 1986
HATHWAY, Dr. D. (University of Durham) 'Herbicide Selectivity'	5th March 1986
IDDON, Dr. B. (University of Salford) 'The Magic of Chemistry'	6th March 1986
JACK, Prof. K.H. (University of Newcastle) 'Chemistry of Si-Al-O-N Engineering Ceramics'	21st November 1985
LANGRIDGE-SMITH, Dr. P.R.R. (University of Edinburgh) 'Naked Metal Clusters - Synthesis, Characterisation and Chemistry'	14th May 1986
LEWIS, Prof. Sir Jack (University of Cambridge) 'Some more Recent Aspects in the Cluster Chemistry of Ruthenium and Osmium Carbonyls'	23rd January 1986
LUDMAN, Dr. C.J. (University of Durham) 'Some Thermochemical Aspects of Explosions'	17th October 1985
MACBRIDE, Dr. J.A.H. (Sunderland Polytechnic) 'A Heterocyclic Tour on a Distorted Tricycle - Biphenylene'	20th November 1985

O'DONNELL, Prof. M.J. (Indiana-Purdue University) — 5th November 1985
'New Methodology for the Synthesis of Amino Acids'

PARMAR, Dr. V.S. (University of Delhi) — 13th September 1985
'Enzyme Assisted ERC Synthesis'

PHILLIPS, Dr. N.J. (University of Technology, Loughborough) — 30th January 1986
'Laser Holography'

PROCTER, Prof. G. (University of Salford) — 19th February 1986
'Approaches to the Synthesis of some Natural Products'

SCHMUTZLER, Prof. R. (University of Braunschweig) — 9th June 1986
'Mixed Valence Diphosphorous Compounds'

SCHRODER, Dr. M. (University of Edinburgh) — 5th March 1986
'Studies on Macrocycle Complexes'

SHEPPARD, Prof. N. (University of East Anglia) — 15th January 1986
'Vibrational and Spectroscopic Determinations of the Structures of Molecules Chemisorbed on Metal Surfaces'

TEE, Prof. O.S. (Concordia University, Montreal) — 12th February 1986
'Bromination of Phenols'

TILL, Miss C. (University of Durham) — 26th February 1986
'ESCA and Optical Emission Studies of the Plasma Polymerisation of Perfluoroaromatics'

TIMMS, Dr. P. (University of Bristol) — 31st October 1985
'Some Chemistry of Fireworks'

WADDINGTON, Prof. D.J. (University of York) — 28th November 1985
'Resources for the Chemistry Teacher'

WHITTLETON, Dr. S.N. (University of Durham) — 30th October 1985
'An Investigation of a Reaction Window'

WILDE, Prof. R.E. (Texas Technical University) — 23rd June 1986
'Molecular Dynamic Processes from Vibrational Bandshapes'

YARWOOD, Dr. J. (University of Durham) — 12th February 1986
'The Structure of Water in Liquid Crystals'

UNIVERSITY OF DURHAM

Board of Studies in Chemistry

COLLOQUIA, LECTURES AND SEMINARS GIVEN BY INVITED SPEAKERS
1ST AUGUST 1986 TO 31ST JULY 1987

ALLEN, Prof. Sir G. (Unilever Research) Biotechnology and the Future of the Chemical Industry	13th November 1986
BARTSCH, Dr. R. (University of Sussex) Low Co-ordinated Phosphorus Compounds	6th May 1987
BLACKBURN, Dr. M. (University of Sheffield) Phosphonates as Analogues of Biological Phosphate Esters	27th May 1987
BORDWELL, Prof. F.G. (Northeastern University, U.S.A.) Carbon Anions, Radicals, Radical Anions and Radical Cations	9th March 1987
CANNING, Dr. N.D.S. (University of Durham) Surface Adsorption Studies of Relevance to Heterogeneous Ammonia Synthesis	26th November 1986
CANNON, Dr. R.D. (University of East Anglia) Electron Transfer in Polynuclear Complexes	11th March 1987
CLEGG, Dr. W. (University of Newcastle-upon-Tyne) Carboxylate Complexes of Zinc; Charting a Structural Jungle	28th January 1987
DÖPP, Prof. D. (University of Duisburg) Cyclo-additions and Cyclo-reversions Involving Captodative Alkenes	5th November 1986
DORFMÜLLER, Prof. T. (University of Bielefeld) Rotational Dynamics in Liquids and Polymers	8th December 1986
GOODGER, Dr. E.M. (Cranfield Institute of Technology) Alternative Fuels for Transport	12th March 1987
GREENWOOD, Prof. N.N. (University of Leeds) Glorious Gaffes in Chemistry	16th October 1986
HARMER, Dr. M. (I.C.I. Chemicals & Polymer Group) The Role of Organometallics in Advanced Materials	7th May 1987
HUBBERSTEY, Dr. P. (University of Nottingham) Demonstration Lecture on Various Aspects of Alkali Metal Chemistry	5th February 1987
HUDSON, Prof. R.F. (University of Kent) Aspects of Organophosphorus Chemistry	17th March 1987
HUDSON, Prof. R.F. (University of Kent) Homolytic Rearrangements of Free Radical Stability	18th March 1987

JARMAN, Dr. M. (Institute of Cancer Research) — 19th February 1987
The Design of Anti Cancer Drugs

KRESPAN, Dr. C. (E.I. Dupont de Nemours) — 26th June 1987
Nickel(0) and Iron(0) as Reagents in Organofluorine Chemistry

KROTO, Prof. H.W. (University of Sussex) — 23rd October 1986
Chemistry in Stars, between Stars and in the Laboratory

LEY, Prof. S.V. (Imperial College) — 5th March 1987
Fact and Fantasy in Organic Synthesis

MILLER, Dr. J. (Dupont Central Research, U.S.A.) — 3rd December 1986
Molecular Ferromagnets; Chemistry and Physical Properties

MILNE/CHRISTIE, Dr. A./Mr. S. (International Paints) — 20th November 1986
Chemical Serendipity - A Real Life Case Study

NEWMAN, Dr. R. (University of Oxford) — 4th March 1987
Change and Decay: A Carbon-13 CP/MAS NMR Study of Humification and Coalification Processes

OTTEWILL, Prof. R.H. (University of Bristol) — 22nd January 1987
Colloid Science a Challenging Subject

PASYNKIEWICZ, Prof. S. (Technical University, Warsaw) — 11th May 1987
Thermal Decomposition of Methyl Copper and its Reactions with Trialkylaluminium

ROBERTS, Prof. S.M. (University of Exeter) — 24th June 1987
Synthesis of Novel Antiviral Agents

RODGERS, Dr. P.J. (I.C.I. Billingham) — 12th February 1987
Industrial Polymers from Bacteria

SCROWSTON, Dr. R.M. (University of Hull) — 6th November 1986
From Myth and Magic to Modern Medicine

SHEPHERD, Dr. T. (University of Durham) — 11th February 1987
Pteridine Natural Products; Synthesis and Use in Chemotherapy

THOMSON, Prof. A. (University of East Anglia) — 4th February 1987
Metalloproteins and Magnetooptics

WILLIAMS, Prof. R.L. (Metropolitan Police Forensic Science) — 27th November 1987
Science and Crime

WONG, Prof. E.H. (University of New Hampshire, U.S.A.) — 29th October 1986
Coordination Chemistry of P-O-P Ligands

WONG, Prof. E.H. (University of New Hampshire, U.S.A.) — 17th February 1987
Symmetrical Shapes from Molecules to Art and Nature

Conferences Attended:

1. Bruker CXP Users Meeting, November, 1985.
2. British Radio Frequency Spectroscopy Group, High Resolution NMR in Solids, University of Oxford, April, 1986.
3. Bruker CXP Users Meeting, November, 1986.
4. Eighth International Meeting on NMR Spectroscopy, University of Kent at Canterbury, July, 1987.

Papers Presented

1. "Multiple pulse techniques in the solid state"
   Bruker CXP Users Meeting, November, 1986.
2. "NMR of Phosphorus-Containing Solids"
   Graduate Symposium, University of Durham, 1987.

Postgraduate Induction Course, October, 1984.

1. Departmental organization
2. Safety matters
3. Electrical appliances and infrared spectroscopy
4. Chromatography and microanalysis
5. Atomic absorptiometry and inorganic analysis
6. Library facilities
7. Mass spectroscopy
8. Nuclear magnetic resonance spectroscopy
9. Glassblowing technique